



# 1 Experimental chemical budgets of OH, HO<sub>2</sub> and RO<sub>2</sub> radicals in 2 rural air in West-Germany during the JULIAC campaign 2019

3 Changmin Cho<sup>1</sup>, Hendrik Fuchs<sup>1</sup>, Andreas Hofzumahaus<sup>1</sup>, Frank Holland<sup>1</sup>, William J. Bloss<sup>3</sup>,  
4 Birger Bohn<sup>1</sup>, Hans-Peter Dorn<sup>1</sup>, Marvin Glowania<sup>1</sup>, Thorsten Hohaus<sup>1</sup>, Lu Liu<sup>1</sup>, Paul S. Monks<sup>2</sup>,  
5 Doreen Niether<sup>1</sup>, Franz Rohrer<sup>1</sup>, Roberto Sommariva<sup>2,3</sup>, Zhaofeng Tan<sup>1</sup>, Ralf Tillmann<sup>1</sup>, Astrid  
6 Kiendler-Scharr<sup>1</sup>, Andreas Wahner<sup>1</sup>, and Anna Novelli<sup>1</sup>

7 <sup>1</sup>Forschungszentrum Jülich, Institute of Energy and Climate Research: Troposphere (IEK-8), Jülich,  
8 Germany

9 <sup>2</sup>Department of Chemistry, University of Leicester, Leicester, UK

10 <sup>3</sup>School of Geography, Earth and Environmental Sciences, University of Birmingham, Birmingham, UK

11 *Correspondence to:* Hendrik Fuchs (h.fuchs@fz-juelich.de) and Anna Novelli (a.novelli@fz-juelich.de)

## 12 **Abstract.**

13 Photochemical processes in ambient air were studied using the atmospheric simulation chamber SAPHIR  
14 at Forschungszentrum Jülich, Germany. Ambient air was continuously drawn into the chamber through a  
15 50 m high inlet line and passed through the chamber for one month in each season throughout 2019. The  
16 residence time of the air inside the chamber was about one hour. As the research center is surrounded by a  
17 mixed deciduous forest and is located close to the city Jülich, the sampled air was influenced by both  
18 anthropogenic and biogenic emissions. Measurements of hydroxyl (OH), hydroperoxyl (HO<sub>2</sub>) and organic  
19 peroxy (RO<sub>2</sub>) radicals were achieved by a laser-induced fluorescence instrument. The radical measurements  
20 together with measurements of OH reactivity ( $k_{OH}$ , the inverse of the OH lifetime) and a comprehensive set  
21 of trace gas concentrations and aerosol properties allowed for the investigation of the seasonal and diurnal  
22 variation of radical production and destruction pathways. In spring and summer periods, median OH  
23 concentrations reached  $6 \times 10^6 \text{ cm}^{-3}$  at noon, and median concentrations of both, HO<sub>2</sub> and RO<sub>2</sub> radicals,  
24 were  $3 \times 10^8 \text{ cm}^{-3}$ . The measured OH reactivity was between 4 and  $18 \text{ s}^{-1}$  in both seasons. The total reaction  
25 rate of peroxy radicals with NO was found to be consistent with production rates of odd oxygen ( $O_x =$   
26  $\text{NO}_2 + \text{O}_3$ ) determined from NO<sub>2</sub> and O<sub>3</sub> concentration measurements. The chemical budgets of radicals were  
27 analysed for the spring and summer seasons, when peroxy radical concentrations were above the detection  
28 limit. For most conditions, the concentrations of radicals were mainly sustained by the regeneration of OH  
29 via reactions of HO<sub>2</sub> and RO<sub>2</sub> radicals with nitric oxide (NO). The median diurnal profiles of the total  
30 radical production and destruction rates showed maxima between 3 to  $8 \text{ ppbv h}^{-1}$  for OH, HO<sub>2</sub> and RO<sub>2</sub>.  
31 Total RO<sub>x</sub> (OH, HO<sub>2</sub>, and RO<sub>2</sub>) initiation and termination rates were below  $3 \text{ ppbv h}^{-1}$ . The highest OH  
32 radical turnover rate of  $13 \text{ ppbv h}^{-1}$  was observed during a high-temperature (max 40°C) period in August.  
33 In this period, the highest HO<sub>2</sub>, RO<sub>2</sub> and RO<sub>x</sub> turnover rates were around 11, 10 and  $4 \text{ ppbv h}^{-1}$ , respectively.  
34 When NO mixing ratios were between 1 ppbv to 3 ppbv, OH and HO<sub>2</sub> production and destruction rates  
35 were balanced, but unexplained RO<sub>2</sub> and RO<sub>x</sub> production reactions with median rates of  $2 \text{ ppbv h}^{-1}$  and  $0.4$   
36  $\text{ppbv h}^{-1}$ , respectively, were required to balance their destruction. For NO mixing ratios above 3 ppbv, the  
37 peroxy radical reaction rates with NO were highly uncertain due to the low peroxy radical concentrations  
38 close to the limit of NO interferences in the HO<sub>2</sub> and RO<sub>2</sub> measurements. For NO mixing ratios below 1  
39 ppbv, a missing OH source with a rate of up to  $3.0 \text{ ppbv h}^{-1}$  was found. This missing OH source consists



40 likely of a combination of a missing primary radical source ( $0.5 \sim 1.4 \text{ ppbv h}^{-1}$ ) and a missing inter-radical  
41  $\text{HO}_2$  to OH conversion reaction with a rate of up to  $2.5 \text{ ppbv h}^{-1}$ . The dataset collected in this campaign  
42 allowed to analyze the potential impact of OH regeneration from  $\text{RO}_2$  isomerization reactions from isoprene,  
43  $\text{HO}_2$  uptake on aerosol, and  $\text{RO}_2$  production from chlorine chemistry on radical production and destruction  
44 rates. These processes were negligible for the chemical conditions encountered in this study.

## 45 1 Introduction

46 The hydroxyl (OH) radical is the dominant daytime atmospheric oxidant. It reacts with most trace gases in  
47 the troposphere and thereby controls the rate of their removal and chemical transformation. In the lower  
48 troposphere, OH is primarily produced by solar photolysis of ozone ( $\text{O}_3$ ) and nitrous acid (HONO). The  
49 reaction of OH with trace gases leads to the formation of hydroperoxy ( $\text{HO}_2$ ) or organic peroxy ( $\text{RO}_2$ , with  
50 R = organic group) radicals, which undergo further radical reactions. Generally, these reactions are cyclic  
51 chain reactions, in which OH,  $\text{HO}_2$ , and  $\text{RO}_2$  are converted into each other, while at the same time emitted  
52 pollutants are oxidized and converted into secondary pollutants such ozone and oxygenated volatile organic  
53 compounds (OVOCs). Because the conversion of radicals occurs on a time scale of seconds to minutes,  
54 they are often referred to as the  $\text{RO}_x$  family ( $\text{OH} + \text{HO}_2 + \text{RO}_2$ ). The most important radical reactions in  
55 the lower are summarized in Table 1. Understanding the radical chemistry is the basis for reliable  
56 predictions of the atmospheric lifetime and chemical transformation of air pollutants and climate-relevant  
57 gases by atmospheric chemistry models (Stone et al., 2012).

58 The level of agreement between simulated and observed radical concentrations in various environments  
59 shows the degree of understanding of the underlying radical chemical mechanism. Even though good  
60 agreement is found in some cases (Tan et al., 2001; Konrad et al., 2003; Mihelcic et al., 2003; Lelieveld et  
61 al., 2008; Kubistin et al., 2010; Whalley et al., 2011), there are significant unexplained discrepancies  
62 between modelled and measured OH in forested regions (Wolfe et al., 2011; Kim et al., 2013; Hens et al.,  
63 2014; Wolfe et al., 2014; Griffith et al., 2016) and of  $\text{HO}_2$  and  $\text{RO}_2$  in polluted areas (Ren et al., 2003; Ren  
64 et al., 2006; Kanaya et al., 2007; Dusanter et al., 2009; Chen et al., 2010; Ren et al., 2013; Brune et al.,  
65 2016; Tan et al., 2018; Slater et al., 2020; Whalley et al., 2021), while different results are found depending  
66 on the abundance of nitric oxide (NO) in rural environments (Hofzumahaus et al., 2009; Lou et al., 2010;  
67 Elshorbany et al., 2012; Kanaya et al., 2012; Tan et al., 2017).

68 A chemical budget analysis using measured OH,  $\text{HO}_2$  and  $\text{RO}_2$  radical concentrations can help assessing  
69 the strength of different radical production and loss paths. This allows to identify possible missing chemical  
70 processes by comparing the total production and destruction rates for the different radicals as concentrations  
71 are expected to be in steady-state due to their short chemical lifetime. A large number of measurements  
72 needs to be available (e.g., OH reactivity, OH, peroxy radicals), therefore, there have been only few studies  
73 focusing on the analysis of the chemical budget for OH radicals so far (Handisides et al., 2003;  
74 Hofzumahaus et al., 2009; Brune et al., 2016; Whalley et al., 2018; Tan et al., 2019; Whalley et al., 2021).

75 Results from field campaigns in China showed a larger OH radical destruction rate compared to its  
76 production rate in the afternoon, which points to an unaccounted OH radical source. Discrepancies were  
77 highest, when NO mixing ratios were lower than 2 ppbv (Hofzumahaus et al., 2009; Tan et al., 2019;  
78 Whalley et al., 2021). On the other hand, studies in urban areas in California (Brune et al., 2016) and in  
79 London (Whalley et al., 2018) as well as in a rural area in Hohenpeissenberg (Handisides et al., 2003)



80 showed no significant gap between the OH production and destruction rates. Recently, radical  
81 measurements including RO<sub>2</sub> enabled the investigation of HO<sub>2</sub>, RO<sub>2</sub>, and RO<sub>x</sub> production and destruction  
82 rates in field campaigns in China (Tan et al., 2019; Whalley et al., 2021). Tan et al. (2019) showed that a  
83 RO<sub>2</sub> loss process was required in a campaign in Wangdu in summer, while HO<sub>2</sub> production and destruction  
84 rates were balanced. This suggests a missing conversion of RO<sub>2</sub> to OH in addition to the reaction of peroxy  
85 radicals with NO. Furthermore, Whalley et al. (2021) found large imbalances between peroxy radical  
86 production and destruction rates in Beijing indicating a substantially slower propagation of RO<sub>2</sub> to HO<sub>2</sub>  
87 radicals than anticipated.

88 In this study, OH, HO<sub>2</sub>, and RO<sub>2</sub> radical concentrations as well as OH reactivity, the inverse of the OH  
89 radical lifetime, were measured in the atmospheric simulation chamber SAPHIR on campus of  
90 Forschungszentrum Jülich (FZJ), Germany, in the Jülich Atmospheric Chemistry Project Campaign  
91 (JULIAC). Ambient air was sampled from 50 m height into the SAPHIR chamber. From this data set, a  
92 chemical budget analysis of OH, HO<sub>2</sub>, RO<sub>2</sub> radicals, and their sum (RO<sub>x</sub>) was done using measured  
93 concentrations allowing to investigate, if all radical production and destruction processes were accounted  
94 for during spring and summer.

95



96 **Table 1.** Chemical reactions and rate constants used for the analysis of the chemical budgets of radicals.  
 97 Values of reaction rate constants are given for standard conditions (298 K, 1 atm). Actual numbers are

| Reaction                                 | $k(298\text{ K, 1 atm}) / \text{cm}^3\text{ s}^{-1}$  | $k_{\text{ERR}}^a$            | Reference                       |
|--|---|-------------------------------|---------------------------------|
| <b>Radical initiation reactions</b>      |   |                               |                                 |
| R1                                       | $\text{HONO} + \text{h}\nu \rightarrow \text{OH} + \text{NO}$                                     | $j_{\text{HONO}}^b$           |                                 |
| R2                                       | $\text{O}_3 + \text{h}\nu \rightarrow \text{O}^1\text{D} + \text{O}_2$                            | $j_{\text{O}^1\text{D}}^b$    |                                 |
| R2a                                      | $\text{O}^1\text{D} + \text{H}_2\text{O} \rightarrow 2\text{OH}$                                  | $2.1 \times 10^{-10}$         | $\pm 13\%$ IUPAC                |
| R2b                                      | $\text{O}^1\text{D} + \text{M} \rightarrow \text{O}^3\text{P} + \text{M}$                         | $3.3 \times 10^{-11}$         | $\pm 10\%$ IUPAC and JPL        |
| R3                                       | $\text{HCHO} + \text{h}\nu \rightarrow 2\text{HO}_2 + \text{CO}$                                  | $j_{\text{HCHO}}^b$           |                                 |
| R4                                       | $\text{CH}_3\text{CHO} + \text{h}\nu \rightarrow \text{CH}_3\text{O}_2 + \text{HO}_2 + \text{CO}$ | $j_{\text{CH}_3\text{CHO}}^b$ |                                 |
| R5                                       | $\text{alkenes} + \text{O}_3 \rightarrow \text{OH, HO}_2, \text{RO}_2 + \text{products}$          |                               |                                 |
| R5a                                      | $\text{propene} + \text{O}_3 \rightarrow \text{products}^c$                                       | $1.0 \times 10^{-17}$         | $\pm 20\%$ IUPAC                |
| R5b                                      | $\text{cis-but-2-ene} + \text{O}_3 \rightarrow \text{product}^d$                                  | $1.3 \times 10^{-16}$         | $\pm 12\%$ IUPAC                |
| R5c                                      | $1\text{-pentene} + \text{O}_3 \rightarrow \text{products}^e$                                     | $1.0 \times 10^{-17}$         | $\pm 20\%$ MCMv3.3.1            |
| R5d                                      | $2\text{-hexene} + \text{O}_3 \rightarrow \text{products}^f$                                      | $1.1 \times 10^{-17}$         | $\pm 20\%$ MCMv3.3.1            |
| R5e                                      | $\text{isoprene} + \text{O}_3 \rightarrow \text{products}^g$                                      | $1.3 \times 10^{-17}$         | $\pm 10\%$ MCMv3.3.1            |
| R5f                                      | $\alpha\text{-pinene} + \text{O}_3 \rightarrow \text{products}^h$                                 | $9.6 \times 10^{-17}$         | $\pm 20\%$ IUPAC                |
| <b>Radical interconversion reactions</b> |   |                               |                                 |
| R6                                       | $\text{HCHO} + \text{OH} + \text{O}_2 \rightarrow \text{CO} + \text{H}_2\text{O} + \text{HO}_2$   | $8.5 \times 10^{-12}$         | $\pm 10\%$ IUPAC                |
| R7                                       | $\text{CO} + \text{OH} + \text{O}_2 \rightarrow \text{CO}_2 + \text{HO}_2$                        | $2.3 \times 10^{-13}$         | $\pm 6\%$ IUPAC                 |
| R8                                       | $\text{VOCs} + \text{OH} + \text{O}_2 \rightarrow \text{RO}_2 + \text{H}_2\text{O}$               | $j$                           |                                 |
| R9                                       | $\text{RO}_2 + \text{NO} \rightarrow \text{products} + \text{HO}_2 + \text{NO}_2$                 | $8.6 \times 10^{-12}$         | $\pm 30\%$ Jenkin et al. (2019) |
| R10                                      | $\text{HO}_2 + \text{NO} \rightarrow \text{OH} + \text{NO}_2$                                     | $8.5 \times 10^{-12}$         | $\pm 13\%$ IUPAC                |
| R11                                      | $\text{HO}_2 + \text{O}_3 \rightarrow \text{OH} + 2\text{O}_2$                                    | $2.0 \times 10^{-15}$         | $\pm 29\%$ IUPAC                |
| <b>Radical termination reactions</b>     |   |                               |                                 |
| R12                                      | $\text{NO}_2 + \text{OH} \rightarrow \text{HNO}_3$  | $1.0 \times 10^{-11}$         | $\pm 30\%$ IUPAC                |
| R13                                      | $\text{NO} + \text{OH} \rightarrow \text{HONO}$   | $9.7 \times 10^{-12}$         | $\pm 13\%$ IUPAC                |
| R14                                      | $\text{RO}_2 + \text{NO} \rightarrow \text{RONO}_2$   | $4.6 \times 10^{-13}$         | $\pm 30\%$ Jenkin et al. (2019) |
| R15                                      | $\text{RO}_2 + \text{RO}_2 \rightarrow \text{products}$   | $3.5 \times 10^{-13}$         | $\pm 50\%$ Jenkin et al. (2019) |
| R16                                      | $\text{RO}_2 + \text{HO}_2 \rightarrow \text{ROOH} + \text{O}_2$                                  | $2.3 \times 10^{-11}$         | $\pm 50\%$ Jenkin et al. (2019) |
| R17                                      | $\text{HO}_2 + \text{HO}_2 \rightarrow \text{H}_2\text{O}_2 + \text{O}_2$                         | $4.5 \times 10^{-12i}$        | $\pm 20\%$ IUPAC                |
| <b>Isoprene reactions</b>                |   |                               |                                 |
| R18                                      | $\text{isoprene} + \text{OH} \rightarrow \text{products}$   | $1.0 \times 10^{-10}$         | $\pm 8\%$ IUPAC                 |
| R19                                      | $\text{isoprene} - \text{RO}_2 (1,6\text{-H shift}) \rightarrow \text{products} + \text{OH}$      | $0.01 - 0.06\text{ s}^{-1}$   | Peeters et al. (2014)           |
| <b>Cl reactions</b>                      |   |                               |                                 |
| R20                                      | $\text{ClNO}_2 + \text{h}\nu \rightarrow \text{Cl} + \text{NO}_2$                                 | $j_{\text{ClNO}_2}^b$         |                                 |
| R21                                      | $\text{Cl}_2 + \text{h}\nu \rightarrow 2\text{Cl}$  | $j_{\text{Cl}_2}^b$           |                                 |
| R22                                      | $\text{VOCs} + \text{Cl} \rightarrow \text{RO}_2 + \text{HCl}$                                    | $j$                           |                                 |

98 used for the calculations.

- 99 <sup>a</sup> 1 $\sigma$  uncertainty  
 100 <sup>b</sup> Measured photolysis frequencies  
 101 <sup>c</sup> Yield for OH: 0.36, HO<sub>2</sub>: 0.10, RO<sub>2</sub>: 0.42 from Novelli et al. (2021)  
 102 <sup>d</sup> Yield for OH: 0.36, HO<sub>2</sub>: 0.15, RO<sub>2</sub>: 0.51 from Novelli et al. (2021)  
 103 <sup>e</sup> Yield for OH: 0.32, HO<sub>2</sub>: 0.09, RO<sub>2</sub>: 0.37 from Novelli et al. (2021)  
 104 <sup>f</sup> Yield for OH: 0.48, HO<sub>2</sub>: 0.11, RO<sub>2</sub>: 0.59 from Novelli et al. (2021)  
 105 <sup>g</sup> Yield for OH: 0.26, HO<sub>2</sub>: 0.26 from Malkin et al. (2010)  
 106 <sup>h</sup> Yield for OH: 0.8 from Cox et al. (2020)  
 107 <sup>i</sup> at 1% water vapour mixing ratio  
 108 <sup>j</sup> Highly variable depending on the specific VOC.  
 109



## 110 2 Methodology

### 111 2.1 The JULIAC campaign

112 The Jülich Atmospheric Chemistry Project (JULIAC) campaign was conducted at Forschungszentrum  
 113 Jülich (FZJ, 50.9° N, 6.4° E), Germany. The project consisted of four one-month long intensive campaigns  
 114 studying atmospheric chemistry in ambient air in each season throughout 2019. The location is surrounded  
 115 by a deciduous forest and is located in a rural environment near a town, Jülich (33,000 inhabitants), 25 km  
 116 northeast, 40 km west, and 43 km southwest from three large cities, Aachen, Cologne and Düsseldorf,  
 117 respectively. Therefore, ambient air is influenced by both biogenic and anthropogenic emission sources.

118 The investigation of the photochemistry was performed in the SAPHIR chamber, which was equipped with  
 119 a large set of instruments measuring radicals, trace gases and aerosol (Table 2). The SAPHIR chamber has  
 120 a cylindrical shape and is made of a double-wall Teflon (FEP) film. A slight overpressure (35 Pa) is

**Table 2.** Specification of instruments used in the JULIAC campaign for the analysis in this work.

| Species  | Measurement technique         | Time resolution (1σ) | Limit of detection  | 1σ accuracy          |
|--|-------------------------------|----------------------|---|----------------------|
| OH   | LIF                           | 270 s                | $0.7 \times 10^6 \text{ cm}^{-3}$   | 18%                  |
| OH   | DOAS                          | 134 s                | $0.8 \times 10^6 \text{ cm}^{-3}$   | 6.5%                 |
| HO <sub>2</sub>  | LIF                           | 47 s                 | $1 \times 10^7 \text{ cm}^{-3}$   | 18%                  |
| RO <sub>2</sub>  | LIF                           | 47s                  | $2 \times 10^7 \text{ cm}^{-3}$   | 18%                  |
| OH reactivity ( $k_{\text{OH}}$ )                        | LP-LIF                        | 180 s                | $0.2 \text{ s}^{-1}$  | 10%                  |
| Photolysis frequencies                                   | Spectroradiometer             | 60 s                 |   | 18%                  |
| O <sub>3</sub>   | UV photometry                 | 60 s                 | 0.5 ppbv  | 2%                   |
| NO <sub>x</sub>  | Chemiluminescence             | 60 s                 | NO: 20 pptv   | NO: 5 %              |
| (NO+NO <sub>2</sub> )                                    |                               |                      | NO <sub>2</sub> : 30 pptv   | NO <sub>2</sub> : 7% |
| CO, CO <sub>2</sub> , CH <sub>4</sub> , H <sub>2</sub> O | Cavity ring-down spectroscopy | 60 s                 | CO and CH <sub>4</sub> : 1 ppbv<br>CO <sub>2</sub> : 25 ppbv<br>H <sub>2</sub> O: 0.1 % | 5%                   |
| HONO   | LOPAP                         | 180 s                | 5 pptv  | 10%                  |
| HCHO   | Cavity ring-down spectroscopy | 300 s                | 0.1 ppbv  | 10%                  |
| ClNO <sub>2</sub>  | I-CIMS                        | 60 s                 | 2.8 pptv  | 8.5%                 |
| VOCs   | PTR-TOF-MS                    | 30 s                 | 15 pptv   | 14%                  |
|  | VOCUS PTR-TOF-MS              | 30 s                 |   |                      |
| Aerosol surface area                                     | SMPS                          | 7 min                | 10nm – 1μm  | N/A                  |



121 maintained in the chamber and the space between the two films is permanently flushed with pure nitrogen  
122 (Linde, purity: > 99:99990 %) to prevent outside air penetrating the inner chamber. The chamber is  
123 equipped with a shutter system allowing the air to be either shielded from or exposed to solar radiation.

124 In the JULIAC campaign, ambient air was sampled at a high flow rate of  $660 \text{ m}^3 \text{ h}^{-1}$  from 50 m high inlet  
125 line (104 mm inner diameter, SilcoNert® coated stainless steel) by means of an oil-free turbo blower  
126 (Aerzener Maschinenfabrik, AERZEN Turbo G3 Typ: TB 50-0.6 S). Large particles ( $>10 \mu\text{m}$  diameter)  
127 were removed by a SilcoNert® coated cyclone (LTG, ZSB-6). The temperatures in the inlet line and cyclone  
128 were controlled to be slightly higher than ambient temperature (+1 to 2 °C) to avoid water vapor  
129 condensation in the inlet system. A 3/2-way valve directed part of the air (flow rate of  $250 \text{ m}^3 \text{ h}^{-1}$ ) into the  
130 chamber. Two fans inside the chamber ensured fast mixing on a time scale of a few minutes. As a result,  
131 the chamber behaved as a continuously stirred photochemical flow reactor with a mean residence time of  
132 air of 1.1 h. During the transition time of 3.5 s from the tip of the inlet to the SAPHIR chamber, atmospheric  
133  $\text{RO}_x$  radicals are lost on walls, but concentrations are rapidly re-established in the sampled ambient air  
134 inside the sunlit chamber.

135 The use of the chamber as a flow reactor has advantages compared to field measurements in the open air.  
136 Perturbations of the studied chemistry due to local emissions of VOCs or  $\text{NO}_x$  can be avoided. Transient  
137 fluctuations of reactants in the sampled air, for example due to spikes of NO from passing cars, are  
138 smoothed out in the chamber. Due to the homogeneous mixing, instruments connected to the chamber  
139 measure the same air composition and segregation effects on reaction rates are insignificant.

140 The air composition could be influenced by the inlet line and chamber surfaces. As the whole inlet line is  
141 heated and chemically inert due to the SilcoNert® coating, no relevant wall loss or desorption of trace gases  
142 is expected from the inlet. This assumption was confirmed by comparing OH reactivity measured at several  
143 positions of the inlet line. No significant differences were found between measurements, if the air was either  
144 sampled upstream of the cyclone or downstream of the blower. Wall losses of trace gases (VOCs,  $\text{NO}_x$ ,  $\text{O}_3$ )  
145 inside the SAPHIR chamber were found to be negligible in previous experiments (e.g., Kaminski et al.,  
146 2017, Rolletter et al., 2020).

147 Nitrous acid (HONO) and formaldehyde (HCHO) are known to be emitted from the chamber film when it  
148 is exposed to solar radiation (Rohrer et al. (2005)). These emissions significantly increase the  
149 concentrations of HONO and HCHO in the chamber. Due to the transmission through the Teflon film and  
150 shading from construction elements of the chamber, the absolute actinic flux density is reduced by 20 to  
151 40 % compared to outside the chamber. It is worth noting, however, that the relative spectral distribution  
152 of the solar radiation is not changed by the transmission through the chamber film (Bohn and Zilken, 2005).

153 The floor underneath the chamber is heated by the solar radiation. Although it is not in direct contact to the  
154 foil, the air temperature in the chamber was on average  $0.7^\circ\text{C}$  higher during winter and autumn and  $1.9^\circ\text{C}$   
155 higher during spring and summer than the temperature outside of the chamber at daytime. Since  
156 photochemistry was studied in the chamber, all data of chemical and physical conditions shown in this work  
157 refer to conditions inside the chamber.

158 The measurements in the campaign were at least once a week interrupted for calibration and maintenance  
159 of instruments. Some days were also excluded from the analysis in this work because the chamber shutter  
160 system was kept closed to protect the chamber film during bad weather from strong wind gusts and/or



161 precipitation. Reference experiments with clean synthetic air were performed to investigate possible  
162 changes in the strength of chamber emissions and to check for instrumental backgrounds.

163

## 164 **2.2 Instrumentation**

### 165 **2.2.1 OH, HO<sub>2</sub> and RO<sub>2</sub> radical and OH reactivity ( $k_{OH}$ ) measurements**

166

167 OH, HO<sub>2</sub>, and RO<sub>2</sub> radicals were measured by the FZJ – LIF which included a newly developed chemical  
168 modulation reactor (CMR) for interference-corrected measurements of OH radicals (Cho et al., 2021). The  
169 signals of the instrument were calibrated against well-defined radical concentrations that were produced  
170 from water photolysis in synthetic air at a wavelength of 185nm using radiation of a mercury lamp. A  
171 detailed description of the LIF instrument and its calibration can be found in previous publications (Holland  
172 et al., 2003; Fuchs et al., 2008; Fuchs et al., 2011; Fuchs et al., 2012).

173 Shortly, the OH radical is sampled through a nozzle with a 0.4 mm diameter pinhole and is excited by a  
174 pulsed laser at a wavelength of 308 nm in a low-pressure (4 hPa) fluorescence cell. The emitted resonant  
175 fluorescence is detected with a time delay by a time-gated micro-channel plate detector (MCP). In the  
176 JULIAC campaign, a chemical modulation reactor (CMR) was implemented on top of the OH cell to  
177 quantify potential interferences. This is achieved by periodically removing ambient OH by an OH scavenger  
178 that is injected in the reactor (propane, Air Liquide, purity>99.95%, (5.0±0.1) % mixture in nitrogen) before  
179 the air enters the fluorescence cell. During the campaign, the observed interference could be fully explained  
180 by the well-characterized interference from the photolysis of ozone in humid air inside the detection cell.  
181 No evidence for an unexplained interference was found (Cho et al., 2021). The limit of detection for OH  
182 was  $0.7 \times 10^6 \text{ cm}^{-3}$  and the accuracy was 18 % ( $1\sigma$ ).

183 OH radical concentrations were also measured by differential optical absorption spectroscopy (DOAS)  
184 using a multiple folded light path for absorption inside along the chamber. The DOAS technique is a  
185 calibration-free technique (Hausmann et al., 1997; Schlosser et al., 2007; Schlosser et al., 2009). The limit  
186 of detection was  $0.8 \times 10^6 \text{ cm}^{-3}$  and the  $1\sigma$ -accuracy was 6.5 %. Due to a technical laser problem, the  
187 DOAS instrument was not available in spring.

188 HO<sub>2</sub> radicals were detected by the LIF instrument in a separate detection cell, where HO<sub>2</sub> is chemically  
189 converted to OH radicals in the reaction with NO (Air Liquide, 1% NO in N<sub>2</sub>, purity > 99.5 %) that is  
190 injected in the fluorescence cell (Fuchs et al., 2011). During the JULIAC campaign, two different  
191 concentrations ( $2.5 \times 10^{13} \text{ cm}^{-3}$  and  $1.0 \times 10^{14} \text{ cm}^{-3}$ ) of NO in the fluorescence cell were used to  
192 observe possible interference from specific RO<sub>2</sub> radicals as highlighted by Fuchs et al. (2011). No difference  
193 between HO<sub>2</sub> measurements at high and low NO concentrations was found suggesting that there was no  
194 significant interference from RO<sub>2</sub>.

195 In addition, the sum of OH, HO<sub>2</sub>, and RO<sub>2</sub> (RO<sub>X</sub>) was measured by the RO<sub>X</sub>-LIF system. Air is sampled  
196 into a chemical converter (pressure of ~ 25 hPa), where a mixture of NO (Air Liquide, 500 ppmv NO in N<sub>2</sub>,  
197 purity > 99.5%) and CO (Air Liquide, 10% CO in N<sub>2</sub>, purity > 99.997%) is injected. The NO converts RO<sub>2</sub>  
198 radicals to HO<sub>2</sub> radicals and CO converts OH radicals formed from the reaction of HO<sub>2</sub> radicals with NO  
199 back to HO<sub>2</sub>. Therefore, an equilibrium between OH and HO<sub>2</sub> is established. Concentrations are chosen, so



200 that the equilibrium is on the side of HO<sub>2</sub>. In a low-pressure cell downstream of the converter HO<sub>2</sub> radicals  
201 are converted to OH radicals by injecting excess NO (Air Liquide, pure NO, purity>99.5%) (Fuchs et al.,  
202 2008) that shifts the equilibrium between OH and HO<sub>2</sub> to OH. The RO<sub>2</sub> concentration is obtained from the  
203 difference between the sum measurement of RO<sub>x</sub> and measurements of OH and HO<sub>2</sub> concentrations in the  
204 other two detection cells. The RO<sub>2</sub> detection sensitivity was calibrated for methyl peroxy radicals (CH<sub>3</sub>O<sub>2</sub>)  
205 which are produced from the reaction of OH with methane (CH<sub>4</sub>) in the calibration system. The resulting  
206 calibration is also applicable to the majority of other atmospheric alkyl peroxy radicals (Fuchs et al., 2008;  
207 Fuchs et al., 2011).

208 The signals in the HO<sub>2</sub> and RO<sub>2</sub> detection systems contain a background signal observed when NO is  
209 injected into the detection cells, even if no radicals are present in the air sampled. The background signal  
210 can be characterized when the inlet of the detection system is overflowed with synthetic air, which is part of  
211 the calibration procedures. During JULIAC the background varied from calibration to calibration and was  
212 often larger than the smallest signals measured in ambient air from the chamber (Table S1). The highest  
213 background signals obtained from calibrations is therefore regarded as an upper limit and the variability is  
214 considered as an additional uncertainty in the measured HO<sub>2</sub> and RO<sub>2</sub> concentrations. HO<sub>2</sub> and RO<sub>2</sub>  
215 background signals, which are subtracted in the evaluation of HO<sub>2</sub> and RO<sub>2</sub> measurements, were taken from  
216 reference experiments in the dark clean chamber, when no HO<sub>2</sub> or RO<sub>2</sub> radicals are expected. The subtracted  
217 signals for each period are available in Table S1 and in most cases were equivalent to concentrations lower  
218 than  $1 \times 10^7 \text{ cm}^{-3}$  for both HO<sub>2</sub> and RO<sub>2</sub> measurements.

219 The total OH reactivity ( $k_{\text{OH}}$ ), the inverse of the chemical lifetime of OH radicals, was measured in ambient  
220 air by a laser-flash photolysis LIF instrument (Lou et al., 2010; Fuchs et al., 2017). A high concentration of  
221 OH radicals is produced by flash photolysis (266 nm, 1 Hz repetition rate) of ozone in humid air (Reaction  
222 R2) in a flow tube that is on top of an OH fluorescence cell. The pseudo first-order decay of OH in the  
223 chemical reactions with atmospheric reactants is measured, giving directly the OH reactivity.

## 224 2.2.2 Other trace gases, aerosol properties and photolysis frequencies measurements

225 A comprehensive set of instruments operated during the JULIAC campaign (Table 2) analyzed the air  
226 composition inside the chamber. Photolysis frequencies inside the chamber were derived from the solar  
227 actinic flux densities measured by a spectroradiometer mounted on the roof of the nearby institute building  
228 (Bohn et al., 2005; Bohn and Zilken, 2005). Formaldehyde (HCHO) was detected by cavity ring-down  
229 spectroscopy (Picarro, G2307, Glowania et al. (2021)). NO and NO<sub>2</sub> were measured by chemiluminescence  
230 (Eco Physics, TR780). In addition, HONO was measured by long-path absorption photometry (LOPAP,  
231 Kleffmann et al. (2006); Häseler et al. (2009)), CO, CO<sub>2</sub>, CH<sub>4</sub>, and H<sub>2</sub>O by cavity ring-down spectroscopy  
232 (Picarro, G2401), and O<sub>3</sub> by UV absorption (Ansyco-41M and Thermo scientific-49I). Volatile organic  
233 compounds (VOCs) were detected by a proton-transfer-reaction time-of-flight mass spectrometer (PTR-  
234 TOF-MS, Ionicon) (Jordan et al., 2009) and a VOCUS PTR-TOF-MS instrument (Aerodyne). The VOCs  
235 included in this study are listed in Table S2 and include isoprene and some carbonyl compounds. Total  
236 aerosol surface area was determined from measurements by a scanning mobility particle sizer (SMPS). In  
237 the summer and autumn periods, nitryl chloride (ClNO<sub>2</sub>) was detected by a chemical ionization mass  
238 spectrometer using iodine as reagent ion (I-CIMS) (Sommariva et al., 2018; Tan et al., 2022).

239 In addition to measurements in the chamber, concentrations of O<sub>3</sub> and NO<sub>x</sub> were also measured in the inlet  
240 system before the air flowed into the SAPHIR chamber. For these measurements, a combined system (Eco





241 Physics, CraNO<sub>x</sub>) consisting of an ozone photometer and a chemiluminescence instrument for NO<sub>x</sub> was  
242 deployed. Measurements were used to determine the photochemical ozone production in the JULIAC  
243 campaign. Further description of the measurement set-up and concept of the evaluation will be discussed  
244 in details in a further publication.

245

## 246 2.3 Chemical budget calculations

247 A chemical budget analysis, similar as in Tan et al. (2019) and Whalley et al. (2021), was applied for OH,  
248 HO<sub>2</sub>, RO<sub>2</sub> and the sum of all three radicals (RO<sub>x</sub>) to the data set from the JULIAC campaign. All reactions  
249 typically considered to be relevant for the generation and destruction of these radicals are considered (Table  
250 1). Rate constants and their uncertainties were mainly taken from IUPAC recommendations (Atkinson et  
251 al., 2004; Atkinson et al., 2006; Cox et al., 2020) or more recent studies. If not otherwise specified, radical  
252 production and destruction rates are calculated from measured concentrations of reactants.

### 253 2.3.1 Chemical budget of OH radicals

254 The production rate of OH radicals includes primary production reactions (Reaction R1, R2 and R5) and  
255 radical interconversion reactions (Reaction R10 and R11):

$$256 \quad P_{\text{OH}} = j_{\text{HONO}}[\text{HONO}] + \varphi_{\text{OH}}j_{\text{O}^1\text{D}}[\text{O}_3] + k_{10}[\text{NO}][\text{HO}_2] + k_{11}[\text{O}_3][\text{HO}_2] \\ 257 \quad + \sum\{\varphi_{\text{OH}}^i k_5^i [\text{alkene}]^i [\text{O}_3]\} + P_{\text{OH,Isop.}} \quad (1)$$

258 Here,  $\varphi_{\text{OH}}$  is the effective OH yield of the ozone photolysis including the reaction of excited oxygen atoms  
259 O(<sup>1</sup>D) with H<sub>2</sub>O producing two OH radicals.  $\varphi_{\text{OH}}^i$  is the OH yield of the ozonolysis reaction of alkenes,  
260 and  $k_5^i$  represents the rate constants of the corresponding reactions.

261  $P_{\text{OH,Isop}}$  is the effective production of OH radicals from unimolecular reactions (1,6-hydrogen shift reactions)  
262 of isoprene-RO<sub>2</sub> radicals (Z- $\delta$ -RO<sub>2</sub>-I and II, Peeters et al. (2014)) and the subsequent chemistry of products..  
263 As there was no measurement of speciated RO<sub>2</sub> radicals, isoprene-RO<sub>2</sub> radical concentrations are estimated  
264 from steady-state conditions considering their production from the reaction of isoprene with OH and their  
265 destruction in bimolecular reaction (reaction rate  $k_{\text{bi}}$ ) and unimolecular reactions (bulk reaction rate  $k_{\text{bulk 1,6-H}}$   
266  $_H$  as defined in Peeters et al. (2014)):

$$267 \quad [\text{RO}_2(\text{isop.})]_{\text{SS}} = \frac{k_{18}[\text{Isoprene}][\text{OH}]}{k_{\text{bi}} + k_{\text{bulk 1,6-H}}} \quad (2)$$

$$268 \quad k_{\text{bi}} = (k_9 + k_{14})[\text{NO}] + k_{15}[\text{RO}_2] + k_{16}[\text{HO}_2] \quad (2a)$$

269 Bimolecular loss reactions include reactions with NO (Reaction R9 and R14), RO<sub>2</sub> (Reaction R15) and HO<sub>2</sub>  
270 (Reaction R16). The OH production from isoprene-RO<sub>2</sub> isomerization reactions is simplified in the  
271 calculation of the total OH production in this work by assuming that each isomerization reaction produces  
272 rapidly one OH radical from the subsequent reactions of products such as photolysis of hydroxy-peroxy  
273 aldehyde (HPALD). In this case, the radical production rate is equal to the loss rate of the isoprene-RO<sub>2</sub>  
274 due to isomerization reactions ( $D_{\text{Z-}\delta\text{-R}_2, \text{Isop.}}$ ):



275  $P_{OH,Isop.} = D_{Z-\delta-RO_2, Isop.} = k_{bulk\ 1,6-H} [RO_2(isop.)]_{ss}$  (4)

276 The total loss rate of OH radicals for the chemical budget analysis is determined by the product of the total  
277 OH reactivity ( $k_{OH}$ ) and the OH radical concentration:

278  $D_{OH} = k_{OH}[OH]$  (5)

### 279 2.3.2 Chemical budget of HO<sub>2</sub> radicals

280 The production rate of HO<sub>2</sub> radicals includes primary reactions (Reaction R3, R4 and R5) and  
281 interconversion reactions (Reaction R6, R7 and R9, Table 1):

283 
$$P_{HO_2} = 2 j_{HCHO}[HCHO] + k_6[HCHO][OH] + k_7[CO][OH] + k_9[NO][RO_2]$$
  
282 
$$+ \Sigma\{\varphi_{HO_2}^i k_5^i [alkene]^i [O_3]\}$$
 (6)

284 Here, the photolysis frequency of HCHO ( $j_{HCHO}$ ) include only paths generating radicals.  $\varphi_{HO_2}^i$  is the HO<sub>2</sub>  
285 yield from the ozonolysis of alkenes. The reactions of OH with H<sub>2</sub> and O<sub>3</sub> are not considered due to their  
286 negligible contributions to the HO<sub>2</sub> production.

287 The loss rate of HO<sub>2</sub> is determined by the reactions with NO (Reaction R10), O<sub>3</sub> (Reaction R11), RO<sub>2</sub>  
288 (Reaction R16) and HO<sub>2</sub> (Reaction R17):

289  $D_{HO_2} = (k_{10}[NO] + k_{11}[O_3] + k_{16}[RO_2] + 2k_{17}[HO_2])[HO_2]$  (7)

290 The reaction of HO<sub>2</sub> radicals with NO<sub>2</sub> is not included as the thermal decomposition of peroxyntic acid  
291 (HO<sub>2</sub>NO<sub>2</sub>) forming back HO<sub>2</sub> radicals and NO<sub>2</sub> is instantaneous for the temperatures experienced during  
292 the JULIAC campaign.

293 In a sensitivity calculation (Section 4.2.3), potential loss of HO<sub>2</sub> due to heterogeneous uptake on aerosol is  
294 investigated. The first order loss rate ( $k_{het.}$ ) can be described as:

295  $k_{het.} = \frac{\gamma_{eff.} v_{HO_2} [AS]}{4}$  (8)

296  $v_{HO_2}$  is the mean molecular velocity of HO<sub>2</sub> ( $4.44 \times 10^5$  cm s<sup>-1</sup> at 298 K), [AS] is the measured aerosol  
297 surface area concentration, and  $\gamma_{eff.}$  is the effective uptake coefficient.

### 298 2.3.3 Chemical budget of RO<sub>2</sub> radicals

299 Primary sources of RO<sub>2</sub> radicals include all oxidation reactions of VOCs with OH, Cl, NO<sub>3</sub> radicals and O<sub>3</sub>.  
300 As the number of measured VOC species in this study was limited (Table S2) and because it is generally  
301 difficult to capture the entire spectrum of atmospheric VOCs (Goldstein and Galbally, 2007; Lou et al.,  
302 2010), the measured total OH reactivity ( $k_{OH}$ ) can be used to calculate the RO<sub>2</sub> radicals production from the  
303 reactions of VOCs with OH. First, the contributions from CO, NO, NO<sub>2</sub>, HCHO and O<sub>3</sub> is removed from  
304 the measured OH reactivity as these species do not form RO<sub>2</sub> radicals in the reaction with OH. It is then  
305 assumed that the remaining fraction can be attributed to organic compounds (VOC reactivity ( $k_{VOC}$ ))  
306 including measured and unmeasured VOCs, which produce RO<sub>2</sub> radicals in their reaction with OH



307 In addition, RO<sub>2</sub> production from ozonolysis needs to be included. In this work, only the reactions of  
 308 measured organic compounds are considered. The contribution to the RO<sub>2</sub> production from the oxidation  
 309 of VOCs by the NO<sub>3</sub> radical was negligible during daytime due to the low VOC load (low OH reactivity),  
 310 so that NO<sub>3</sub> destruction by photolysis and reaction with NO dominated.

311 Reactions of chloride (Cl) also produce RO<sub>2</sub> radicals, but the concentration was not measured in the  
 312 JULIAC campaign. However, one of the most important precursor species, nitryl chloride (ClNO<sub>2</sub>), was  
 313 detected during the campaign (except in spring, Tan et al. (2022)). ClNO<sub>2</sub> can accumulate during nighttime,  
 314 but it is photolyzed after sunrise yielding NO<sub>2</sub> and Cl atoms (Reaction R20). Assuming as an upper limit  
 315 that each Cl atom reacts with a VOCs (Tanaka et al., 2003), the RO<sub>2</sub> production rate from Cl radicals can  
 316 be calculated as:

$$317 \quad P_{\text{RO}_2, \text{Cl}} = j_{\text{ClNO}_2} [\text{ClNO}_2] \quad (9)$$

318 The total RO<sub>2</sub> production rate is then calculated as:

$$319 \quad P_{\text{RO}_2} = k_{\text{VOC}} [\text{OH}] + \sum (\varphi_{\text{RO}_2}^i k_{\text{R5}}^i [\text{alkene}]^i [\text{O}_3]) + P_{\text{RO}_2, \text{Cl}} \quad (10)$$

320 Here,  $\varphi_{\text{RO}_2}^i$  is the RO<sub>2</sub> yield from the ozonolysis of alkenes species (Table 1).

321 With respect to the destruction rate of RO<sub>2</sub>, its reactions with NO, HO<sub>2</sub>, and other RO<sub>2</sub> and unimolecular  
 322 reactions of specific isoprene-RO<sub>2</sub> radicals (D<sub>Z-δ-R<sub>2</sub>, Isop.</sub>) (Eq. 4) are considered in this work:

$$323 \quad D_{\text{RO}_2} = ((k_9 + k_{14})[\text{NO}] + 2k_{15}[\text{RO}_2] + k_{16}[\text{HO}_2])[\text{RO}_2] + D_{\text{Z-}\delta\text{-R}_2, \text{ Isop.}} \quad (11)$$

### 324 2.3.4 Chemical budget of RO<sub>x</sub> radicals

325 In the chemical budget of the sum of OH, HO<sub>2</sub> and RO<sub>2</sub> (RO<sub>x</sub>), inter-radical conversion reactions cancel  
 326 out and only initiation and termination reactions are included. Therefore, the RO<sub>x</sub> radical budget analysis  
 327 allows to investigate if primary radical source reactions or termination processes are missing in the chemical  
 328 mechanism used (Table 1).

329 The production rate of the RO<sub>x</sub> radicals is given by the sum of rates from radical initiation reactions  
 330 (Reaction R1-R5, R20-R22, Table 1):

$$331 \quad P_{\text{RO}_x} = j_{\text{HONO}} [\text{HONO}] + \varphi_{\text{OH}} j_{\text{O}^1\text{D}} [\text{O}_3] + 2j_{\text{HCHO}} [\text{HCHO}] \\ 332 \quad + \sum ((\varphi_{\text{OH}}^i + \varphi_{\text{HO}_2}^i + \varphi_{\text{RO}_2}^i) k_5^i [\text{alkene}]^i [\text{O}_3]) + P_{\text{RO}_2, \text{Cl}} \quad (12)$$

333 Radicals can be additionally produced from the photolysis of other oxygenated organic compounds  
 334 (OVOCs, e.g., Reaction R4) not included in Eq. 12. Their potential impact is further discussed in Section  
 335 4.2.2.

336 The loss rate of the RO<sub>x</sub> radical is calculated by the sum of rates from radical termination reactions  
 337 (Reaction R12-R17):

$$338 \quad D_{\text{RO}_x} = (k_{13}[\text{NO}] + k_{12}[\text{NO}_2])[\text{OH}] + k_{14}[\text{NO}][\text{RO}_2] + 2k_{15}[\text{RO}_2]^2 + 2k_{16}[\text{HO}_2][\text{RO}_2] + 2k_{17}[\text{HO}_2]^2 \\ 339 \quad (13)$$



### 340 2.3.5 Uncertainties in the calculated production and destruction rates

341 The uncertainty of each production or loss rate is calculated by Gaussian summation of the  $1\sigma$  errors of the  
342 measured quantities (Table 2) and the uncertainties of the reaction rate constants (Table 1).

343 For reactions of  $\text{RO}_2$  with NO (Reaction R9, R14),  $\text{HO}_2$  (Reaction R16) and  $\text{RO}_2$  (Reaction R15), generic  
344 rate constants are used for the sum of  $\text{RO}_2$  radicals (Table 1, Jenkin et al. (2019)). Rate constants of the NO  
345 reaction with  $\text{RO}_2$  derived from hydrocarbons ( $<C_5$ ) and with oxygenated peroxy radicals range from  
346  $7.7 \times 10^{-12} \text{ cm}^3 \text{ s}^{-1}$  to  $1.1 \times 10^{-11} \text{ cm}^3 \text{ s}^{-1}$  (Jenkin et al., 2019). The  $1\sigma$ -uncertainty of the rate constants  
347 varies from 6 to 30 %. In the error calculations here, an upper limit value of 30 % is applied. However, for  
348 reactions of  $\text{RO}_2$  with  $\text{HO}_2$  and with  $\text{RO}_2$ , the range of rate constants varies by more than an order of  
349 magnitude. In the calculations, an uncertainty of 50% is used for the reaction rate constants of  $\text{RO}_2$  with  
350  $\text{HO}_2$  and with  $\text{RO}_2$ .

351 As there are no measurements of speciated  $\text{RO}_2$  radicals, a yield of 5% for the formation of organic nitrates  
352 is assumed for all  $\text{RO}_2$  but the yield can vary between 1% for methyl peroxy radicals ( $\text{CH}_3\text{O}_2$ ) and more  
353 than 20 % for  $\text{RO}_2$  from monoterpene species. This simplification can introduce systematic errors in the  
354 calculations (Section 4.2.1).

355

### 356 2.4 Odd oxygen production rate

357 In the troposphere, ozone is formed exclusively by the oxidation of NO to  $\text{NO}_2$  through reaction with  $\text{RO}_2$   
358 (Reaction R9) and  $\text{HO}_2$  (Reaction R10), followed by  $\text{NO}_2$  photolysis (Fishman and Carney, 1984; Sillman  
359 et al., 1990; Kleinman et al., 2002).

360 During the day, the photolysis of  $\text{NO}_2$  and the back reaction of NO with  $\text{O}_3$  form a rapid photochemical  
361 equilibrium between  $\text{O}_3$  and  $\text{NO}_2$ . The sum of  $\text{O}_3$  and  $\text{NO}_2$  is therefore defined as odd oxygen ( $\text{O}_x$ ) (Han et  
362 al., 2011; Goldberg et al., 2015). The relative composition of  $\text{O}_x$  depends on the  $\text{NO}_2$  photolysis frequency  
363 and the NO concentration. For the conditions of the spring and summer periods in the JULIAC campaign,  
364  $\text{O}_x$  consisted predominantly ( $> 85\%$ ) of  $\text{O}_3$ .

365 In this work, the net production rate of  $\text{O}_x$  ( $P_{\text{O}_x}$ ) was determined experimentally from the increase of  $\text{O}_x$  in  
366 the sunlit SAPHIR chamber. Furthermore, measurements of radicals and  $\text{NO}_x$  were used to calculate  $P_{\text{O}_x}$   
367 from the rate of  $\text{O}_x$  formation reactions (Reaction R9, R10), and  $\text{O}_x$  loss by the reaction of  $\text{NO}_2$  with OH  
368 (Reaction R12) (Mihelcic et al., 2003; Cazorla et al., 2012; Niether et al., 2022)):

$$369 P_{\text{O}_x,\text{net}} = k_9[\text{NO}][\text{RO}_2] + k_{10}[\text{NO}][\text{HO}_2] - k_{12}[\text{NO}_2][\text{OH}] \quad (14)$$

370 This calculation neglects minor  $\text{O}_x$  destruction processes such as the reaction of  $\text{O}_3$  with  $\text{NO}_2$ , OH,  $\text{HO}_2$  or  
371 Cl since they did not play a notable role during the day in this campaign.

## 372 3 Results

### 373 3.1 Data quality of radical measurements



374 Performing measurements in the SAPHIR chamber allowed to test the accuracy of radical measurements  
375 in different ways that are typically not available in field experiments. First, OH radicals was measured by  
376 2 independent instruments, the OH-DOAS and LIF instruments (Cho et al., 2021). Second, the O<sub>x</sub>  
377 production rate calculated from measured concentrations of HO<sub>2</sub> and RO<sub>2</sub> could be compared to the  
378 observed increase of O<sub>x</sub> concentrations in the chamber, which can be solely attributed to chemical reactions.  
379 This is possible, because other factors typically impacting the O<sub>x</sub> concentration in field experiments such  
380 as transportation processes are not effective.

381 OH concentrations were measured by the LIF instrument applying the chemical modulation scheme and  
382 the DOAS in the winter, summer and autumn periods of the campaign. As OH concentrations were close  
383 to the limit of detection in autumn and winter, a meaningful comparison of measurements was only possible  
384 for the summer period. A detailed comparison of measurements can be found in Cho et al. (2021). In general,  
385 the OH measurements of the two instruments agreed within their measurement errors (Table 1) giving a  
386 slope of  $1.1 \pm 0.02$  in a linear regression analysis. The good agreement confirms that the newly developed  
387 chemical modulation system of the LIF instrument allowed for interference-free OH concentration  
388 measurements for conditions of the campaign. Only in the period from 22 to 26 August, which was  
389 characterized by exceptionally high temperatures (30 to 40°C), OH concentrations measured by the LIF  
390 instrument were systematically higher by 25% than those measured by the DOAS instrument for unknown  
391 reasons (Cho et al., 2021). OH concentrations measured by the DOAS instrument were used for the analysis  
392 of the radical budgets in this period.

393 Net O<sub>x</sub> production rates were determined from the measured increase of O<sub>x</sub> concentrations in the chamber  
394 and compared to calculations from the turnover rates of HO<sub>2</sub> and RO<sub>2</sub> reactions with NO. This calculation  
395 takes also the NO<sub>2</sub> loss due to its reaction with OH into account (Eq. 14). The odd oxygen production rate  
396 did not exceed 1 ppbv h<sup>-1</sup> in winter and autumn due to the general low photochemical activity in these  
397 seasons. In spring and summer, the O<sub>x</sub> production rate showed clear diurnal variations with noontime  
398 maxima that reached up to 16 ppbv h<sup>-1</sup>. In these seasons, both methods for determining the O<sub>x</sub> production  
399 rate agreed within  $\pm 15\%$  ( $1\sigma$ ). Observed discrepancies were less than 1 ppbv h<sup>-1</sup>, when NO mixing ratios  
400 were lower than 1 ppbv, but reached values of 3 ppbv h<sup>-1</sup> for NO mixing ratios of 3 - 4 ppbv NO. The  
401 largest discrepancy of 8.5 ppbv h<sup>-1</sup> was found in the morning on 29 April, when the NO mixing ratio  
402 exceeded 9 ppbv. High NO values suppressed HO<sub>2</sub> and RO<sub>2</sub> concentrations to values below  $2.0 \times 10^7$  cm<sup>-3</sup>,  
403 which is within the range of the background corrections for the HO<sub>2</sub> and RO<sub>2</sub> measurements (Table S1).  
404 Under these conditions, an erroneous background subtraction may have caused the observed discrepancies.

405

406

407

408

409

410



### 411 3.2 Meteorological and chemical conditions during the JULIAC campaign

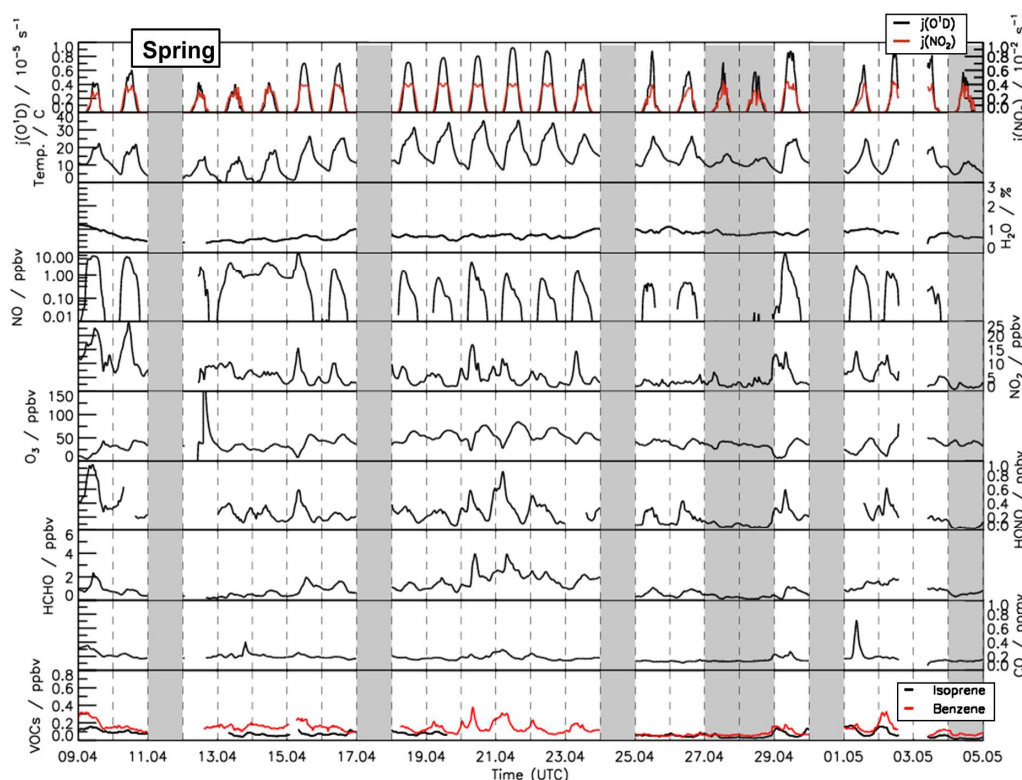


**Figure 1:** Time series of temperature and trace gas concentrations during the spring period of the JULIAC campaign (Cho et al., 2022). Vertical dashed lines denote midnight. Grey shaded areas indicate calibration days, when no measurements were done and days when the chamber roof was closed due to bad weather conditions.

412 A broad range of meteorological and chemical conditions was encountered during the JULIAC campaign.  
413 During the winter and autumn periods (Fig. S1 and S2), the sky was often overcast and it rained frequently.  
414 Temperatures were generally below 10°C and the photolysis frequencies of ozone ( $j_{O1D}$ ) and nitrogen  
415 dioxide ( $j_{NO2}$ ) mostly remained below  $1.5 \times 10^{-6} \text{ s}^{-1}$  and  $2 \times 10^{-3} \text{ s}^{-1}$ , respectively. During spring and  
416 summer, temperatures in the chamber were up to 35°C in mid-April and 40°C between 24 and 31 August  
417 (Fig. 1 and 2). Photolysis frequencies in the chamber were  $1 \times 10^{-5} \text{ s}^{-1}$  ( $j_{O1D}$ ) and  $4 \times 10^{-3} \text{ s}^{-1}$  ( $j_{NO2}$ ).

418 The air was sampled at all times from 50 m above ground. The temperature at different heights measured  
419 between 5 m and 120 m at a meteorological tower near the SAPHIR chamber showed that the air was well  
420 mixed within this height range during the day. Therefore, it can be assumed for the chemical composition  
421 of the air sampled into the chamber to be representative for the air within the atmospheric boundary layer.  
422 At night, vertical temperature profiles showed atmospheric stratification below 100 m. The air at 50 m can



423 be assumed to be isolated from the ground and therefore not being affected by surface emissions or  
 424 deposition on surfaces at the ground.

425 Overall, relatively clean air was sampled during the whole JULIAC campaign indicated by CO and NO  
 426 mixing ratios below 0.3 ppmv and 2 ppbv, respectively. Concentrations of anthropogenic organic  
 427 compounds (e.g. benzene and toluene) were low with mixing ratios of less than 0.5 ppbv. Even though the  
 428 measurement site is surrounded by a deciduous forest, the concentrations of biogenic organic compounds  
 429 such as isoprene and monoterpenes were also low (median 0.8 ppbv and 0.15 ppbv, respectively) compared  
 430 to previously reported values measured on the campus of FZJ in summer, when isoprene concentrations  
 431 ranged between 0.5 to 4 ppbv (Komenda et al., 2003; Spirig et al., 2005; Kanaya et al., 2012). A possible  
 432 reason for the low values could be damages of trees from severe droughts in the previous year (BMEL,  
 433 2021).

434

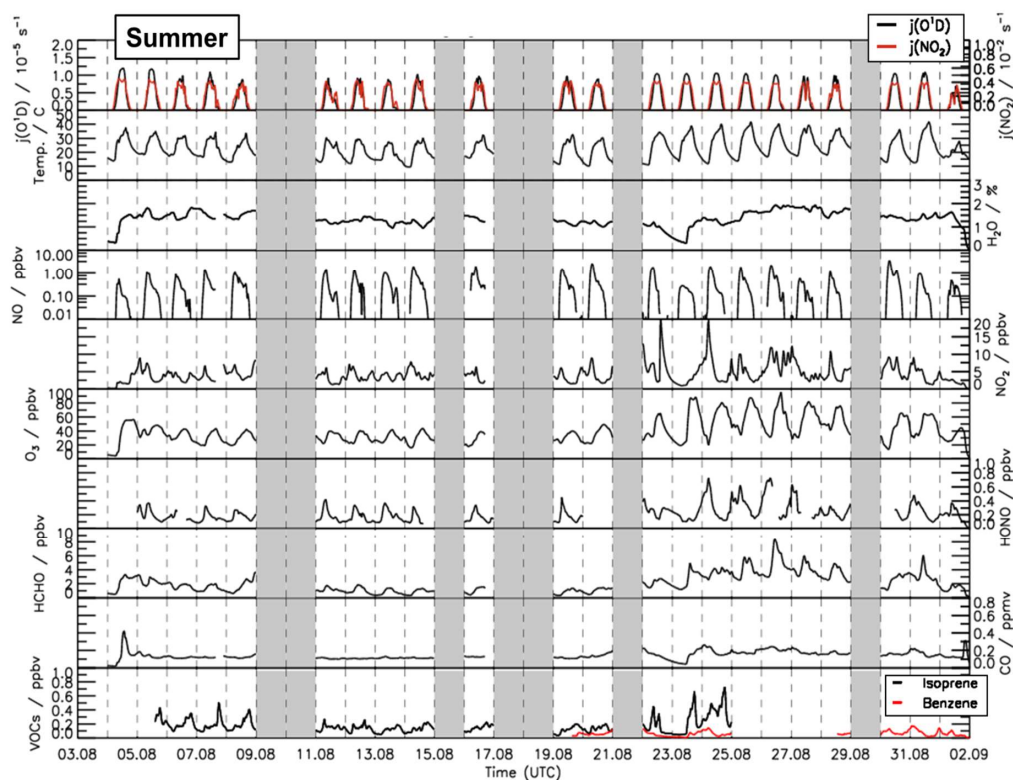


**Figure 2:** Time series of temperature and trace gas concentrations during the summer period of the JULIAC campaign (Cho et al., 2022). Vertical dashed lines denote midnight. Grey shaded areas indicate calibration days, when no measurements were done and days when the chamber roof was closed due to bad weather conditions.

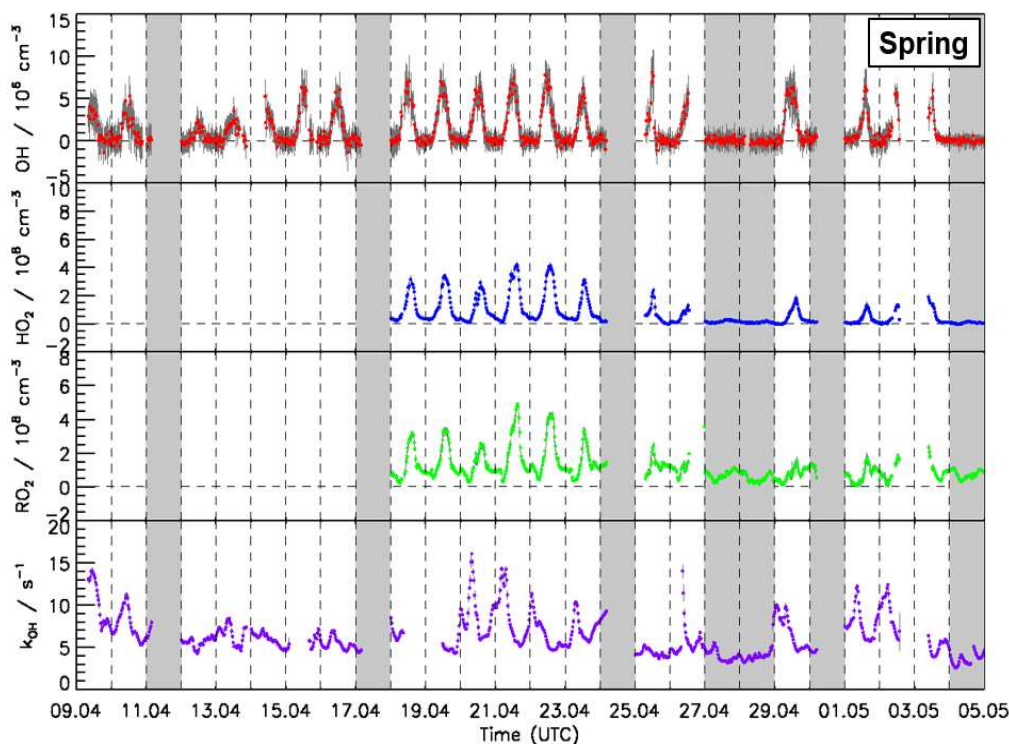


**Figure 3:** Time series of OH, HO<sub>2</sub>, and RO<sub>2</sub> radical concentration measured by the FZJ-LIF-CMR instrument and measurements of the OH reactivity ( $k_{\text{OH}}$ ) measured in the spring period of the JULIAC campaign (Cho et al., 2022). Vertical dashed lines denote midnight. Grey shaded areas indicate calibration days when no measurements were done and days when the chamber roof was closed due to bad weather conditions.

435 **3.3 OH, HO<sub>2</sub>, and RO<sub>2</sub> radical concentrations and OH reactivity during winter and autumn periods**  
436 **of the JULIAC campaign**

437 During winter (Fig. S3) and autumn (Fig. S4), daytime OH radical concentrations were below  $1 \times 10^6 \text{ cm}^{-3}$   
438 <sup>3</sup>, mainly due to a low primary radical production. Daytime peroxy radical (HO<sub>2</sub> and RO<sub>2</sub>) concentrations  
439 during these periods were also very low with average values below  $2 \times 10^7 \text{ cm}^{-3}$  (Fig. S5) close to the limit  
440 of detection of RO<sub>2</sub> radicals (Table 2) and within the uncertainty of the background corrections for HO<sub>2</sub>  
441 and RO<sub>2</sub> (Table S1). During winter and autumn, HO<sub>2</sub> concentrations typically increased in the morning and  
442 reached peak concentrations of  $2 \times 10^7 \text{ cm}^{-3}$  at noon. Concentrations decreased in the evening and night  
443 with minimum values right before sunrise. In contrast, nighttime RO<sub>2</sub> concentrations increased to values  
444 between 3 to  $4 \times 10^7 \text{ cm}^{-3}$  after sunset, when the chemical loss due to their reaction with NO became  
445 negligible, while RO<sub>2</sub> radicals were still produced from reactions of VOC with NO<sub>3</sub> and O<sub>3</sub>. NO  
446 concentrations were essentially zero at that time, because NO production by the photolysis of NO<sub>2</sub> stopped  
447 and NO rapidly reacted with ozone. RO<sub>2</sub> radical concentrations decreased in the morning to values that





448 were similar to that of HO<sub>2</sub> radicals as can be expected for conditions with high NO mixing ratios, which  
449 lead to a fast loss of RO<sub>2</sub> and HO<sub>2</sub> in their reactions with NO.

450 The measured OH reactivity ( $k_{OH}$ ) ranged between 4 and 33 s<sup>-1</sup> during winter and autumn periods. The  
451 highest value was observed on 21 January, when a highly polluted plume containing 50 ppbv of NO was  
452 sampled.

453 The measured OH reactivity can be compared to OH reactivity calculated by summing up the product  
454 between measured OH reactant concentrations and their reaction rate constants with the OH radical. On  
455 average, 1.3 s<sup>-1</sup> (18 %) of the measured OH reactivity could not be explained by the measured OH reactants  
456 during the winter and autumn periods (Fig. S5). NO<sub>x</sub>, CH<sub>4</sub>, CO, and VOCs contributed approximately 43,  
457 3, 20 and 13 %, respectively, to the measured OH reactivity.

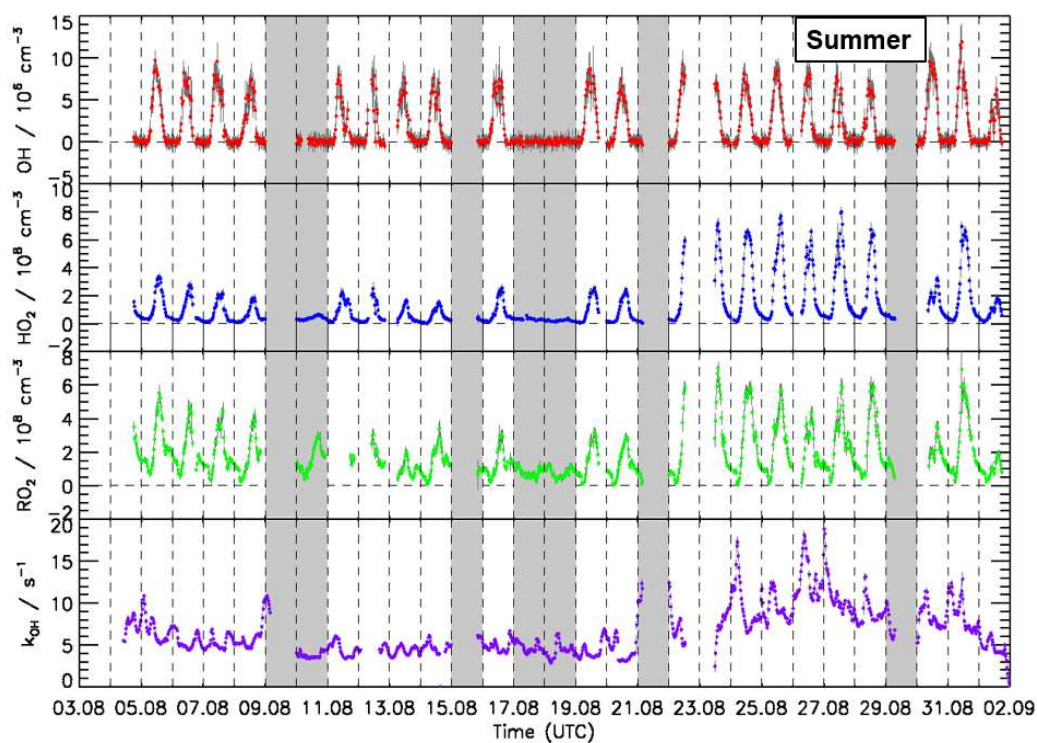


**Figure 4:** Time series of OH, HO<sub>2</sub>, and RO<sub>2</sub> concentration measured by the FZJ-LIF-CMR instrument and measurements of the OH reactivity ( $k_{OH}$ ) in the summer period of the JULIAC campaign (Cho et al., 2022). Vertical dashed lines denote midnight. Grey shaded areas indicate calibration days when no measurements were done and days when the chamber roof was closed due to bad weather conditions.

458

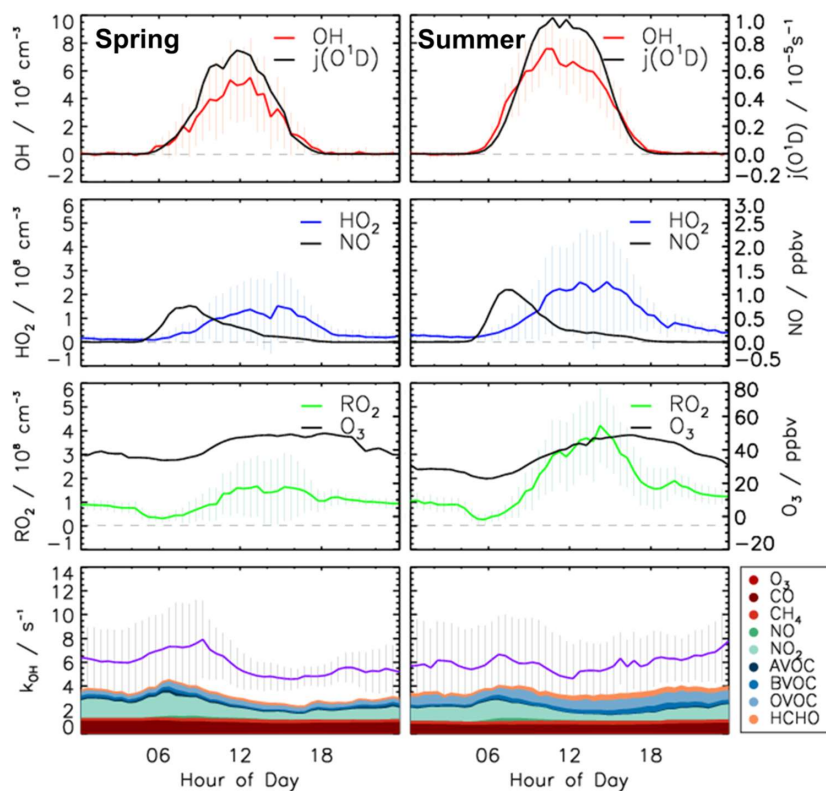


**Figure 5:** Median values of the diurnal profiles of OH, HO<sub>2</sub>, RO<sub>2</sub>,  $k_{OH}$ ,  $j_{O^1D}$ , NO, O<sub>3</sub> measured in the spring and summer periods of the JULIAC campaign. Colored areas represent the contributions of measured reactants to the total OH reactivity. Vertical lines give 25<sup>th</sup> and 75<sup>th</sup> percentile values.

459

### 460 3.4 OH, HO<sub>2</sub>, and RO<sub>2</sub> radical concentrations and OH reactivity during the spring and summer 461 periods of the JULIAC campaign

462 During spring and summer (Fig. 3, 4 and 5), maximum daytime OH concentrations were between 6 and 8  
 463  $\times 10^6 \text{ cm}^{-3}$ . The highest OH concentration ( $1.2 \times 10^7 \text{ cm}^{-3}$ ) occurred on 31 August. The diurnal OH  
 464 concentration profile shows a high correlation with the ozone photolysis frequency ( $j_{O^1D}$ ) as observed in  
 465 previous field campaigns (e.g., Ehhalt and Rohrer (2000); Handisides et al. (2003); Holland et al. (2003)).

466 Unfortunately, the measurements of HO<sub>2</sub> and RO<sub>2</sub> radicals were not available for the first two weeks of the  
 467 spring campaign due to a malfunction of the instrument. Daily maximum HO<sub>2</sub> and RO<sub>2</sub> concentrations were  
 468 in the range of 2 to 4  $\times 10^8 \text{ cm}^{-3}$  during the spring period and the first half of the summer period. Maximum  
 469 HO<sub>2</sub> and RO<sub>2</sub> concentrations were 8.0  $\times 10^8 \text{ cm}^{-3}$  and 7.0  $\times 10^8 \text{ cm}^{-3}$ , respectively, during the second half  
 470 of summer period. In spring and summer, peroxy radical concentrations showed a distinct diurnal pattern.  
 471 Both HO<sub>2</sub> and RO<sub>2</sub> radical concentrations were suppressed in the early morning (between 04:00 and 07:00)  
 472 due to the reaction with elevated NO mixing ratios of up to 1.5 ppbv. Maximum peroxy radical  
 473 concentrations were usually reached in the afternoon (~14:00), when NO concentrations were lowest.



474 The measured OH reactivity values were in the range of 4 to 18 s<sup>-1</sup>. High values were observed between 23  
475 and 31 August due to high emissions of biogenic volatile organic compounds (BVOCs) from plants at high  
476 ambient temperatures. The OH reactivity that cannot be attributed to the measured OH reactants was on  
477 average, 2.5 s<sup>-1</sup> (40%), which is much higher than observed in the winter and autumn periods (Fig. S5). CO  
478 and CH<sub>4</sub> contributed 10% and 4%, respectively. Due to the high emissions of biogenic organic compounds  
479 in spring and summer, the attributed contribution of organic compounds to the total measured OH reactivity  
480 was 20 % and the contribution of NO<sub>x</sub> was only 19 %, much less compared to the winter and autumn  
481 periods. Isoprene had the largest contribution among all VOCs accounting for up to 5 % of the total  
482 measured OH reactivity. Unfortunately, the number of detected VOC species in the JULIAC campaign was  
483 small (Table S2). This, however, does not impact the analysis in this study as the measured OH reactivity  
484 is used to determine the loss rate of OH radicals.

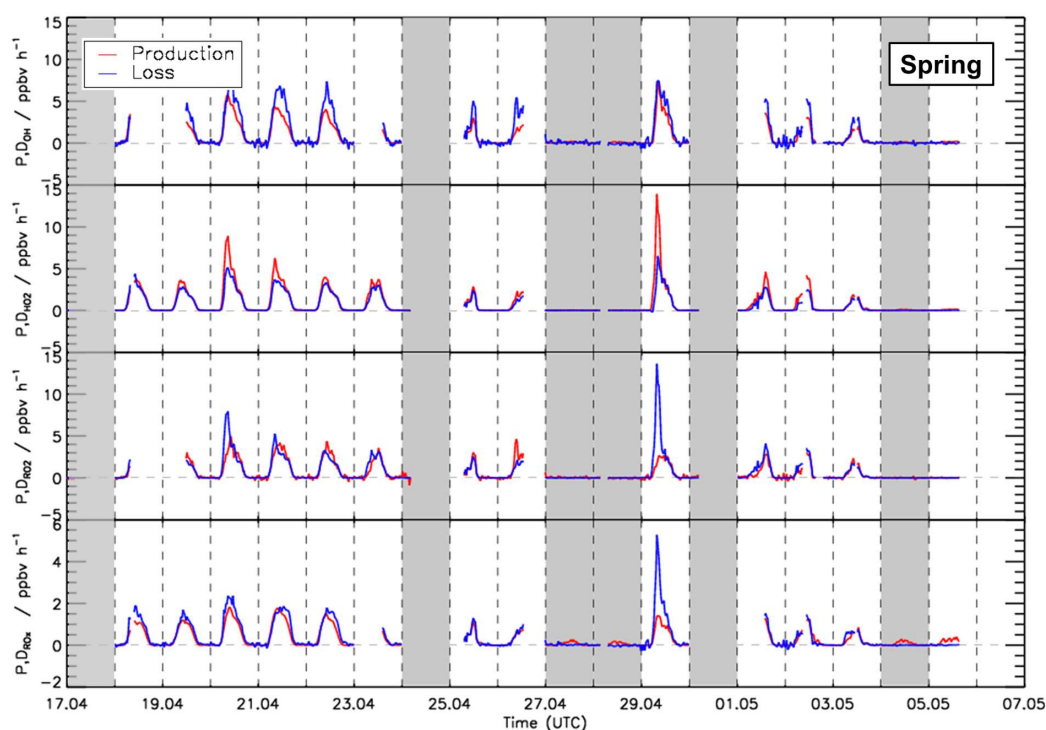


**Figure 6:** Time series of total production and destruction rates of OH, HO<sub>2</sub>, RO<sub>2</sub>, and RO<sub>x</sub> radicals in the spring period of the JULIAC campaign. Vertical dashed lines denote midnight. Grey areas indicate calibration days and days when the chamber roof was closed.

485 In the JULIAC campaign, nighttime OH concentrations were clearly below the limit of detection of the  
486 FZJ-CMR-LIF instrument ( $0.7 \times 10^6$  cm<sup>-3</sup>). When all nighttime data are averaged, mean OH  
487 concentrations with 1σ standard errors of  $(3 \pm 1) \times 10^4$  cm<sup>-3</sup> and  $(5 \pm 3) \times 10^4$  cm<sup>-3</sup> are obtained for  
488 the spring and summer periods, respectively. These low values support the absence of instrumentally  
489 produced OH and indicate a very low nocturnal OH production at 50 m height in the absence of NO and  
490 solar UV.

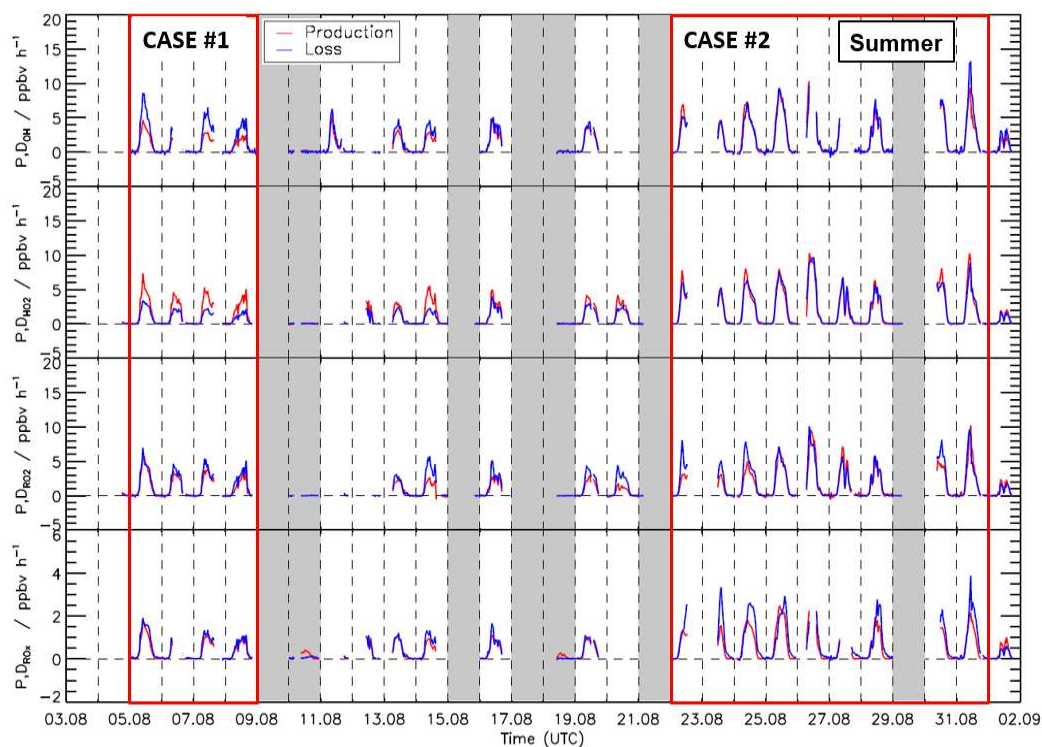


**Figure 7:** Time series of total production and destruction rates of OH, HO<sub>2</sub>, RO<sub>2</sub>, and RO<sub>x</sub> radicals in the summer period of the JULIAC campaign. Vertical dashed lines denote midnight. Grey areas indicate calibration days and days when the chamber roof was closed. The red boxes denote periods that are discussed in more detail (Case 1 and Case 2).

491

### 492 3.5 Chemical budgets of OH, HO<sub>2</sub>, RO<sub>2</sub> and RO<sub>x</sub> radicals in the spring and summer periods

493 Due to the very low photochemical activity observed in autumn and winter, which resulted in radical  
494 concentrations close to the detection limit of the instrument, the chemical budget analysis is only discussed  
495 for data from the spring and summer periods. It focuses on daytime conditions.

496 Time series of turnover rates of reactions involving OH, HO<sub>2</sub>, RO<sub>2</sub> and RO<sub>x</sub> radicals in the spring and  
497 summer periods are presented in Fig. 6 and 7, respectively, and median diurnal profiles in Fig. 8. Typical  
498 daytime turnover rates of OH, HO<sub>2</sub> and RO<sub>2</sub> radicals were between 3 ppbv h<sup>-1</sup> and 10 ppbv h<sup>-1</sup>. The rates of  
499 RO<sub>x</sub> production and destruction ranged from 1 ppbv hr<sup>-1</sup> to 3 ppbv hr<sup>-1</sup>, which is 2 to 4 times lower than  
500 those of OH, HO<sub>2</sub>, and RO<sub>2</sub>, because radical conversion reactions cancel out. The highest OH turnover rate  
501 of 13 ppbv h<sup>-1</sup> was observed on 31 August, when the air temperature in the chamber reached up to 40°C.  
502 Unusually high turnover rates for HO<sub>2</sub>, RO<sub>2</sub>, and RO<sub>x</sub> radicals occurred on 29 April with values of 14 ppbv  
503 h<sup>-1</sup>, 15 ppbv h<sup>-1</sup>, and 4 ppbv h<sup>-1</sup>, respectively, when the NO mixing ratio exceeded 9 ppbv. For the reasons



504 stated in Section 3.1, the HO<sub>2</sub> and RO<sub>2</sub> data on this date are considered highly uncertain and were excluded  
505 from further analysis of the chemical budgets.

506 Diurnal variations of total radical production and destruction rates, as well as of the contributions of the  
507 most important reactions, are shown as median values for the entire spring and summer period in Fig. 8.  
508 For OH, the reaction of HO<sub>2</sub> with NO (Reaction R10) was the dominant production pathway contributing  
509 more than 70 % to the total production rate in both spring and summer periods. The photolysis of HONO  
510 (Reaction R1) was the most important primary OH source during daytime contributing approximately 20 %  
511 to the total OH production. The reaction of HO<sub>2</sub> with ozone (Reaction R11), the photolysis of ozone  
512 (Reaction R2), and the ozonolysis of alkenes (Reaction R5) contributed less than 3 % to the total OH  
513 production. The maximum median total OH production rate of 3.5 ppbv hr<sup>-1</sup> was observed in the morning  
514 shortly after the peak NO concentration in both spring and summer (Fig. 5). Values gradually decreased  
515 until sunset. Median total OH destruction rates were higher than production rates and reached up to 5 ppbv  
516 hr<sup>-1</sup> and 6 ppbv hr<sup>-1</sup> at noon in spring and summer, respectively. The contributions of different reactions to  
517 the total OH destruction rate is described by the contribution of OH reactants to the OH reactivity (Section  
518 3.4, Fig. 5).

519 Short-lived radicals are expected to be in a steady state, and therefore radical production and destruction  
520 rates must be balanced. An imbalance between the calculated rates indicates inaccurate data or a missing  
521 radical production or destruction process. The daily peak of the OH production rates was typically lower  
522 than the destruction rate by approximately 1.8 ppbv h<sup>-1</sup> in the spring and 2.5 ppbv h<sup>-1</sup> in the summer period  
523 (36 and 43 % of the total OH destruction rate). These discrepancies are higher than the uncertainty of the  
524 calculation (Fig. 8).

525 80% of the HO<sub>2</sub> production rate consisted of the reaction of RO<sub>2</sub> with NO (Reaction R9). The remaining  
526 part of the HO<sub>2</sub> production rate was due to the photolysis of formaldehyde (9 %) and the reaction of  
527 formaldehyde with OH (10 %). Other reactions producing HO<sub>2</sub> played a minor role (< 1 %). The HO<sub>2</sub>  
528 destruction was mostly due to the reaction of HO<sub>2</sub> with NO (Reaction R10) contributing on average 88 %  
529 to the total production rate. The loss due to reaction of HO<sub>2</sub> with RO<sub>2</sub> radicals (Reaction R16) contributed  
530 on average 9 % to the total loss.

531 Median values of the total HO<sub>2</sub> destruction and production rates were well balanced in the spring period,  
532 with the production rate being slightly higher than the destruction rate. The maximum difference of 1 ppbv  
533 hr<sup>-1</sup>, however, was insignificant compared to the uncertainty of the calculation. A similar tendency but more  
534 pronounced feature was observed in summer. Here, the median value of production rate was higher than  
535 that of the destruction rate by 1.8 ppbv hr<sup>-1</sup> (38 % of the total HO<sub>2</sub> production rate) but differences were  
536 variable (Fig. 7). This aspect is discussed in more detail for two periods (Sections 3.7 and 3.8), which  
537 exhibited different degrees of imbalances in the radical budgets.

538 The RO<sub>2</sub> production rate was dominated by the reaction of VOCs with OH (Reaction R8). The contributions  
539 of ozonolysis of measured alkenes to the RO<sub>2</sub> production were very small (less than 1 %). The reaction of  
540 RO<sub>2</sub> with NO (Reaction R9) dominated the RO<sub>2</sub> destruction and contributed more than 90 % to the total  
541 loss rate. In the late afternoon, the RO<sub>2</sub> termination reaction with HO<sub>2</sub> gained in importance with  
542 contributions of up to 10 %. Although slight imbalances of up to 1 ppbv were observed in the early morning,  
543 the RO<sub>2</sub> production and destruction rates were generally balanced within the uncertainty of calculations in  
544 both spring and summer.



545 Figure 9 shows the calculated RO<sub>x</sub> production and destruction rates. The photolysis of HONO (Reaction  
 546 R1), HCHO (Reaction R3) and O<sub>3</sub> (Reaction R2) were the dominant processes initiating radical chemistry  
 547 and contributed to the total RO<sub>x</sub> production rate on average 45 %, 38 % and 15 %, respectively, in both  
 548 periods. In the morning, the reaction of OH with NO<sub>2</sub> (Reaction R12) was the most important radical  
 549 termination process contributing up to 65 % to the total RO<sub>x</sub> destruction rate. In addition, due to relatively  
 550 high NO mixing ratios in the early morning, the reactions of OH with NO (Reaction R13) and RO<sub>2</sub> with  
 551 NO, which yields organic nitrate (Reaction R14), were also significant radical termination processes  
 552 contributing 13 % and 17 % to the total RO<sub>x</sub> destruction rate, respectively. In the afternoon, radical self-  
 553 reactions (Reaction R15 – R17), and, in particular, the reaction of RO<sub>2</sub> with HO<sub>2</sub> (Reaction R16), dominated

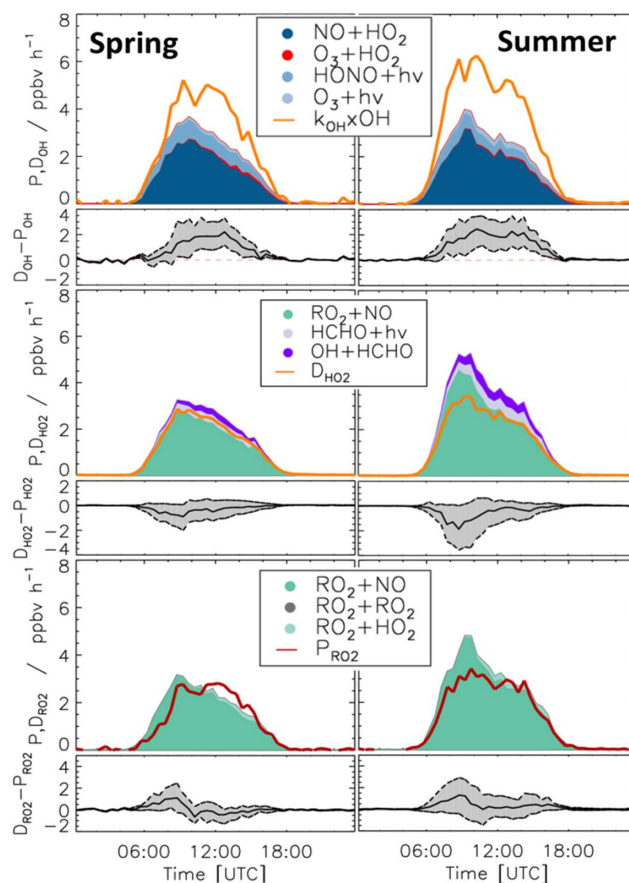


**Figure 8:** Median values of production and destruction rates of OH, HO<sub>2</sub>, and RO<sub>2</sub> radicals in the spring and summer periods of the JULIAC campaign, with data from 29 April excluded. In addition, the differences between the destruction and production rates are shown. Grey areas indicate the uncertainty derived from experimental errors of the measured quantities (Table 2) and of the reaction rate constants (Table 1). The reactions that have insignificant contributions to the production or destruction rates are not shown.



554 the RO<sub>x</sub> destruction due to the low NO and NO<sub>2</sub> mixing ratios. In both periods, spring and summer, the  
555 total RO<sub>x</sub> destruction rate was slightly higher than the production rate, in particular, in the afternoon. The  
556 imbalance was up to 0.5 ppbv h<sup>-1</sup>, which is higher than the uncertainty of the calculations.

557 Meteorological and chemical conditions were variable especially in the summer period causing variations  
558 in the balance between radical production and destruction rates (Fig. 7 and Table S3). In the following, the  
559 chemical budgets with the largest and smallest observed imbalances are discussed: August 5-8 (Case 1) and  
560 August 22-31 (Case 2).

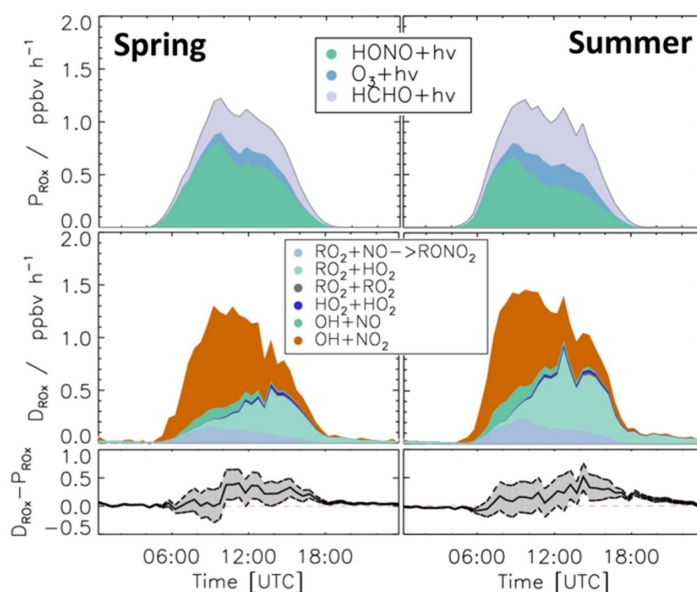


**Figure 9:** Median values of production and destruction rates of RO<sub>x</sub> radicals during the spring and summer periods of the JULIAC campaign. In addition, the differences between the destruction and production rates are shown. Grey areas indicate the uncertainty derived from experimental errors of the measured quantities (Table 2) and of the reaction rate constants (Table 1). The reactions that have insignificant contributions to the production or destruction rates are not shown.

### 561 3.5.1 Case 1: 5 - 8 August 2019

562 For the period between 5 and 8 August, relatively low NO mixing ratios (maximum: 1 ppbv, median: 0.26  
563 ppbv) and typical summer temperature for this region (median: 27°C) were observed (Fig. 10 and Table  
564 S3).

565 As for the whole summer period (Fig. 8), the reactions of peroxy radicals with NO (Reaction R9, R10)  
566 dominated the inter-radical conversion reactions of OH, HO<sub>2</sub> and RO<sub>2</sub> in this period (Fig. 10). A significant  
567 imbalance between the OH production and destruction rates of up to 3.0 ppbv h<sup>-1</sup> (51 % of the total OH  
568 destruction rate) is found, which cannot be explained by the uncertainty of the calculations. The total HO<sub>2</sub>  
569 production rate was 2.0 ppbv h<sup>-1</sup> higher than the destruction rate (48 % of the total HO<sub>2</sub> production rate),



570 whilst the  $\text{RO}_2$  production and destruction rates were well balanced. Relatively small but nevertheless  
 571 significant differences between  $\text{RO}_x$  production and destruction rates ( $0.5 \text{ ppbv h}^{-1}$ ) were observed during  
 572 daytime (Fig. 11).

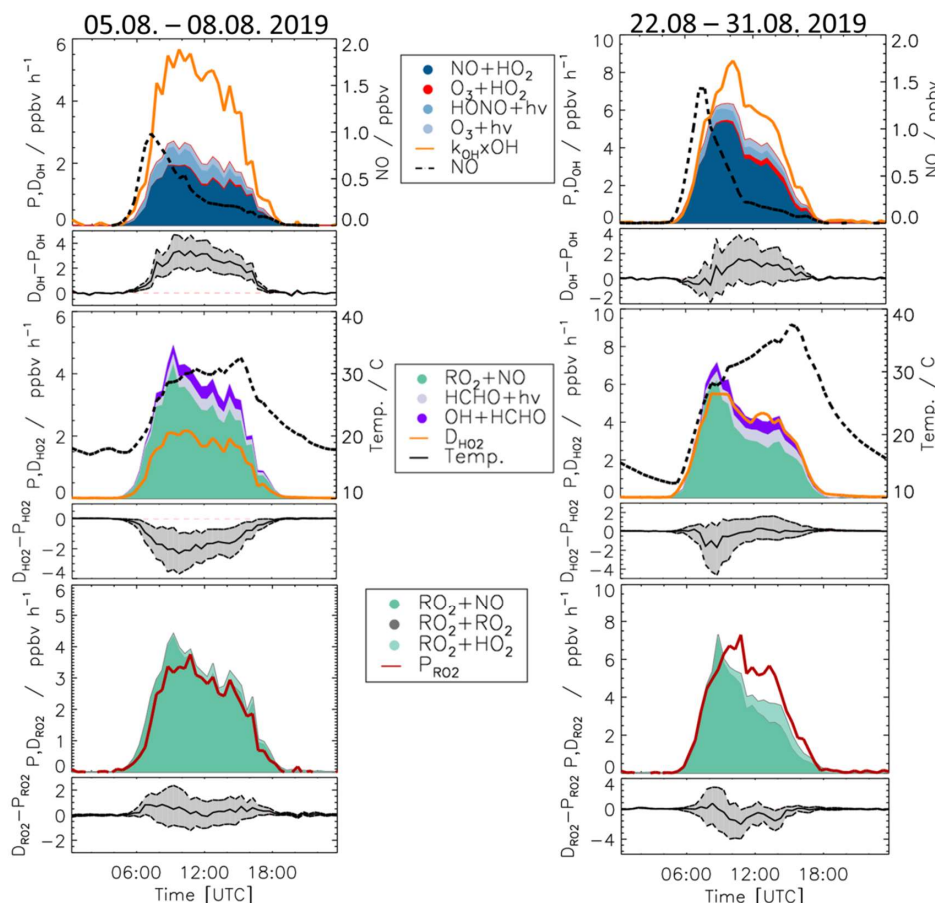


**Figure 10:** Production and destruction rates of OH,  $\text{HO}_2$ , and  $\text{RO}_2$  radicals for Case 1 (05.08. - 08.08 2019) and Case 2 (22.08 - 31.08 2019). In addition, the differences between the destruction and production rates are shown. Grey areas give the uncertainty derived from experimental errors of the measured quantities (Table 2) and of the reaction rate constants (Table 1). The reactions that have insignificant contributions to the production or destruction rates are not shown.

573





574 3.5.2 Case 2: 22 - 31 August 2019

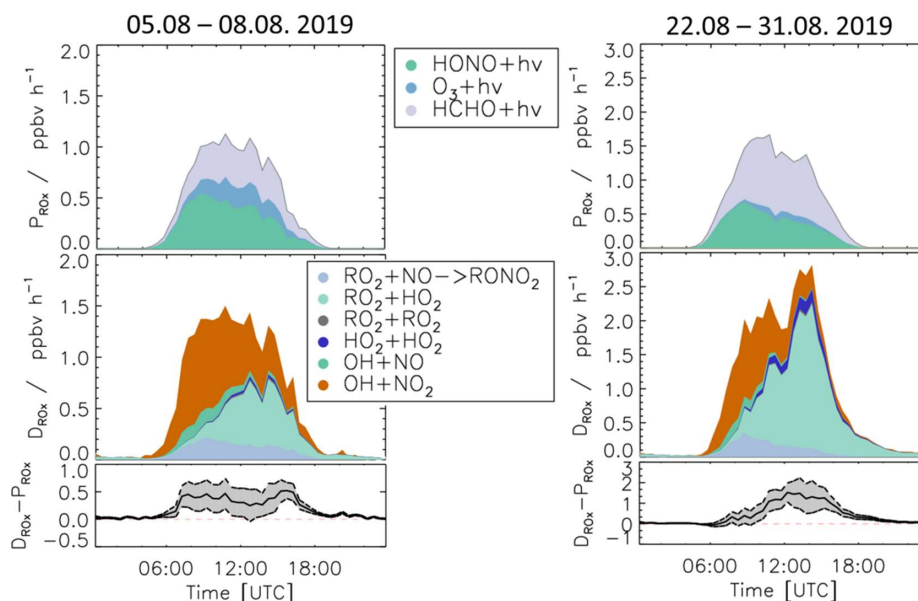


**Figure 11:** Production and destruction rates of  $RO_x$  for the periods of the case studies (Case 1 and Case 2). In addition, the differences between the destruction and production rates are shown. Grey areas indicate the uncertainty derived from experimental errors of the measured quantities (Table 2) and of the reaction rate constants (Table 1). The reactions that have insignificant contributions to the production or destruction rates are not shown.

575 During the period from 22 to 31 August, the temperature was generally high and reached a maximum value  
576 of 42°C inside the chamber. The concentrations of radical precursors, HONO, HCHO and  $O_3$ , were higher  
577 than those observed in Case 1 (Table S3). Ozone mixing ratios reached values up to 100 ppbv, while  
578 daytime NO mixing ratios were similar as in Case 1 (<1.5 ppbv, median value of 0.22 ppbv). The conditions  
579 outside the chamber were characterized by stagnant air (wind speed < 4 m/s at 50 m height) with no  
580 precipitation. At these conditions, vigorous biogenic emissions can be expected (Vilà-Guerau de Arellano  
581 et al., 2009; Sarkar et al., 2020). Enhanced biogenic VOC emissions and their photochemical degradation  
582 can therefore explain the higher VOC and HCHO concentrations in Case 2 compared to the cooler period  
583 beginning of the month (Table S3). The larger VOC reactivity and comparable OH concentrations resulted in  
584 in  $HO_2$  and  $RO_2$  concentrations that were approximately 2 to 3 times higher than in Case 1 (Table S3).

585 Imbalances between the radical production and destruction rates were a factor of 2 smaller in the warmer  
586 and more photochemically active period of Case 2 compared to Case 1. OH destruction rates were up to 1.5  
587 ppbv  $h^{-1}$  (25 % of the total OH destruction rate) higher than the total production rate (Fig. 10). The  $HO_2$   
588 production and destruction rates agree within  $\pm 1$  ppbv  $h^{-1}$ . The contributions from photolysis of HCHO and  
589 the reaction of HCHO with OH to the  $HO_2$  production rate were larger compared to other periods with



590 values of up to 15% and 13%, respectively, due to high HCHO mixing ratios of up to 8 ppbv (Fig. 2). The  
591 RO<sub>2</sub> production and destruction rates showed imbalances by up to 1.5 ppbv h<sup>-1</sup> in the late afternoon.

592 While HONO photolysis was the dominating RO<sub>x</sub> source during most of the time in spring and summer  
593 (Fig. 9), HO<sub>2</sub> production from the photolysis of HCHO was the most important primary radical source in  
594 Case 2 due to the high concentration of HCHO (Fig. 11). Although the chemical budgets for each radical  
595 species were essentially closed within the experimental uncertainty, the total loss rate of RO<sub>x</sub> was  
596 consistently higher than the production rate during daytime. The deviation was higher than the experimental  
597 uncertainty and reached a maximum value of 1.4 ppbv h<sup>-1</sup> at noontime.

### 598 3.5.3 NO dependence of radical production and destruction rates

599 One of the most influential parameters for the radical chemistry is the concentration of NO, since the  
600 reaction with NO dominates the conversion rate of RO<sub>2</sub> to HO<sub>2</sub> (Reaction R10) and HO<sub>2</sub> to OH (Reaction  
601 R9) (Fig. 10). Figure 12 shows the NO dependence of median values of the calculated production and  
602 destruction rates for the different radicals for the spring and summer period.

603 For OH, the production rates are consistently lower than the destruction rates by about 1.5 ppbv h<sup>-1</sup> for NO  
604 mixing ratios lower than 1 ppbv NO. At higher NO, the OH budget is balanced within the experimental  
605 uncertainty. For HO<sub>2</sub>, an inverse pattern is observed. Below 1 ppbv NO, the production rate is higher than  
606 the destruction rate by about 1 ppbv h<sup>-1</sup>. Only for lowest NO mixing ratios, the production and destruction  
607 rates are balanced. For NO mixing ratios above 1 ppbv, the chemical budget of HO<sub>2</sub> is essentially closed.  
608 For NO mixing ratios of 3.5 ppbv, the difference between production and destruction rate is noticeably high  
609 with 4 ppbv h<sup>-1</sup> but has also a large uncertainty. For RO<sub>2</sub> radicals, the chemical budget is closed for NO  
610 mixing ratios below 1 ppbv but an increasing discrepancy between the loss and production rates is observed  
611 with increasing NO mixing ratios. While the production rate is relatively constant with a value of 2.5 ppbv  
612 h<sup>-1</sup>, the loss rate increases to values of up to 7.5 ppbv h<sup>-1</sup> at 3.5 ppbv NO. The budget of RO<sub>x</sub>, in which  
613 radical inter-conversion reactions cancel out, is mostly balanced over the whole range of NO. Only for  
614 lowest and highest NO mixing ratios the destruction rate is 0.6 ppbv h<sup>-1</sup> higher than the production rate.

615

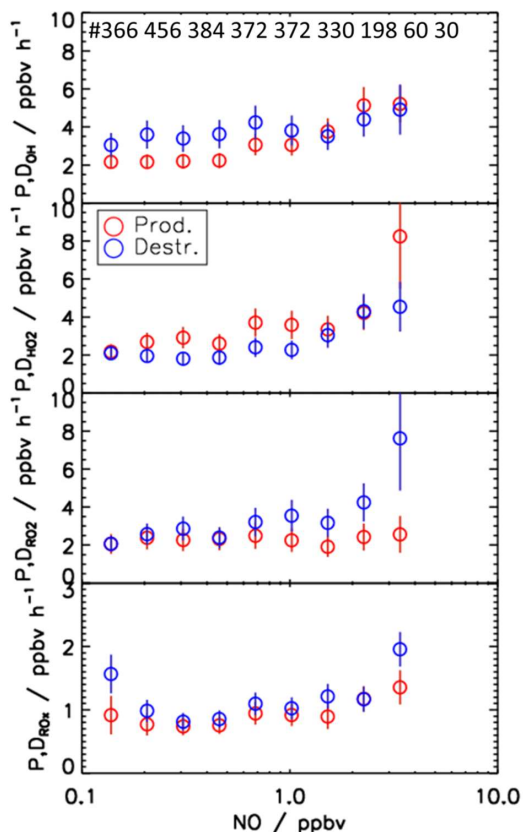


**Figure 12:** NO dependence of median production and destruction rates of OH, HO<sub>2</sub>, RO<sub>2</sub>, and RO<sub>x</sub> radicals. Median values include all data from the spring and summer periods of the JULIAC campaign (NO intervals 0.4 ppbv). Vertical bars represent the uncertainty from experimental errors of the measured quantities (Table 2) and of the reaction rate constants (Table 1).

616

617 **4 Discussion**

618 **4.1 Discrepancies in the chemical budgets of radicals**

619 The highest imbalances in the chemical budgets of radicals are found for OH radicals. In spring and summer,  
 620 their production rate was consistently lower than the loss rate (Fig. 8). This deficit was largest beginning of  
 621 August (Case 1, Fig. 10) when the discrepancy reached  $(3.0 \pm 1)$  ppbv h<sup>-1</sup>.

622 Imbalances in the radical budgets can be observed for different reasons. They can be caused by missing  
 623 processes or incorrect rate constants in the calculations of the production or destruction rates (Section 4.2).  
 624 It is also possible that measured concentrations that are used for the calculation contain unknown errors.



625 The technically difficult radical measurements have a large potential for artefacts (Hofzumahaus and Heard,  
626 2016). Precautions were taken to minimize measurement interferences for OH and HO<sub>2</sub> in this campaign:

- 627 • The measurements of OH by the LIF instrument were interference-corrected using chemical  
628 modulation and agreed with simultaneous OH measurements by the DOAS instrument within the  
629 experimental uncertainties. The measured OH reactivity quantifies the total chemical loss rate of  
630 OH caused by atmospheric reactants and has a total accuracy of 10%. Thus, the destruction rate of  
631 OH, which is the product of the concentration and reactivity of OH, is known within 20 % and is  
632 unlikely biased by unknown OH interferences or unknown atmospheric reactants.
- 633 • The O<sub>x</sub> production rate calculated from the reaction of peroxy radicals with NO agrees with the  
634 measured increase of O<sub>x</sub> concentrations within ±1 ppbv h<sup>-1</sup> for most conditions (Section 3.1). As  
635 more than 70 % of the OH production is due to the reaction of HO<sub>2</sub> with NO (Reaction R10), a bias  
636 of more than 1 ppbv h<sup>-1</sup> due to an unaccounted HO<sub>2</sub> measurement error seems unlikely.
- 637 • The analysis of the chemical budget of OH in previous chamber experiments performed at various  
638 chemical conditions showed no evidence for a missing OH source originating from chamber wall  
639 effects (Kaminski et al., 2017; Fuchs et al., 2018; Novelli et al., 2018; Rolletter et al., 2019;  
640 Rolletter et al., 2020).

641 Thus, there is no evidence for instrumental errors that are not included in the estimated errors of the  
642 calculated turnover rates. The observed imbalances in the OH budget of up to 3 ppbv h<sup>-1</sup> are therefore most  
643 likely due to a missing OH source.

644 The missing OH production is correlated with the imbalance in the HO<sub>2</sub> budget, for which the production  
645 rate is larger than the loss rate at low NO mixing ratios (Fig. 12). This is most clearly seen in the period of  
646 Case 1, when the discrepancy reaches (2.0±1) ppbv h<sup>-1</sup> (Fig. 10). The production rate of HO<sub>2</sub> is nearly equal  
647 to the RO<sub>2</sub> loss rate (P<sub>HO2</sub> ≈ D<sub>RO2</sub>) because both are controlled by the reaction of RO<sub>2</sub> with NO (Reaction  
648 R9). Furthermore, the RO<sub>2</sub> loss rate is well balanced by the RO<sub>2</sub> production rate within the experimental  
649 uncertainty of ±1 ppbv h<sup>-1</sup> (Fig. 8 and 10). Thus, there is no hint that the calculated turnover rate of the RO<sub>2</sub>  
650 + NO reaction had a bias higher than 1 ppbv h<sup>-1</sup>. In addition, turnover rates of the reactions of HO<sub>2</sub> and RO<sub>2</sub>  
651 with NO producing ozone are consistent with the observed O<sub>x</sub> increase in the chamber (Section 3.1). This  
652 suggests that these rates are correct in the chemical budget analysis. For the above reasons, the discrepancy  
653 between HO<sub>2</sub> production and destruction rates is most likely due to a missing HO<sub>2</sub> loss process and not by  
654 measurement errors of HO<sub>2</sub>, RO<sub>2</sub> or NO.

655 RO<sub>x</sub> destruction rates are generally higher than the production rates but differences are on average lower  
656 than 0.5 ppbv h<sup>-1</sup> (Fig. 9). In the periods of Case 1 and Case 2, the corresponding discrepancies reach 0.5  
657 ppbv h<sup>-1</sup> and 1.4 ppbv h<sup>-1</sup>, respectively (Fig. 10). If these discrepancies were due to a missing primary OH  
658 source, they could also explain a small part (17 %) of the imbalance in the chemical OH budget in Case 1,  
659 and the complete imbalance in the OH budget in Case 2.

660 It is difficult to identify the exact cause for the differences in OH and HO<sub>2</sub> budgets observed for Case 1 and  
661 2 only with the available data. Case 2 was characterized by high temperature with increased BVOC  
662 emissions and high levels of HCHO (Table S3). No clear correlation was found between the ratio of the  
663 production and destruction rates of the radicals and the concentration of chemical species such as NO, NO<sub>2</sub>,  
664 O<sub>3</sub>, HCHO, etc. A weak correlation was observed with temperature with an improved balance in the budgets  
665 the higher the temperature was. This could indicate that the unaccounted processes become less competitive



666 for high radical turnover rates with chemical conditions being dominated by organic compounds from  
667 biogenic emissions.

668 In conclusion, the radical budget analysis suggests the presence of a missing OH source and a missing HO<sub>2</sub>  
669 loss process with a similar turnover rate at NO mixing ratios below 1 ppbv for typical temperatures in  
670 summer. The opposing imbalances in the OH and HO<sub>2</sub> budgets could be due to an unknown mechanism  
671 that converts HO<sub>2</sub> to OH, or they could indicate a missing primary OH source and a similar fast, but  
672 independent termination reaction removing HO<sub>2</sub>. The remaining imbalance in the RO<sub>x</sub> budget would be  
673 consistent with an unaccounted primary OH source. This fits best the observations in Case 2 characterized  
674 by high temperatures and VOC emissions.

675 For NO mixing ratios that are higher than 1 ppbv, production and destruction rates of OH and HO<sub>2</sub> radicals  
676 are generally balanced (Fig. 12). An exception is observed for HO<sub>2</sub> for highest NO mixing ratios of 3.5  
677 ppbv, for which the production rate is 3.5 ppbv h<sup>-1</sup> higher than the loss rate.

678 For RO<sub>2</sub>, the radical budget is not closed, but the loss rate increases with NO in contrast to the production  
679 rate. The difference reaches a value of 5 ppbv h<sup>-1</sup> at 3.5 ppbv NO. In the same range of NO mixing ratios,  
680 the odd oxygen production rate ( $P_{O_x}$ ) calculated by peroxy radicals (Eq. 14) overestimates the observed  
681 increase in the O<sub>x</sub> mixing ratio by about 3 ppbv h<sup>-1</sup>. This difference points to a systematic error in the peroxy  
682 radical measurements explaining a considerable part of the imbalance in the RO<sub>2</sub> budget. A reduction of  
683 the RO<sub>2</sub> concentration by  $3 \times 10^7$  cm<sup>-3</sup> would reduce the HO<sub>2</sub> production rate by 3 ppbv h<sup>-1</sup> and resolve  
684 the discrepancy in the odd oxygen production calculations for the highest NO mixing ratio. The presumed  
685 bias in the RO<sub>2</sub> measurement may be caused by an incorrect background subtraction that becomes most  
686 relevant at high NO concentrations (Section 3.1). However, even after correction of this bias a discrepancy  
687 in the RO<sub>2</sub> budget would remain requiring an additional RO<sub>2</sub> source of approximately 2 ppbv h<sup>-1</sup> to be  
688 balanced.

689 Further information on the nature of the missing RO<sub>2</sub> source can be obtained from the chemical budget of  
690 RO<sub>x</sub>, for which the production rate is 0.5 ppbv h<sup>-1</sup> smaller than the loss rate at 3.5 ppbv NO (Fig. 12). This  
691 discrepancy cannot be explained by the instrumental uncertainties in HO<sub>2</sub> and RO<sub>2</sub> measurements, because  
692 the RO<sub>x</sub> budget at high NO in the morning was dominated by OH reactions with NO<sub>2</sub> and (Fig. 9). Thus,  
693 the imbalance in the RO<sub>x</sub> budget at high NO indicates a missing primary radical source, which on a single  
694 day (29 April) even reached 3 ppbv hr<sup>-1</sup> (Fig. 6). As the OH budget is balanced for most of the time and  
695 the corresponding HO<sub>2</sub> budget does not require an additional HO<sub>2</sub> source, a missing primary RO<sub>2</sub> source is  
696 a likely explanation for the discrepancy in the RO<sub>x</sub> budget. This would also explain part of the imbalance  
697 in the RO<sub>2</sub> budget at high NO concentrations.

698

#### 699 **4.2 Potentially missing chemical processes**

700 The above discussion shows that imbalances between calculated production and destruction rates are highly  
701 variable over time and change with chemical conditions. As main general features in spring and summer,  
702 the radical budget analysis indicates unaccounted OH production processes with a typical strength of 1.5 –  
703 3 ppbv h<sup>-1</sup> at low NO concentrations, which coincides with a missing HO<sub>2</sub> sink of 1 – 2 ppbv h<sup>-1</sup>. At high  
704 NO mixing ratios (> 1 ppbv), the radical budgets for OH and HO<sub>2</sub> radicals are relatively well balanced, but



705 RO<sub>2</sub> production processes of about 2 ppbv h<sup>-1</sup> appear to be missing in the RO<sub>2</sub> radical budget. In the  
706 following, potential reasons for the observed discrepancies in the radical budgets are discussed.

#### 707 **4.2.1 Differences in the chemical behavior of specific RO<sub>2</sub> radicals**

708 As no speciated RO<sub>2</sub> radicals were detected but the sum of all RO<sub>2</sub> species, effective rate coefficients for  
709 the reaction of all RO<sub>2</sub> species with NO (Reaction R9, R14), RO<sub>2</sub> (Reaction R15), and HO<sub>2</sub> (Reaction R16)  
710 are used from structure-activity relationship (SAR) by Jenkin et al. (2019) for the calculations of turnover  
711 rates. Potential systematic errors due to this simplification for reactions of RO<sub>2</sub> with RO<sub>2</sub> and HO<sub>2</sub> are  
712 expected to be negligible due to their small contributions to the total turnover rates.

713 In contrast, the reaction of RO<sub>2</sub> with NO plays an important role in the chemical budgets of HO<sub>2</sub> and RO<sub>2</sub>.  
714 The reaction has one channel that converts RO<sub>2</sub> to HO<sub>2</sub> (Reaction R9) and one radical termination channel  
715 that produces organic nitrates (RONO<sub>2</sub>) (Reaction R14). The unknown speciation of RO<sub>2</sub> causes uncertainty  
716 with respect to the total rate constant of the RO<sub>2</sub> + NO reaction ( $k_9 + k_{14}$ ). An effective value of  
717  $9 \times 10^{-12} \text{ cm}^3 \text{ s}^{-1}$  was taken from (Jenkin et al., 2019). A high limit for the total rate coefficient of RO<sub>2</sub>  
718 +NO (for example  $1.1 \times 10^{-11} \text{ cm}^3 \text{ s}^{-1}$ , 298K for c-C<sub>3</sub>H<sub>9</sub>O<sub>2</sub>) would slightly increase the imbalances  
719 between production and destruction rates for HO<sub>2</sub> and RO<sub>2</sub> radicals by 13 % for both spring and summer.  
720 A lower limit would be the rate constant of the reaction of methyl peroxy radicals (CH<sub>3</sub>O<sub>2</sub>) with NO having  
721 a value of  $7.7 \times 10^{-12} \text{ cm}^3 \text{ s}^{-1}$  (298 K)., Applying this number in the calculations for HO<sub>2</sub> production and  
722 RO<sub>2</sub> destruction rates (Fig. S6) for the period when observed discrepancies in the HO<sub>2</sub> budget were highest  
723 (Case 1) further improves the already well balanced budget of RO<sub>2</sub> radicals. This also reduces the imbalance  
724 between HO<sub>2</sub> destruction and destruction rates, but the effect is rather small (approximately 10%) and not  
725 sufficient to explain the total difference. For the other periods such as the spring period and the period of  
726 Case 2, a reduced reaction rate would worsen the observed imbalances.

727 An additional uncertainty in the HO<sub>2</sub> production rate comes from the assumed yield of organic nitrates in  
728 the reaction of RO<sub>2</sub> with NO. Typical organic nitrate yields range from 5 % to 20 % (Jenkin et al., 2019).  
729 The low limit value is applied in the calculations above. Using a value of 20 % decreases the discrepancy  
730 between HO<sub>2</sub> production and destruction rates from 2.0 to 1.5 ppbv h<sup>-1</sup> for the period of Case 1.

731 It is worth noting that the organic nitrate yield is generally higher for larger hydrocarbons, but the rate  
732 constant for the RO<sub>2</sub> + NO reaction is also often higher, so that there are compensating effects in the  
733 production efficiency of HO<sub>2</sub>. In addition, it is expected that only a fraction of RO<sub>2</sub> radicals is produced  
734 from large hydrocarbons due to the major composition of RO<sub>2</sub> would be methyl peroxy radicals.

735 For the above reasons, the unknown speciation of RO<sub>2</sub> is unlikely the reason for the observed imbalances  
736 in the HO<sub>2</sub> budget that are most prominent in the period of Case 1.

#### 737 **4.2.2 Unaccounted primary radical sources**

738 Primary RO<sub>x</sub> radical production that may not be appropriately accounted for in the calculations could be  
739 OH, HO<sub>2</sub>, and RO<sub>2</sub> production from the ozonolysis of alkenes. Only few alkene compounds were measured  
740 in the JULIAC campaign. The contribution from the ozonolysis of these alkenes to the radical production  
741 was very small with values in the range of 0.005 to 0.03 ppbv h<sup>-1</sup> (Section 3.5). The ozonolysis of small  
742 alkenes such as propene and cis-2-butene that were not measured but are often abundant for example in



743 forested areas (Goldstein et al., 1996; Rhew et al., 2017), may have significantly contributed to the radical  
744 production.

745 The potential impact of unmeasured alkenes on the primary radical production is tested by assuming that  
746 the OH reactivity that cannot be explained by measured OH reactants (on average,  $2.5 \text{ s}^{-1}$ ) originates from  
747 1.5 ppbv propene and 1.0 ppbv cis-2-butene. The radical production by ozonolysis of the additional propene  
748 and cis-2-butene increases the production from ozonolysis of measured species by more than an order of  
749 magnitude in both spring and summer periods of the JULIAC campaign (Fig. S7) The discrepancies  
750 between the total  $\text{RO}_x$  production and destruction rates is significantly decreased for the period of the 2  
751 Case studies by approximately  $0.2 \text{ ppbv h}^{-1}$ . However, the additional OH production is by far insufficient  
752 to explain the missing OH source that was generally found during the JULIAC campaign. In addition, the  
753 corresponding OH and  $\text{O}_3$  reactivity from the additional alkene compounds is about a factor of 6 larger than  
754 of alkenes (e.g., ethene, propene, trans-2-butene, cis-2-pentene) that were measured in ambient air next to  
755 the SAPHIR chamber in the HO<sub>x</sub>Comp campaign in July 2005 (Elshorbany et al., 2012; Kanaya et al.,  
756 2012).

757 The photolysis of oxygenated organic compounds is another source for radicals that could be  
758 underestimated in the calculations. Only the photolysis of HCHO is included in the production rate of  $\text{HO}_2$   
759 and  $\text{RO}_x$  at all times of the campaign. In addition, acetaldehyde ( $\text{CH}_3\text{CHO}$ ), methyl vinyl ketone (MVK),  
760 methacrolein (MACR), and methylglyoxal were measured during part of the campaign and were not  
761 included in the analysis in Section 3. Calculations show that radical production rate from their photolysis  
762 was less than  $0.1 \text{ ppbv h}^{-1}$ . Thus, photolysis of unmeasured OVOCs was very likely unimportant in the  
763 present study. This is consistent with similar small contributions from photolysis of OVOCs other than  
764 HCHO found in in the HO<sub>x</sub>Comp campaign (Kanaya et al., 2012).

765 The photolysis of  $\text{ClNO}_2$  constitutes a primary radical source (Reaction R20, R22) that can be found in  
766 coastal environments (e.g., Osthoff et al. (2008)) and mid-continental regions (e.g., Thornton et al. (2010)).  
767 The availability of  $\text{ClNO}_2$  data during the summer period allowed assessing the potential impact of its  
768 photolysis on the  $\text{RO}_2$  radical production (Eq. 9). Due to the low mixing ratio of  $\text{ClNO}_2$  of less than 0.4  
769 ppbv (Tan et al., 2022), the  $\text{RO}_2$  production from Cl oxidation processes was insignificant ( $<0.1 \text{ ppbv h}^{-1}$ )  
770 and cannot explain the observed discrepancies in the primary production and destruction rates of radicals  
771 in the summer period and in the case studies. The instrument detecting  $\text{ClNO}_2$  was not available in the  
772 spring period of the campaign. Therefore, the extent to which  $\text{ClNO}_2$  photolysis contributed in spring, for  
773 example to the large missing  $\text{RO}_x$  source (up to  $3 \text{ ppbv hr}^{-1}$ ) on 29 April, remains unknown.

#### 774 4.2.3 Unaccounted radical termination reactions

775 Heterogeneous uptake of  $\text{HO}_2$  on aerosol is a potential termination reaction that is not included in the  $\text{HO}_2$   
776 and  $\text{RO}_x$  destruction rates above. However, the impact of including the heterogeneous  $\text{HO}_2$  loss on aerosol  
777 surface (Eq. 8) on the total loss rate is insignificant (less than 1 %), even if a high effective uptake  
778 coefficient of 0.2 is assumed (Fig. S7).

779 As  $\text{HO}_2$  uptake is a radical termination process, its relative contribution to the total  $\text{RO}_x$  loss rate can be  
780 higher compared to the relative contribution to the total  $\text{HO}_2$  loss rate. However, the only notable influence  
781 would be for the period of Case 2 (8 % of total  $\text{RO}_x$  loss rate), when the aerosol surface area concentration  
782 was high with values of up to  $3.0 \times 10^2 \mu\text{m}^2 \text{ cm}^{-3}$ .



783 The estimate for the heterogeneous HO<sub>2</sub> loss rate has a high uncertainty because the uptake coefficient  
784 highly depends on the aerosol properties that were not fully characterized in this campaign. Previous  
785 laboratory investigations showed a large variability for the uptake coefficient with values ranging from 0.08  
786 to 0.6 depending on the aerosol chemical composition and the physical state (George et al., 2007; Taketani  
787 et al., 2008, 2009; George et al., 2013; Lakey et al., 2015; Song et al., 2020; Tan et al., 2020). Even the  
788 largest reported HO<sub>2</sub> uptake coefficients cannot explain the observed differences in the chemical budget of  
789 HO<sub>2</sub> radicals. Therefore, heterogeneous HO<sub>2</sub> reactions can be ruled out as an explanation for the  
790 unexplained HO<sub>2</sub> loss rate.

#### 791 **4.2.4 Unaccounted radical inter-conversion reactions**

792 In the last decade, it has been discovered that unimolecular reactions of RO<sub>2</sub> can significantly increase  
793 atmospheric OH concentrations in low-NO environments where they can compete with the reaction of RO<sub>2</sub>  
794 with NO. The most important, atmospherically relevant example is the production of OH from the  
795 isomerization of isoprene-RO<sub>2</sub> radicals (Peeters et al., 2009; da Silva et al., 2010; Peeters and Müller, 2010;  
796 Crouse et al., 2011; Fuchs et al., 2013; Peeters et al., 2014; Teng et al., 2017; Novelli et al., 2020). The  
797 SAPHIR chamber is surrounded by a deciduous forest that emits isoprene especially in summer. Compared  
798 to previous campaigns on the campus where up to several ppbv of isoprene were measured (Komenda et  
799 al., 2003; Spirig et al., 2005; Kanaya et al., 2012), concentrations were relatively low during the JULIAC  
800 campaign (< 0.4 ppbv, on average).

801 The effect of the conversion of RO<sub>2</sub> to OH by the isomerization of isoprene-RO<sub>2</sub> (Eq. 4) is tested in the  
802 analysis of the OH and RO<sub>2</sub> budgets. In the afternoon of days in the spring period and the period of Case 2,  
803 the total OH production increases only 1 % due to the low isoprene mixing ratios (< 0.2 ppbv) and the  
804 competition of unimolecular reactions with bimolecular reactions of RO<sub>2</sub> with NO. Even in the summer  
805 period, when isoprene mixing ratios were up to 0.8 ppbv, the contribution of isomerization reactions from  
806 isoprene-RO<sub>2</sub> radicals to the total turnover rate of RO<sub>2</sub> is still small with values of less than 4 %. This  
807 implies that unimolecular decomposition reactions of isoprene-RO<sub>2</sub> radicals made a minor contribution to  
808 the RO<sub>2</sub> destruction and OH production rates.

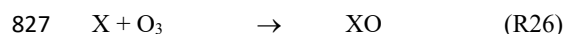
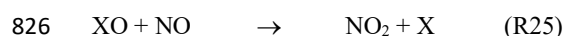
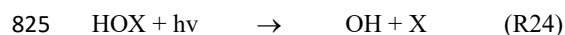
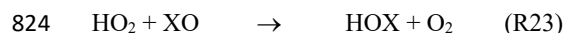
809 Another known isomerization process that produces OH applies to RO<sub>2</sub> that are formed by OH oxidation  
810 of methacrolein (MACR) (Crouse et al., 2012; Fuchs et al., 2014), which is an oxidation product of  
811 isoprene. MACR mixing ratios were up to 0.5 ppbv in the JULIAC campaign. Because the rate constant for  
812 the OH reaction of MACR is smaller than for isoprene, OH regeneration from MACR-RO<sub>2</sub> radicals is even  
813 less important than from isoprene-RO<sub>2</sub>.

814 For acyl and carbonyl peroxy radicals it was shown that the reaction of RO<sub>2</sub> with HO<sub>2</sub>, which mainly forms  
815 hydroperoxides (ROOH) (Reaction R16), can produce OH with yields up to 80% (Hasson et al., 2004;  
816 Dillon and Crowley, 2008; Groß et al., 2014; Praske et al., 2015; Winiberg et al., 2016; Jenkin et al., 2019).  
817 It is also noteworthy that the rate constant for the reaction of HO<sub>2</sub> with this class of RO<sub>2</sub> species is almost  
818 a factor of 2 higher than for other RO<sub>2</sub> species (Jenkin et al., 2019). However, even if it is assumed that all  
819 the measured RO<sub>2</sub> are acyl and carbonyl peroxy radicals, the formation of OH from their reaction with NO  
820 could only explain up to 0.5 ppbv h<sup>-1</sup> of the imbalances in both OH and HO<sub>2</sub> budgets.





821 Studies in the remote marine boundary layer show that HO<sub>2</sub> to OH conversion mediated by halogen oxides  
822 (XO, X = Cl, Br, I) (e.g., Bloss et al. (2005); Sommariva et al. (2006); Kanaya et al. (2007); Stone et al.  
823 (2018); Fan and Li (2022)) can significantly contribute to the interconversion of radicals and destroy ozone:



828 This conversion mechanism would only be effective at low NO, when the consumption of XO by NO  
829 (Reaction R25) is comparatively slow and when X is not depleted by other reactions as in the case of Cl by  
830 reactions with VOCs (Reaction R22).

831 For BrO, the rate constants for Reaction R23 and R25 are about the same ( $2.1 \times 10^{-11} \text{ cm}^3 \text{ s}^{-1}$  at 298 K,  
832 (Burkholder, 2019). Thus, the reaction of BrO with HO<sub>2</sub> would only be dominant, if the NO concentration  
833 were smaller than the concentration of HO<sub>2</sub>, i.e., less than 10 pptv in this campaign. For IO, the situation is  
834 similar and NO mixing ratios would need to be less than 40 pptv. Such low NO mixing ratios were not  
835 observed during daytime and rule out significant halogen oxide mediated HO<sub>2</sub> to OH conversion. The  
836 required XO concentrations to achieve an HO<sub>2</sub> loss rate of 1 ppbv h<sup>-1</sup> at an HO<sub>2</sub> concentration of  
837  $2 \times 10^8 \text{ cm}^3$  would be 66 pptv BrO or 16 pptv IO, which exceeds the abundances reported for marine  
838 environments, where halogen sources are known to exist, by more than an order of magnitude. For these  
839 reasons, halogen oxide chemistry cannot explain the missing HO<sub>2</sub> sink and missing OH source in this study.

#### 840 **4.3 Comparison with results from other field campaigns**

841 Although the chemical and physical conditions were partly influenced by the chamber properties (Section  
842 2.1), the radical concentrations observed during spring and summer were within the range of values that  
843 have been observed in other field studies in summertime in urban and suburban areas (Tan et al., 2001; Ren  
844 et al., 2003; Kanaya et al., 2007; Mao et al., 2010; Lu et al., 2013; Brune et al., 2016; Tan et al., 2017;  
845 Whalley et al., 2018; Tan et al., 2019). The impact of the decreased solar radiation by the chamber  
846 transmission on the radical production was compensated by the radical production from the photolysis of  
847 HONO and HCHO emitted from the chamber film.

848 This effect is also shown in the relationship between the OH concentration and the photolysis frequencies  
849 of ozone,  $j_{\text{O}^1\text{D}}$  (Section 3.4). The slope ( $8.0 \times 10^{11} \text{ cm}^3 \text{ s}^{-1}$ ) of the correlation for the data from the  
850 JULIAC campaign is much higher than obtained for data in other field campaigns in similar environments  
851 (Ehhalt and Rohrer, 2000; Handisides et al., 2003; Holland et al., 2003; Tan et al., 2017) due to the high  
852 OH production by the photolysis of chamber-produced HONO (Reaction R1). This is further confirmed by  
853 the similarity in OH and HO<sub>2</sub> radical concentrations between this campaign and what was observed in the  
854 HOxComp campaign when measurements were performed in front of the SAPHIR chamber for 3 days in  
855 July 2005 (Elshorbany et al., 2012).

856 In contrast, daytime OH concentrations observed during winter and autumn in the JULIAC campaign were  
857 lower than OH concentrations observed in previous wintertime field campaigns (Heard et al., 2004; Ren et



858 al., 2006; Kanaya et al., 2007; Tan et al., 2018; Ma et al., 2019). This is due to the lower photolysis  
859 frequencies in the chamber compared to outdoors, which is not compensated by chamber-produced HONO  
860 in wintertime, because the emission strength is low at low temperature and low solar radiation.

861 Very low nighttime OH concentration in all seasons of the JULIAC campaign (Section 3.4) is consistent  
862 with observations in previous field campaigns in rural areas in Germany (Ehhalt and Rohrer, 2000;  
863 Handisides et al., 2003; Holland et al., 2003), in which nighttime OH concentrations were less than  $1 \times 10^5$   
864  $\text{cm}^{-3}$ . However, in several other field studies performed in urban areas, nighttime OH concentrations were  
865 in the range of 0.2 to  $3 \times 10^6 \text{ cm}^{-3}$ , for example in China (Lu et al., 2014; Rohrer et al., 2014; Tan et al.,  
866 2017; Tan et al., 2018; Ma et al., 2019; Tan et al., 2019; Wang et al., 2019; Whalley et al., 2021), in the US  
867 (Martinez et al., 2003; Brune et al., 2016; Griffith et al., 2016), and in the UK (Ren et al., 2003; Vaughan  
868 et al., 2012). In these studies, the high nighttime OH concentrations could not be explained by model  
869 predictions and raised questions about the presence of potential interferences in nighttime OH signals  
870 measured by LIF instruments (Mao et al., 2012; Lu et al., 2014; Novelli et al., 2014).

871 Similar studies investigating the chemical budgets of OH, HO<sub>2</sub>, RO<sub>2</sub>, and RO<sub>x</sub> radicals like in this study  
872 have been performed for data from field campaigns in a suburban area in the Pearl River Delta (PRD),  
873 China, in autumn 2014 (Tan et al., 2019), and in central Beijing, China, (Whalley et al., 2021) in summer  
874 2017.

875 Tan et al. (2019) observed median values of turnover rates of OH, HO<sub>2</sub> and RO<sub>2</sub> radicals ranging from 10  
876 to 15 ppbv h<sup>-1</sup>, while rates for RO<sub>x</sub> initiation and termination rates were on the order of 3 to 4 ppbv h<sup>-1</sup>  
877 during daytime for chemical conditions affected by anthropogenic emissions. From the comparison between  
878 the radical production and destruction rates, a missing OH source and a missing RO<sub>2</sub> sink with a similar  
879 rate up to 7 ppbv h<sup>-1</sup> (45 % of the total OH turnover) were found at low NO mixing ratios below 1 ppbv,  
880 while HO<sub>2</sub> production and destruction rates were balanced. The authors suggested that an additional  
881 chemical mechanism is required that efficiently converts RO<sub>2</sub> to OH without the involvement of NO. One  
882 possibility proposed by Tan et al. (2019) is that HO<sub>x</sub> radicals are formed from the auto-oxidation of specific  
883 RO<sub>2</sub> species which include multifunctional groups such as -OH, -OOH, or -CHO groups.

884 The analysis of the chemical budget of OH radicals in the JULIAC campaign shows that an unaccounted  
885 OH source with a rate ranging between 2 and 3 ppbv h<sup>-1</sup> (about 50 % of the total OH destruction rate) is  
886 required at low NO mixing ratios to balance OH production and destruction rates. This rate is smaller than  
887 the rate determined in Tan et al. (2019). However, considering that the OH radical turnover rates in the  
888 JULIAC campaign were about half compared to values in the campaign in the PRD area, the relative  
889 importance of the unaccounted OH source was comparable in both campaigns. However, the mechanism  
890 suggested by Tan et al. (2019) is likely not the only explanation for discrepancies in the radical budgets  
891 observed in this study. In the JULIAC campaign, to balance the budget of RO<sub>2</sub> radicals rather requires an  
892 additional radical source than additional loss processes particularly at high NO mixing ratios above 1 ppbv,  
893 and the missing OH sources are likely originating from an HO<sub>2</sub> to OH conversion process and/or a missing  
894 primary OH source.

895 Whalley et al. (2021) also investigated the chemical budgets for radicals over a wide range of NO mixing  
896 ratios (0.1 to 104 ppbv) from measurement performed in central Beijing, China. Compared to the results in  
897 Tan et al. (2019) and to results in this study, the rates of RO<sub>x</sub> initiation and termination reactions were 2 to  
898 4 times higher. Also, the rates of radical propagation reactions for OH, HO<sub>2</sub> and RO<sub>2</sub> radicals were 5 to 10



899 times higher due to fast inter-radical conversion reactions at conditions with high concentrations of NO.  
900 Similar to the results in this study, an OH source with a high rate of up to 15 ppbv h<sup>-1</sup> (50 % of the total OH  
901 destruction) was required to balance OH production and destruction rates for low NO mixing ratios. This  
902 unaccounted OH source is more than 3 times higher than that determined in the JULIAC campaign and in  
903 the campaign in China reported by Tan et al. (2019). The HO<sub>2</sub> production rate observed in Beijing largely  
904 exceeded the destruction rate by 3 to 5 times for low NO mixing ratios. In contrast, production and  
905 destruction of RO<sub>2</sub> and RO<sub>x</sub> radicals were well balanced. On the other hand, results for conditions of low  
906 NO concentrations, production and destruction of OH radicals were balanced at high NO mixing ratios,  
907 while very high imbalances of up to 50 ppbv h<sup>-1</sup> were observed for HO<sub>2</sub> and RO<sub>2</sub> radicals. Whalley et al.  
908 (2021) showed that reducing the rate constant of the reaction between RO<sub>2</sub> and NO by a factor of 10 could  
909 close the gaps between production and destruction rates. The authors suggested that the presence of a  
910 significant fraction of RO<sub>2</sub> radicals from the oxidation of large and multifunctional VOCs such as  
911 monoterpenes and long-chain alkanes could explain observations. These radicals can undergo multiple RO<sub>2</sub>  
912 to RO<sub>2</sub> conversion reactions by unimolecular isomerization of alkoxy radicals (RO), which are formed from  
913 the reaction of RO<sub>2</sub> with NO, so that no HO<sub>2</sub> is produced. Such a RO<sub>2</sub> radical reaction chain would be  
914 equivalent to an increased chemical lifetime of RO<sub>2</sub> radicals, if RO<sub>2</sub> species cannot be distinguished by  
915 instruments like in the sum measurements performed by RO<sub>x</sub>-LIF instruments. Whalley et al. (2021)  
916 showed that RO<sub>2</sub> production by this mechanism would largely reconcile discrepancies between modelled  
917 and measured RO<sub>2</sub> concentrations (the model-measurement ratio decreases from 6.2 to 1.8), if the OH  
918 reactivity that could not be accounted for by measured OH reactants is attributed to  $\alpha$ -pinene.

919 Applying a reduced rate constant for RO<sub>2</sub> to HO<sub>2</sub> propagation reactions as suggested in Whalley et al. (2021)  
920 in the calculations in this study could help explaining the observed discrepancies between HO<sub>2</sub> and RO<sub>2</sub>  
921 production and destruction rates. The largest effect is expected when high NO mixing ratios up to 10 ppbv  
922 like on 29 April is experienced. In this case, a high reduction of the rate constant by a factor of 2 for all  
923 measured RO<sub>2</sub> would be required to close the observed gaps between production and destruction rates.  
924 Reduced reaction rate constants of the RO<sub>2</sub>+NO reaction could be expected for RO<sub>2</sub> from large VOCs.  
925 However, the fraction of these RO<sub>2</sub> species is expected to be small for conditions of this campaign, even if  
926 OH reactivity that is not explained by measured OH reactants is attributed to large VOCs. Therefore, it  
927 seems unlikely that the mechanism suggested by Whalley et al. (2021) affects the observed discrepancies  
928 in the radical budgets in this study.

929 It is interesting to point out that similar discrepancies in the OH and HO<sub>2</sub> budgets have been observed during  
930 the HO<sub>x</sub>Comp campaign in July 2005 (Elshorbany et al., 2012). Although measurements were only done  
931 for 3 days and despite that these were 14 years earlier than measurements in this work, the chemical  
932 composition was similar with comparable values of NO<sub>x</sub>, O<sub>3</sub>, isoprene concentrations and of OH reactivity.  
933 As observed in this study, a missing OH radical source in the range of 2 to 4 ppbv h<sup>-1</sup> was needed to close  
934 the OH budget for low-NO chemical regimes. The lack of measured RO<sub>2</sub> radicals did not allow to perform  
935 a measurement-only budget for HO<sub>2</sub> radicals. Nevertheless, model calculations overestimated measured  
936 HO<sub>2</sub> radicals after the correction for RO<sub>2</sub> radical interferences (Fuchs et al., 2011) by up to 30% at low NO  
937 (Kanaya et al., 2012; Elshorbany et al., 2012). Like in this study, good agreement was found between  
938 modelled and measured OH and HO<sub>2</sub> radical concentrations only if an unknown loss process for HO<sub>2</sub>  
939 radicals that would recycle OH was introduced.

#### 940 4.4 Potential role of the missing radical processes on the evaluation of the ozone production rate



941 The good agreement of the odd oxygen production rates calculated by the two different methods (Section  
942 3.1) not only gives high confidence in the measured peroxy radical concentrations but also confirms the  
943 current chemical understanding of tropospheric ozone formation from the reaction of peroxy radicals with  
944 NO. Therefore, results demonstrate that accurate predictions of radical concentrations in atmospheric  
945 models are crucial to accurately predict the surface ozone level.

946 However, the significant level of the missing radical processes found in this study implies the difficulties  
947 in the prediction of the radical concentrations by the models without constraining radicals by their  
948 measurements. In low NO mixing ratios, there are two opposing effects of the missing radical processes on  
949 the O<sub>3</sub> formation. At first, a missing OH source and therefore an underestimation of OH concentrations by  
950 the models would lower the loss of NO<sub>2</sub> by the reduced reaction rate with OH, and essentially produce more  
951 O<sub>3</sub> by its photolysis. Furthermore, the production of RO<sub>2</sub> would be under-predicted due to the lower OH  
952 concentrations in the models. At the same time, an unexplained HO<sub>2</sub> sink would result in the over-prediction  
953 in HO<sub>2</sub> concentrations and thus O<sub>3</sub> production. In high NO environments, missing RO<sub>2</sub> and RO<sub>x</sub> production  
954 processes would result in an underestimation of the O<sub>3</sub> production.

955

## 956 **5 Summary and conclusions**

957 Ambient measurements of atmospheric radicals, trace gases, and aerosol properties were performed during  
958 the Jülich Atmospheric Chemistry Project campaign (JULIAC) using the atmospheric simulation chamber  
959 SAPHIR at Forschungszentrum Jülich, Germany. Ambient air was continuously drawn at a high rate into  
960 the chamber (1 hour residence time) through a 50 m high inlet line for one month in each season throughout  
961 2019.

962 For parts of the campaign, measurements of OH concentrations were achieved by two different methods,  
963 laser-induced fluorescence with a chemical modulation system for zeroing (FZJ-LIF-CMR) and differential  
964 optical absorption spectroscopy (FZJ-DOAS). Measurements of both instruments agreed within 11 % (Cho  
965 et al., 2021).

966 The production rate of odd oxygen (O<sub>x</sub>) was determined by using either measured HO<sub>2</sub> and RO<sub>2</sub>  
967 concentrations or O<sub>3</sub> and NO<sub>2</sub> concentrations measured in the chamber and in the incoming flow. Results  
968 showed excellent agreement between the two different methods confirming that HO<sub>2</sub> and RO<sub>2</sub> are  
969 responsible for the formation of tropospheric O<sub>3</sub> and giving additional confidence in the reliability of peroxy  
970 radical concentration measurements performed in the JULIAC campaign.

971 An analysis of the chemical budgets of OH, HO<sub>2</sub>, RO<sub>2</sub> and RO<sub>x</sub> radicals was performed for data obtained  
972 in the spring and summer periods of the campaign. On average, daytime radical turnover rates ranged  
973 between 3 to 6 ppbv h<sup>-1</sup> and 4 to 10 ppbv h<sup>-1</sup> in spring and summer, respectively, for OH, HO<sub>2</sub> and RO<sub>2</sub>  
974 radicals, while total rates of RO<sub>x</sub> initiation and termination reactions were below 2.0 ppbv h<sup>-1</sup>. For most  
975 conditions, radical production and destruction rates highly depended on the turnover rate of the reaction of  
976 peroxy radicals with NO. For the total turnover rate of the sum of all radicals (RO<sub>x</sub>), the photolysis of  
977 HONO and HCHO contributed most to the primary radical production and the reactions of OH with NO<sub>2</sub>  
978 and RO<sub>2</sub> with HO<sub>2</sub> dominated the radical termination processes.



979 Differences between radical production and destruction rates were often small and below the accuracy of  
980 the calculations in the JULIAC campaign in winter and autumn. However, for both spring and summer, an  
981 additional OH source is required to explain the observed discrepancy between production and destruction  
982 rates. The OH production rate of this source would need be on average 2 ppbv h<sup>-1</sup> and 3 ppbv h<sup>-1</sup> in the  
983 spring and summer period, respectively. This discrepancy is in the same range as observed for  
984 measurements at the same location during the HO<sub>x</sub>Comp campaign in July 2005 (Elshorbany et al., 2012).

985 Discrepancies between production and destruction rates of OH radicals were highest for conditions with  
986 low NO mixing ratios in this study. This is similar to findings in other field campaigns in China (Tan et al.,  
987 2017; Tan et al., 2019; Whalley et al., 2021). The high reliability of radical data in this study gives further  
988 confidence that the discrepancies arise from unaccounted chemical processes rather than from instrumental  
989 artefacts.

990 The highest unaccounted OH source with a rate of 3.0 ppbv h<sup>-1</sup> (51 % of the observed total OH destruction  
991 rate) is observed in the period from 5 August to 8 August (Case 1), when NO mixing ratios were less than  
992 1 ppbv and median maximum temperature in the chamber were 31 ° C. At the same time, an additional  
993 HO<sub>2</sub> destruction process with a rate of up to 2.0 ppbv h<sup>-1</sup> is required to balance the HO<sub>2</sub> production rate,  
994 while production and destruction rates for RO<sub>2</sub> radicals are well balanced. This indicates that an  
995 unaccounted HO<sub>2</sub> to OH radical propagation process could be present. In addition, part of the missing OH  
996 source could have been originated from a missing primary OH production process, because also a small  
997 difference between the total RO<sub>x</sub> production and destruction rates are observed. The missing RO<sub>x</sub> source  
998 was up to 0.5 ppbv h<sup>-1</sup> for Case 1, but was even higher with a rate of 1.4 ppbv h<sup>-1</sup> in the summer, when  
999 temperature were highest (Case 2).

1000 For NO mixing ratios in range of 1 to 3 ppbv, production and destruction rates for OH and HO<sub>2</sub> radicals  
1001 were balanced, while additional sources of RO<sub>2</sub> and RO<sub>x</sub> having on average rates of 1.6 ppbv h<sup>-1</sup> and 0.4  
1002 ppbv h<sup>-1</sup>, respectively, were required to balance their production and destruction rates. Therefore, part of  
1003 the missing RO<sub>2</sub> source can be explained by a primary radical source, but the remaining RO<sub>2</sub> source is still  
1004 unresolved.

1005 For high NO mixing ratios above 3 ppbv, 4 to 5 ppbv h<sup>-1</sup>, large discrepancies between production and  
1006 destruction rates of HO<sub>2</sub> and RO<sub>2</sub> radicals were found, but the calculations for these conditions have a higher  
1007 uncertainty due to low HO<sub>2</sub> and RO<sub>2</sub> concentrations close to background signals. Whereas the imbalance in  
1008 the budget for HO<sub>2</sub> radicals is due to an unaccounted loss processes, an additional RO<sub>2</sub> production processes  
1009 is required to close the chemical budget for RO<sub>2</sub> radicals. For the same conditions, a primary RO<sub>x</sub> source  
1010 with a rate of 0.5 ppbv h<sup>-1</sup> was needed to balance the RO<sub>x</sub> destruction rate. Therefore, the missing primary  
1011 RO<sub>x</sub> source is likely an unaccounted primary RO<sub>2</sub> source.

1012 Production of radicals from the oxidation of organic compounds by chlorine could have been one additional  
1013 source. Unfortunately, the potential impact of chlorine chemistry could not be examined in the spring  
1014 periods, when these conditions were experienced, because ClNO<sub>2</sub> measurements were not available. During  
1015 times when ClNO<sub>2</sub> concentrations were measured, chlorine chemistry initiated by the photolysis of ClNO<sub>2</sub>  
1016 did not significantly contribute to the radical production.

1017 For chemical conditions when the contribution of the reaction of HO<sub>2</sub> with NO to the OH production was  
1018 reduced, i.e. at lower NO levels, other radical formation pathways such as isomerization reactions of RO<sub>2</sub>



1019 radicals, OH formation from ozonolysis of alkenes or photolysis of multifunctional organic compounds  
1020 could gain in importance and need to be properly accounted for. These processes remain relatively poorly  
1021 constrained due to the lack of direct measurements of e.g., multifunctional organic compounds.

1022 Although the exact mechanism for the missing production or destruction processes for OH, HO<sub>2</sub> and RO<sub>2</sub>  
1023 radicals could not be determined from measurements in this campaign, knowing the magnitudes of the  
1024 missing radical processes gives indicative information about the disagreements of model simulations and  
1025 observations for radicals and secondary air pollutants.

1026 More investigations of the chemical budgets of radicals for example in environments with high NO mixing  
1027 ratios including the determination of the impact of chlorine chemistry and with a detailed characterization  
1028 of the chemical composition of air masses with respect to the presence of complex organic compounds  
1029 would be beneficial for the understanding of radical chemistry as well as of the formation of secondary air  
1030 pollution such as ozone.

1031

#### 1032 **Code and data availability**

1033 Data of the JULIAC campaign analyzed in this work is available from the Jülich Data repository  
1034 (<https://doi.org/10.26165/JUELICH-DATA/3J80BW>, Cho et al., 2022).

1035

#### 1036 **Author contributions**

1037 AH designed JULIAC campaign and organized it together with HF and FH. CC performed the  
1038 measurements of radicals, analyzed the data, and wrote the paper together with AN and HF. All co-authors  
1039 contributed with data and helped the writing by intensive discussions of the manuscript.

1040

#### 1041 **Competing interests**

1042 The authors declare that they have no conflict of interest.

1043

#### 1044 **Financial Support**

1045 This project has received funding from the European Research Council (ERC) under the European Union's  
1046 Horizon 2020 research and innovation program (SARLEP grant agreement no. 681529) and from the  
1047 European Commission (EC) (Eurochamp 2020 project, grant agreement no. 730997).

1048

#### 1049 **References**

1050 Atkinson, R., Baulch, D. L., Cox, R. A., Crowley, J. N., Hampson, R. F., Hynes, R. G., Jenkin, M. E., Rossi, M.  
1051 J., and Troe, J.: Evaluated kinetic and photochemical data for atmospheric chemistry: Volume I - gas



- 1052 phase reactions of Ox, HOx, NOx and SOx species, *Atmos. Chem. Phys.*, 4, 1461-1738, doi:10.5194/acp-4-  
1053 1461-2004, 2004.
- 1054  
1055 Atkinson, R., Baulch, D. L., Cox, R. A., Crowley, J. N., Hampson, R. F., Hynes, R. G., Jenkin, M. E., Rossi, M.  
1056 J., Troe, J., and Subcommittee, I.: Evaluated kinetic and photochemical data for atmospheric chemistry:  
1057 Volume II - gas phase reactions of organic species, *Atmos. Chem. Phys.*, 6, 3625-4055, doi:10.5194/acp-  
1058 6-3625-2006, 2006.
- 1059  
1060 Bloss, W. J., Lee, J. D., Johnson, G. P., Sommariva, R., Heard, D. E., Saiz-Lopez, A., Plane, J. M. C.,  
1061 McFiggans, G., Coe, H., Flynn, M., Williams, P., Rickard, A. R., and Fleming, Z. L.: Impact of halogen  
1062 monoxide chemistry upon boundary layer OH and HO<sub>2</sub> concentrations at a coastal site, *Geophysical*  
1063 *Research Letters*, 32, doi:10.1029/2004GL022084, 2005.
- 1064  
1065 BMEL: (Federal Ministry of Food and Agriculture) : Ergebnisse der Waldzustandserhebung 2020, in,  
1066 Bonn, Germany, 2021.
- 1067  
1068 Bohn, B., Rohrer, F., Brauers, T., and Wahner, A.: Actinometric measurements of NO<sub>2</sub> photolysis  
1069 frequencies in the atmosphere simulation chamber SAPHIR, *Atmos. Chem. Phys.*, 5, 493-503,  
1070 doi:10.5194/acp-5-493-2005, 2005.
- 1071  
1072 Bohn, B., and Zilken, H.: Model-aided radiometric determination of photolysis frequencies in a sunlit  
1073 atmosphere simulation chamber, *Atmos. Chem. Phys.*, 5, 191-206, doi:10.5194/acp-5-191-2005, 2005.
- 1074  
1075 Brune, W. H., Baier, B. C., Thomas, J., Ren, X., Cohen, R. C., Pusede, S. E., Browne, E. C., Goldstein, A. H.,  
1076 Gentner, D. R., Keutsch, F. N., Thornton, J. A., Harrold, S., Lopez-Hilfiker, F. D., and Wennberg, P. O.:  
1077 Ozone production chemistry in the presence of urban plumes, *Faraday Discuss.*, 189, 169-189,  
1078 doi:10.1039/C5FD00204D, 2016.
- 1079  
1080 Cazorla, M., Brune, W. H., Ren, X., and Lefer, B.: Direct measurement of ozone production rates in  
1081 Houston in 2009 and comparison with two estimation methods, *Atmos. Chem. Phys.*, 12, 1203-1212,  
1082 doi:10.5194/acp-12-1203-2012, 2012.
- 1083  
1084 Chen, S., Ren, X., Mao, J., Chen, Z., Brune, W. H., Lefer, B., Rappenglück, B., Flynn, J., Olson, J., and  
1085 Crawford, J. H.: A comparison of chemical mechanisms based on TRAMP-2006 field data, *Atmos.*  
1086 *Environ.*, 44, 4116-4125, doi:10.1016/j.atmosenv.2009.05.027, 2010.
- 1087  
1088 Cho, C., Hofzumahaus, A., Fuchs, H., Dorn, H. P., Glowania, M., Holland, F., Rohrer, F., Vardhan, V.,  
1089 Kiendler-Scharr, A., Wahner, A., and Novelli, A.: Characterization of a chemical modulation reactor  
1090 (CMR) for the measurement of atmospheric concentrations of hydroxyl radicals with a laser-induced  
1091 fluorescence instrument, *Atmos. Meas. Tech.*, 14, 1851-1877, do



- 1092 Cho, C., Fuchs, H., Hofzumahaus, A., Holland, F., Bohn, B., Glowania, M., Hohaus, T., Lu, L., Niether, D.,  
1093 Rohrer, F., Sommariva, R., Tan, Z., Tillmann, R., Kiendler-Scharr, A., Wahner, A., and Novelli, A.: Data  
1094 Experiments SAPHIR chamber Campaign JULIAC 2019, Jülich Data [Data set],  
1095 <https://doi.org/10.26165/JUELICH-DATA/3J80BW>, 2022
- 1096  
1097 Cox, R. A., Ammann, M., Crowley, J. N., Herrmann, H., Jenkin, M. E., McNeill, V. F., Mellouki, A., Troe, J.,  
1098 and Wallington, T. J.: Evaluated kinetic and photochemical data for atmospheric chemistry: Volume VII –  
1099 Criegee intermediates, *Atmos. Chem. Phys.*, 20, 13497-13519, doi:10.5194/acp-20-13497-2020, 2020.
- 1100  
1101 Crouse, J. D., Paulot, F., Kjaergaard, H. G., and Wennberg, P. O.: Peroxy radical isomerization in the  
1102 oxidation of isoprene, *Phys. Chem. Chem. Phys.*, 13, 13607-13613, doi:10.1039/C1CP21330J, 2011.
- 1103  
1104 Crouse, J. D., Knap, H. C., Ørnsø, K. B., Jørgensen, S., Paulot, F., Kjaergaard, H. G., and Wennberg, P. O.:  
1105 Atmospheric Fate of Methacrolein. 1. Peroxy Radical Isomerization Following Addition of OH and O<sub>2</sub>, *J.*  
1106 *Phys. Chem. A*, 116, 5756-5762, doi:10.1021/jp211560u, 2012.
- 1107  
1108 da Silva, G., Graham, C., and Wang, Z.-F.: Unimolecular  $\beta$ -hydroxyperoxy radical decomposition with OH  
1109 recycling in the photochemical oxidation of isoprene, *Environ. Sci. Technol.*, 44, 250-256,  
1110 doi:10.1021/es900924d, 2010.
- 1111  
1112 Dillon, T. J., and Crowley, J. N.: Direct detection of OH formation in the reactions of HO<sub>2</sub> with CH<sub>3</sub>C(O)O<sub>2</sub>  
1113 and other substituted peroxy radicals, *Atmos. Chem. Phys.*, 8, 4877-4889, doi:10.5194/acp-8-4877-2008,  
1114 2008.
- 1115  
1116 Dusanter, S., Vimal, D., Stevens, P. S., Volkamer, R., Molina, L. T., Baker, A., Meinardi, S., Blake, D.,  
1117 Sheehy, P., Merten, A., Zhang, R., Zheng, J., Fortner, E. C., Junkermann, W., Dubey, M., Rahn, T.,  
1118 Eichinger, B., Lewandowski, P., Prueger, J., and Holder, H.: Measurements of OH and HO<sub>2</sub> concentrations  
1119 during the MCMA-2006 field campaign – Part 2: Model comparison and radical budget, *Atmos. Chem.*  
1120 *Phys.*, 9, 6655-6675, doi:10.5194/acp-9-6655-2009, 2009.
- 1121  
1122 Ehhalt, D. H., and Rohrer, F.: Dependence of the OH concentration on solar UV, *J. Geophys. Res.: Atmos.*,  
1123 105, 3565-3571, doi:10.1029/1999jd901070, 2000.
- 1124  
1125 Elshorbany, Y. F., Kleffmann, J., Hofzumahaus, A., Kurtenbach, R., Wiesen, P., Brauers, T., Bohn, B., Dorn,  
1126 H.-P., Fuchs, H., Holland, F., Rohrer, F., Tillmann, R., Wegener, R., Wahner, A., Kanaya, Y., Yoshino, A.,  
1127 Nishida, S., Kajii, Y., Martinez, M., Kubistin, D., Harder, H., Lelieveld, J., Elste, T., Plass-Dülmer, C., Stange,  
1128 G., Berresheim, H., and Schurath, U.: HO<sub>x</sub> budgets during HO<sub>x</sub>Comp: A case study of HO<sub>x</sub> chemistry  
1129 under NO<sub>x</sub>-limited conditions, *J. Geophys. Res.: Atmos.*, 117, doi:10.1029/2011JD017008, 2012.
- 1130  
1131 Fan, S., and Li, Y.: The impacts of marine-emitted halogens on OH radicals in East Asia during summer,  
1132 *Atmos. Chem. Phys.*, 22, 7331-7351, doi:10.5194/acp-22-7331-2022, 2022.





- 1133  
1134 Fishman, J., and Carney, T. A.: A one-dimensional photochemical model of the troposphere with  
1135 planetary boundary-layer parameterization, *J. Atmos. Chem.*, 1, 351-376, doi:10.1007/BF00053800,  
1136 1984.
- 1137  
1138 Fuchs, H., Holland, F., and Hofzumahaus, A.: Measurement of tropospheric RO<sub>2</sub> and HO<sub>2</sub> radicals by a  
1139 laser-induced fluorescence instrument, *Rev. Sci. Instrum.*, 79, 084104, doi:10.1063/1.2968712, 2008.
- 1140  
1141 Fuchs, H., Bohn, B., Hofzumahaus, A., Holland, F., Lu, K. D., Nehr, S., Rohrer, F., and Wahner, A.:  
1142 Detection of HO<sub>2</sub> by laser-induced fluorescence: calibration and interferences from RO<sub>2</sub> radicals, *Atmos.*  
1143 *Meas. Tech.*, 4, 1209-1225, doi:10.5194/amt-4-1209-2011, 2011.
- 1144  
1145 Fuchs, H., Dorn, H. P., Bachner, M., Bohn, B., Brauers, T., Gomm, S., Hofzumahaus, A., Holland, F., Nehr,  
1146 S., Rohrer, F., Tillmann, R., and Wahner, A.: Comparison of OH concentration measurements by DOAS  
1147 and LIF during SAPHIR chamber experiments at high OH reactivity and low NO concentration, *Atmos.*  
1148 *Meas. Tech.*, 5, 1611-1626, doi:10.5194/amt-5-1611-2012, 2012.
- 1149  
1150 Fuchs, H., Hofzumahaus, A., Rohrer, F., Bohn, B., Brauers, T., Dorn, H. P., Häsel, R., Holland, F.,  
1151 Kaminski, M., Li, X., Lu, K., Nehr, S., Tillmann, R., Wegener, R., and Wahner, A.: Experimental evidence  
1152 for efficient hydroxyl radical regeneration in isoprene oxidation, *Nat. Geosci.*, 6, 1023-1026,  
1153 doi:10.1038/ngeo1964, 2013.
- 1154  
1155 Fuchs, H., Acir, I. H., Bohn, B., Brauers, T., Dorn, H. P., Häsel, R., Hofzumahaus, A., Holland, F.,  
1156 Kaminski, M., Li, X., Lu, K., Lutz, A., Nehr, S., Rohrer, F., Tillmann, R., Wegener, R., and Wahner, A.: OH  
1157 regeneration from methacrolein oxidation investigated in the atmosphere simulation chamber SAPHIR,  
1158 *Atmos. Chem. Phys.*, 14, 7895-7908, doi:10.5194/acp-14-7895-2014, 2014.
- 1159  
1160 Fuchs, H., Novelli, A., Rolletter, M., Hofzumahaus, A., Pfannerstill, E. Y., Kessel, S., Edtbauer, A., Williams,  
1161 J., Michoud, V., Dusanter, S., Locoge, N., Zannoni, N., Gros, V., Truong, F., Sarda-Estève, R., Cryer, D. R.,  
1162 Brumby, C. A., Whalley, L. K., Stone, D., Seakins, P. W., Heard, D. E., Schoemaeker, C., Blocquet, M.,  
1163 Coudert, S., Batut, S., Fittschen, C., Thames, A. B., Brune, W. H., Ernest, C., Harder, H., Müller, J. B. A.,  
1164 Elste, T., Kubistin, D., Andres, S., Bohn, B., Hohaus, T., Holland, F., Li, X., Rohrer, F., Kiendler-Scharr, A.,  
1165 Tillmann, R., Wegener, R., Yu, Z., Zou, Q., and Wahner, A.: Comparison of OH reactivity measurements in  
1166 the atmospheric simulation chamber SAPHIR, *Atmos. Meas. Tech.*, 10, 4023-4053, doi:10.5194/amt-10-  
1167 4023-2017, 2017.
- 1168  
1169 Fuchs, H., Albrecht, S., Acir, I., Bohn, B., Breitenlechner, M., Dorn, H. P., Gkatzelis, G. I., Hofzumahaus, A.,  
1170 Holland, F., Kaminski, M., Keutsch, F. N., Novelli, A., Reimer, D., Rohrer, F., Tillmann, R., Vereecken, L.,  
1171 Wegener, R., Zaytsev, A., Kiendler-Scharr, A., and Wahner, A.: Investigation of the oxidation of methyl  
1172 vinyl ketone (MVK) by OH radicals in the atmospheric simulation chamber SAPHIR, *Atmos. Chem. Phys.*,  
1173 18, 8001-8016, doi:10.5194/acp-18-8001-2018, 2018.
- 1174



- 1175 George, I. J., Vlasenko, A., Slowik, J. G., Broekhuizen, K., and Abbatt, J. P. D.: Heterogeneous oxidation of  
1176 saturated organic aerosols by hydroxyl radicals: uptake kinetics, condensed-phase products, and particle  
1177 size change, *Atmos. Chem. Phys.*, 7, 4187-4201, doi:10.5194/acp-7-4187-2007, 2007.
- 1178  
1179 George, I. J., Matthews, P. S. J., Whalley, L. K., Brooks, B., Goddard, A., Baeza-Romero, M. T., and Heard,  
1180 D. E.: Measurements of uptake coefficients for heterogeneous loss of HO<sub>2</sub> onto submicron inorganic salt  
1181 aerosols, *Phys. Chem. Chem. Phys.*, 15, 12829-12845, doi:10.1039/C3CP51831K, 2013.
- 1182  
1183 Glowania, M., Rohrer, F., Dorn, H. P., Hofzumahaus, A., Holland, F., Kiendler-Scharr, A., Wahner, A., and  
1184 Fuchs, H.: Comparison of formaldehyde measurements by Hantzsch, CRDS and DOAS in the SAPHIR  
1185 chamber, *Atmos. Meas. Tech. Discuss.*, 2021, 1-23, doi:10.5194/amt-2021-10, 2021.
- 1186  
1187 Goldberg, D. L., Vinciguerra, T. P., Hosley, K. M., Loughner, C. P., Canty, T. P., Salawitch, R. J., and  
1188 Dickerson, R. R.: Evidence for an increase in the ozone photochemical lifetime in the eastern United  
1189 States using a regional air quality model, *J. Geophys. Res.: Atmos.*, 120, 12778-12793,  
1190 doi:10.1002/2015JD023930, 2015.
- 1191  
1192 Goldstein, A. H., Fan, S. M., Goulden, M. L., Munger, J. W., and Wofsy, S. C.: Emissions of ethene,  
1193 propene, and 1-butene by a midlatitude forest, *Journal of Geophysical Research: Atmospheres*, 101,  
1194 9149-9157, doi:10.1029/96JD00334, 1996.
- 1195  
1196 Goldstein, A. H., and Galbally, I. E.: Known and Unexplored Organic Constituents in the Earth's  
1197 Atmosphere, *Environ. Sci. Technol.*, 41, 1514-1521, doi:10.1021/es072476p, 2007.
- 1198  
1199 Griffith, S. M., Hansen, R. F., Dusanter, S., Michoud, V., Gilman, J. B., Kuster, W. C., Veres, P. R., Graus,  
1200 M., de Gouw, J. A., Roberts, J., Young, C., Washenfelder, R., Brown, S. S., Thalman, R., Waxman, E.,  
1201 Volkamer, R., Tsai, C., Stutz, J., Flynn, J. H., Grossberg, N., Lefer, B., Alvarez, S. L., Rappenglueck, B.,  
1202 Mielke, L. H., Osthoff, H. D., and Stevens, P. S.: Measurements of hydroxyl and hydroperoxy radicals  
1203 during CalNex-LA: Model comparisons and radical budgets, *J. Geophys. Res.: Atmos.*, 121, 4211-4232,  
1204 doi:10.1002/2015jd024358, 2016.
- 1205  
1206 Groß, C. B. M., Dillon, T. J., Schuster, G., Lelieveld, J., and Crowley, J. N.: Direct Kinetic Study of OH and  
1207 O<sub>3</sub> Formation in the Reaction of CH<sub>3</sub>C(O)O<sub>2</sub> with HO<sub>2</sub>, *J. Phys. Chem. A*, 118, 974-985,  
1208 doi:10.1021/jp412380z, 2014.
- 1209  
1210 Han, S., Bian, H., Feng, Y., Liu, A., Li, X., Zeng, F., and Zhang, X.: Analysis of the Relationship between O<sub>3</sub>,  
1211 NO and NO<sub>2</sub> in Tianjin, China, *Aerosol Air Qual. Res.*, 11, 128-139, doi:10.4209/aaqr.2010.07.0055, 2011.
- 1212  
1213 Handisides, G. M., Plass-Dülmer, C., Gilge, S., Bingemer, H., and Berresheim, H.: Hohenpeissenberg  
1214 Photochemical Experiment (HOPE 2000): Measurements and photostationary state calculations of OH  
1215 and peroxy radicals, *Atmos. Chem. Phys.*, 3, 1565-1588, doi:10.5194/acp-3-1565-2003, 2003.



- 1216  
1217 Häsel, R., Brauers, T., Holland, F., and Wahner, A.: Development and application of a new mobile  
1218 LOPAP instrument for the measurement of HONO altitude profiles in the planetary boundary layer,  
1219 Atmos. Meas. Tech. Discuss., 2009, 2027-2054, doi:10.5194/amtd-2-2027-2009, 2009.
- 1220  
1221 Hasson, A. S., Tyndall, G. S., and Orlando, J. J.: A Product Yield Study of the Reaction of HO<sub>2</sub> Radicals with  
1222 Ethyl Peroxy (C<sub>2</sub>H<sub>5</sub>O<sub>2</sub>), Acetyl Peroxy (CH<sub>3</sub>C(O)O<sub>2</sub>), and Acetonyl Peroxy (CH<sub>3</sub>C(O)CH<sub>2</sub>O<sub>2</sub>) Radicals, J. Phys.  
1223 Chem. A, 108, 5979-5989, doi:10.1021/jp048873t, 2004.
- 1224  
1225 Hens, K., Novelli, A., Martinez, M., Auld, J., Axinte, R., Bohn, B., Fischer, H., Keronen, P., Kubistin, D.,  
1226 Nölscher, A. C., Oswald, R., Paasonen, P., Petäjä, T., Regelin, E., Sander, R., Sinha, V., Sipilä, M.,  
1227 Taraborrelli, D., Tatum Ernest, C., Williams, J., Lelieveld, J., and Harder, H.: Observation and modelling of  
1228 HOx radicals in a boreal forest, Atmos. Chem. Phys., 14, 8723-8747, doi:10.5194/acp-14-8723-2014,  
1229 2014.
- 1230  
1231 Hofzumahaus, A., Rohrer, F., Lu, K., Bohn, B., Brauers, T., Chang, C.-C., Fuchs, H., Holland, F., Kita, K.,  
1232 Kondo, Y., Li, X., Lou, S., Shao, M., Zeng, L., Wahner, A., and Zhang, Y.: Amplified trace gas removal in the  
1233 troposphere, Science, 324, 1702-1704, doi:10.1126/science.1164566, 2009.
- 1234  
1235 Hofzumahaus, A., and Heard, D. H.: Assessment of local HOx and ROx measurement techniques:  
1236 achievements, challenges, and future directions - Outcomes of the 2015 international HOx workshop,  
1237 Forschungszentrum Jülich, Jülich, 20-21, 2016.
- 1238  
1239 Holland, F., Hofzumahaus, A., Schäfer, J., Kraus, A., and Pätz, H.-W.: Measurements of OH and HO<sub>2</sub>  
1240 radical concentrations and photolysis frequencies during BERLIOZ, J. Geophys. Res.: Atmos., 108, 8246,  
1241 doi:10.1029/2001jd001393, 2003.
- 1242  
1243 J. B. Burkholder, S. P. S., J. Abbatt, J. R. Barker, C. Cappa, J. D. Crouse, T. S. Dibble, R. E. Huie, C. E. Kolb,  
1244 M. J. Kurylo, V. L. Orkin, C. J. Percival, D. M. Wilmouth, and P. H. Wine: Chemical Kinetics and  
1245 Photochemical Data for Use in Atmospheric Studies, Evaluation No. 19, Jet Propulsion Laboratory,  
1246 Pasadena, 2019.
- 1247  
1248 Jenkin, M. E., Valorso, R., Aumont, B., and Rickard, A. R.: Estimation of rate coefficients and branching  
1249 ratios for reactions of organic peroxy radicals for use in automated mechanism construction, Atmos.  
1250 Chem. Phys., 19, 7691-7717, doi:10.5194/acp-19-7691-2019, 2019.
- 1251  
1252 Jordan, A., Haidacher, S., Hanel, G., Hartungen, E., Märk, L., Seehauser, H., Schottkowsky, R., Sulzer, P.,  
1253 and Märk, T. D.: A high resolution and high sensitivity proton-transfer-reaction time-of-flight mass  
1254 spectrometer (PTR-TOF-MS), Int. J. Mass Spectrom., 286, 122-128, doi:10.1016/j.ijms.2009.07.005,  
1255 2009.
- 1256



1257 Kaminski, M., Fuchs, H., Acir, I. H., Bohn, B., Brauers, T., Dorn, H. P., Häsel, R., Hofzumahaus, A., Li, X.,  
1258 Lutz, A., Nehr, S., Rohrer, F., Tillmann, R., Vereecken, L., Wegener, R., and Wahner, A.: Investigation of  
1259 the  $\beta$ -pinene photooxidation by OH in the atmosphere simulation chamber SAPHIR, *Atmos. Chem. Phys.*,  
1260 17, 6631-6650, doi:10.5194/acp-17-6631-2017, 2017.

1261  
1262 Kanaya, Y., Cao, R., Akimoto, H., Fukuda, M., Komazaki, Y., Yokouchi, Y., Koike, M., Tanimoto, H.,  
1263 Takegawa, N., and Kondo, Y.: Urban photochemistry in central Tokyo: 1. Observed and modeled OH and  
1264 HO<sub>2</sub> radical concentrations during the winter and summer of 2004, *J. Geophys. Res.: Atmos.*, 112,  
1265 doi:10.1029/2007jd008670, 2007.

1266  
1267 Kanaya, Y., Hofzumahaus, A., Dorn, H. P., Brauers, T., Fuchs, H., Holland, F., Rohrer, F., Bohn, B.,  
1268 Tillmann, R., Wegener, R., Wahner, A., Kajii, Y., Miyamoto, K., Nishida, S., Watanabe, K., Yoshino, A.,  
1269 Kubistin, D., Martinez, M., Rudolf, M., Harder, H., Berresheim, H., Elste, T., Plass-Dülmer, C., Stange, G.,  
1270 Kleffmann, J., Elshorbany, Y., and Schurath, U.: Comparisons of observed and modeled OH and HO<sub>2</sub>  
1271 concentrations during the ambient measurement period of the HOxComp field campaign, *Atmos. Chem.*  
1272 *Phys.*, 12, 2567-2585, doi:10.5194/acp-12-2567-2012, 2012.

1273  
1274 Kim, S., Wolfe, G. M., Mauldin, L., Cantrell, C., Guenther, A., Karl, T., Turnipseed, A., Greenberg, J., Hall,  
1275 S. R., Ullmann, K., Apel, E., Hornbrook, R., Kajii, Y., Nakashima, Y., Keutsch, F. N., DiGangi, J. P., Henry, S.  
1276 B., Kaser, L., Schnitzhofer, R., Graus, M., Hansel, A., Zheng, W., and Flocke, F. F.: Evaluation of HO<sub>x</sub>  
1277 sources and cycling using measurement-constrained model calculations in a 2-methyl-3-butene-2-ol  
1278 (MBO) and monoterpene (MT) dominated ecosystem, *Atmos. Chem. Phys.*, 13, 2031-2044,  
1279 doi:10.5194/acp-13-2031-2013, 2013.

1280  
1281 Kleffmann, J., Lörzer, J. C., Wiesen, P., Kern, C., Trick, S., Volkamer, R., Rodenas, M., and Wirtz, K.:  
1282 Intercomparison of the DOAS and LOPAP techniques for the detection of nitrous acid (HONO), *Atmos.*  
1283 *Environ.*, 40, 3640-3652, doi:10.1016/j.atmosenv.2006.03.027, 2006.

1284  
1285 Kleinman, L. I., Daum, P. H., Lee, Y.-N., Nunnermacker, L. J., Springston, S. R., Weinstein-Lloyd, J., and  
1286 Rudolph, J.: Ozone production efficiency in an urban area, *J. Geophys. Res.: Atmos.*, 107, ACH 23-21-ACH  
1287 23-12, doi:10.1029/2002JD002529, 2002.

1288  
1289 Komenda, M., Schaub, A., and Koppmann, R.: Description and characterization of an on-line system for  
1290 long-term measurements of isoprene, methyl vinyl ketone, and methacrolein in ambient air, *J.*  
1291 *Chromatogr. A*, 995, 185-201, doi:10.1016/S0021-9673(03)00518-1, 2003.

1292  
1293 Konrad, S., Schmitz, T., Buers, H.-J., Houben, N., Mannschreck, K., Mihelcic, D., Müsgen, P., Pätz, H.-W.,  
1294 Holland, F., Hofzumahaus, A., Schäfer, H.-J., Schröder, S., Volz-Thomas, A., Bächmann, K., Schlomski, S.,  
1295 Moortgat, G., and Großmann, D.: Hydrocarbon measurements at Pabstthum during the BERLIOZ  
1296 campaign and modeling of free radicals, *J. Geophys. Res.: Atmos.*, 108, doi:10.1029/2001JD000866,  
1297 2003.

1298



- 1299 Kubistin, D., Harder, H., Martinez, M., Rudolf, M., Sander, R., Bozem, H., Eerdeken, G., Fischer, H., Gurk,  
1300 C., Klupfel, T., Konigstedt, R., Parchatka, U., Schiller, C. L., Stickler, A., Taraborrelli, D., Williams, J., and  
1301 Lelieveld, J.: Hydroxyl radicals in the tropical troposphere over the Suriname rainforest: comparison of  
1302 measurements with the box model MECCA, *Atmos. Chem. Phys.*, **10**, 9705-9728, doi:10.5194/acp-10-  
1303 9705-2010, 2010.
- 1304  
1305 Lakey, P. S. J., George, I. J., Whalley, L. K., Baeza-Romero, M. T., and Heard, D. E.: Measurements of the  
1306 HO<sub>2</sub> Uptake Coefficients onto Single Component Organic Aerosols, *Environ. Sci. Technol.*, **49**, 4878-4885,  
1307 doi:10.1021/acs.est.5b00948, 2015.
- 1308  
1309 Lelieveld, J., Butler, T. M., Crowley, J. N., Dillon, T. J., Fischer, H., Ganzeveld, L., Harder, H., Lawrence, M.  
1310 G., Martinez, M., Taraborrelli, D., and Williams, J.: Atmospheric oxidation capacity sustained by a  
1311 tropical forest, *Nature*, **452**, 737, doi:10.1038/nature06870, 2008.
- 1312  
1313 Lou, S., Holland, F., Rohrer, F., Lu, K., Bohn, B., Brauers, T., Chang, C. C., Fuchs, H., Häsel, R., Kita, K.,  
1314 Kondo, Y., Li, X., Shao, M., Zeng, L., Wahner, A., Zhang, Y., Wang, W., and Hofzumahaus, A.: Atmospheric  
1315 OH reactivities in the Pearl River Delta – China in summer 2006: measurement and model results,  
1316 *Atmos. Chem. Phys.*, **10**, 11243-11260, doi:10.5194/acp-10-11243-2010, 2010.
- 1317  
1318 Lu, K. D., Hofzumahaus, A., Holland, F., Bohn, B., Brauers, T., Fuchs, H., Hu, M., Häsel, R., Kita, K.,  
1319 Kondo, Y., Li, X., Lou, S. R., Oebel, A., Shao, M., Zeng, L. M., Wahner, A., Zhu, T., Zhang, Y. H., and Rohrer,  
1320 F.: Missing OH source in a suburban environment near Beijing: observed and modelled OH and HO<sub>2</sub>  
1321 concentrations in summer 2006, *Atmos. Chem. Phys.*, **13**, 1057-1080, doi:10.5194/acp-13-1057-2013,  
1322 2013.
- 1323  
1324 Lu, K. D., Rohrer, F., Holland, F., Fuchs, H., Brauers, T., Oebel, A., Dlugi, R., Hu, M., Li, X., Lou, S. R., Shao,  
1325 M., Zhu, T., Wahner, A., Zhang, Y. H., and Hofzumahaus, A.: Nighttime observation and chemistry of HO<sub>x</sub>  
1326 in the Pearl River Delta and Beijing in summer 2006, *Atmos. Chem. Phys.*, **14**, 4979-4999,  
1327 doi:10.5194/acp-14-4979-2014, 2014.
- 1328  
1329 Ma, X., Tan, Z., Lu, K., Yang, X., Liu, Y., Li, S., Li, X., Chen, S., Novelli, A., Cho, C., Zeng, L., Wahner, A., and  
1330 Zhang, Y.: Winter photochemistry in Beijing: Observation and model simulation of OH and HO<sub>2</sub> radicals  
1331 at an urban site, *Sci. Tot. Environ.*, **685**, 85-95, doi:10.1016/j.scitotenv.2019.05.329, 2019.
- 1332  
1333 Malkin, T. L., Goddard, A., Heard, D. E., and Seakins, P. W.: Measurements of OH and HO<sub>2</sub>  
1334 yields from the gas phase ozonolysis of isoprene, *Atmos. Chem. Phys.*, **10**, 1441-1459, doi:10.5194/acp-  
1335 10-1441-2010, 2010.
- 1336  
1337 Mao, J., Ren, X., Chen, S., Brune, W. H., Chen, Z., Martinez, M., Harder, H., Lefer, B., Rappenglück, B.,  
1338 Flynn, J., and Leuchner, M.: Atmospheric oxidation capacity in the summer of Houston 2006:  
1339 Comparison with summer measurements in other metropolitan studies, *Atmos. Environ.*, **44**, 4107-4115,  
1340 doi:doi.org/10.1016/j.atmosenv.2009.01.013, 2010.



- 1341  
1342 Mao, J., Ren, X., Zhang, L., Van Duin, D. M., Cohen, R. C., Park, J. H., Goldstein, A. H., Paulot, F., Beaver,  
1343 M. R., Crounse, J. D., Wennberg, P. O., DiGangi, J. P., Henry, S. B., Keutsch, F. N., Park, C., Schade, G. W.,  
1344 Wolfe, G. M., Thornton, J. A., and Brune, W. H.: Insights into hydroxyl measurements and atmospheric  
1345 oxidation in a California forest, *Atmos. Chem. Phys.*, 12, 8009-8020, doi:10.5194/acp-12-8009-2012,  
1346 2012.
- 1347  
1348 Martinez, M., Harder, H., Kovacs, T. A., Simpas, J. B., Bassis, J., Leshner, R., Brune, W. H., Frost, G. J.,  
1349 Williams, E. J., Stroud, C. A., Jobson, B. T., Roberts, J. M., Hall, S. R., Shetter, R. E., Wert, B., Fried, A.,  
1350 Alicke, B., Stutz, J., Young, V. L., White, A. B., and Zamora, R. J.: OH and HO<sub>2</sub> concentrations, sources, and  
1351 loss rates during the Southern Oxidants Study in Nashville, Tennessee, summer 1999, *J. Geophys. Res.*:  
1352 *Atmos.*, 108, doi:10.1029/2003JD003551, 2003.
- 1353  
1354 Mihelcic, D., Holland, F., Hofzumahaus, A., Hoppe, L., Konrad, S., Müsgen, P., Pätz, H.-W., Schäfer, H.-J.,  
1355 Schmitz, T., Volz-Thomas, A., Bächmann, K., Schlomski, S., Platt, U., Geyer, A., Alicke, B., and Moortgat,  
1356 G. K.: Peroxy radicals during BERLIOZ at Pabstthum: Measurements, radical budgets and ozone  
1357 production, *J. Geophys. Res.*: *Atmos.*, 108, doi:10.1029/2001JD001014, 2003.
- 1358  
1359 Novelli, A., Hens, K., Tatum Ernest, C., Kubistin, D., Regelin, E., Elste, T., Plass-Dülmer, C., Martinez, M.,  
1360 Lelieveld, J., and Harder, H.: Characterisation of an inlet pre-injector laser-induced fluorescence  
1361 instrument for the measurement of atmospheric hydroxyl radicals, *Atmos. Meas. Tech.*, 7, 3413-3430,  
1362 doi:10.5194/amt-7-3413-2014, 2014.
- 1363  
1364 Novelli, A., Kaminski, M., Rolletter, M., Acir, I. H., Bohn, B., Dorn, H. P., Li, X., Lutz, A., Nehr, S., Rohrer, F.,  
1365 Tillmann, R., Wegener, R., Holland, F., Hofzumahaus, A., Kiendler-Scharr, A., Wahner, A., and Fuchs, H.:  
1366 Evaluation of OH and HO<sub>2</sub> concentrations and their budgets during photooxidation of 2-methyl-3-  
1367 butene-2-ol (MBO) in the atmospheric simulation chamber SAPHIR, *Atmos. Chem. Phys.*, 18, 11409-  
1368 11422, doi:10.5194/acp-18-11409-2018, 2018.
- 1369  
1370 Novelli, A., Vereecken, L., Bohn, B., Dorn, H. P., Gkatzelis, G. I., Hofzumahaus, A., Holland, F., Reimer, D.,  
1371 Rohrer, F., Rosanka, S., Taraborrelli, D., Tillmann, R., Wegener, R., Yu, Z., Kiendler-Scharr, A., Wahner, A.,  
1372 and Fuchs, H.: Importance of isomerization reactions for OH radical regeneration from the photo-  
1373 oxidation of isoprene investigated in the atmospheric simulation chamber SAPHIR, *Atmos. Chem. Phys.*,  
1374 20, 3333-3355, doi:10.5194/acp-20-3333-2020, 2020.
- 1375  
1376 Novelli, A., Cho, C., Fuchs, H., Hofzumahaus, A., Rohrer, F., Tillmann, R., Kiendler-Scharr, A., Wahner, A.,  
1377 and Vereecken, L.: Experimental and theoretical study on the impact of a nitrate group on the chemistry  
1378 of alkoxy radicals, *Phys. Chem. Chem. Phys.*, 23, 5474-5495, doi:10.1039/d0cp05555g, 2021.
- 1379  
1380 Osthoff, H. D., Roberts, J. M., Ravishankara, A. R., Williams, E. J., Lerner, B. M., Sommariva, R., Bates, T.  
1381 S., Coffman, D., Quinn, P. K., Dibb, J. E., Stark, H., Burkholder, J. B., Talukdar, R. K., Meagher, J.,  
1382 Fehsenfeld, F. C., and Brown, S. S.: High levels of nitryl chloride in the polluted subtropical marine  
1383 boundary layer, *Nature Geoscience*, 1, 324-328, doi:10.1038/ngeo177, 2008.



- 1384  
1385 Peeters, J., Nguyen, T., and Vereecken, L.: HO<sub>x</sub> radical regeneration in the oxidation of isoprene, *Phys.*  
1386 *Chem. Chem. Phys.*, 11, 5935-5939, doi:10.1039/b908511d, 2009.
- 1387  
1388 Peeters, J., and Müller, J.-F.: HO<sub>x</sub> radical regeneration in isoprene oxidation via peroxy radical  
1389 isomerisations. II: experimental evidence and global impact, *Phys. Chem. Chem. Phys.*, 12, 14227-14235,  
1390 doi:10.1039/c0cp00811g, 2010.
- 1391  
1392 Peeters, J., Müller, J. F., Stavrou, T., and Vinh Son, N.: Hydroxyl radical recycling in isoprene oxidation  
1393 driven by hydrogen bonding and hydrogen tunneling: The upgraded LIM1 mechanism, *J. Phys. Chem. A*,  
1394 118, doi:10.1021/jp5033146, 2014.
- 1395  
1396 Praske, E., Crouse, J. D., Bates, K. H., Kurtén, T., Kjaergaard, H. G., and Wennberg, P. O.: Atmospheric  
1397 Fate of Methyl Vinyl Ketone: Peroxy Radical Reactions with NO and HO<sub>2</sub>, *J. Phys. Chem. A*, 119, 4562-  
1398 4572, doi:10.1021/jp5107058, 2015.
- 1399  
1400 Ren, X., Harder, H., Martinez, M., Leshner, R. L., Oligier, A., Simpas, J. B., Brune, W. H., Schwab, J. J.,  
1401 Demerjian, K. L., He, Y., Zhou, X., and Gao, H.: OH and HO<sub>2</sub> Chemistry in the urban atmosphere of New  
1402 York City, *Atmos. Environ.*, 37, 3639-3651, doi:doi.org/10.1016/S1352-2310(03)00459-X, 2003.
- 1403  
1404 Ren, X., Brune, W. H., Mao, J., Mitchell, M. J., Leshner, R. L., Simpas, J. B., Metcalf, A. R., Schwab, J. J., Cai,  
1405 C., Li, Y., Demerjian, K. L., Felton, H. D., Boynton, G., Adams, A., Perry, J., He, Y., Zhou, X., and Hou, J.:  
1406 Behavior of OH and HO<sub>2</sub> in the winter atmosphere in New York City, *Atmos. Environ.*, 40, 252-263,  
1407 doi:10.1016/j.atmosenv.2005.11.073, 2006.
- 1408  
1409 Ren, X., van Duin, D., Cazorla, M., Chen, S., Mao, J., Zhang, L., Brune, W. H., Flynn, J. H., Grossberg, N.,  
1410 Lefter, B. L., Rappenglück, B., Wong, K. W., Tsai, C., Stutz, J., Dibb, J. E., Thomas Jobson, B., Luke, W. T.,  
1411 and Kelley, P.: Atmospheric oxidation chemistry and ozone production: Results from SHARP 2009 in  
1412 Houston, Texas, *J. Geophys. Res.: Atmos.*, 118, 5770-5780, doi:10.1002/jgrd.50342, 2013.
- 1413  
1414 Rhew, R. C., Deventer, M. J., Turnipseed, A. A., Warneke, C., Ortega, J., Shen, S., Martinez, L., Koss, A.,  
1415 Lerner, B. M., Gilman, J. B., Smith, J. N., Guenther, A. B., and de Gouw, J. A.: Ethene, propene, butene  
1416 and isoprene emissions from a ponderosa pine forest measured by relaxed eddy accumulation, *Atmos.*  
1417 *Chem. Phys.*, 17, 13417-13438, doi:10.5194/acp-17-13417-2017, 2017.
- 1418  
1419 Rohrer, F., Bohn, B., Brauers, T., Brüning, D., Johnen, F. J., Wahner, A., and Kleffmann, J.:  
1420 Characterisation of the photolytic HONO-source in the atmosphere simulation chamber SAPHIR, *Atmos.*  
1421 *Chem. Phys.*, 5, 2189-2201, doi:10.5194/acp-5-2189-2005, 2005.
- 1422  
1423 Rohrer, F., Lu, K., Hofzumahaus, A., Bohn, B., Brauers, T., Chang, C.-C., Fuchs, H., Häsel, R., Holland, F.,  
1424 Hu, M., Kita, K., Kondo, Y., Li, X., Lou, S., Oebel, A., Shao, M., Zeng, L., Zhu, T., Zhang, Y., and Wahner, A.:



- 1425 Maximum efficiency in the hydroxyl-radical-based self-cleansing of the troposphere, *Nat. Geosci.*, 7, 559,  
1426 doi:10.1038/ngeo2199, 2014.
- 1427  
1428 Rolletter, M., Kaminski, M., Acir, I. H., Bohn, B., Dorn, H. P., Li, X., Lutz, A., Nehr, S., Rohrer, F., Tillmann,  
1429 R., Wegener, R., Hofzumahaus, A., Kiendler-Scharr, A., Wahner, A., and Fuchs, H.: Investigation of the  $\alpha$ -  
1430 pinene photooxidation by OH in the atmospheric simulation chamber SAPHIR, *Atmos. Chem. Phys.*, 19,  
1431 11635-11649, doi:10.5194/acp-19-11635-2019, 2019.
- 1432  
1433 Rolletter, M., Blocquet, M., Kaminski, M., Bohn, B., Dorn, H. P., Hofzumahaus, A., Holland, F., Li, X.,  
1434 Rohrer, F., Tillmann, R., Wegener, R., Kiendler-Scharr, A., Wahner, A., and Fuchs, H.: Photooxidation of  
1435 pinonaldehyde at ambient conditions investigated in the atmospheric simulation chamber SAPHIR,  
1436 *Atmos. Chem. Phys.*, 20, 13701-13719, doi:10.5194/acp-20-13701-2020, 2020.
- 1437  
1438 Sarkar, C., Guenther, A. B., Park, J. H., Seco, R., Alves, E., Batalha, S., Santana, R., Kim, S., Smith, J., Tóta,  
1439 J., and Vega, O.: PTR-TOF-MS eddy covariance measurements of isoprene and monoterpene fluxes from  
1440 an eastern Amazonian rainforest, *Atmos. Chem. Phys.*, 20, 7179-7191, doi:10.5194/acp-20-7179-2020,  
1441 2020.
- 1442  
1443 Sillman, S., Logan, J. A., and Wofsy, S. C.: The sensitivity of ozone to nitrogen oxides and hydrocarbons in  
1444 regional ozone episodes, *J. Geophys. Res.: Atmos.*, 95, 1837-1851, doi:10.1029/JD095iD02p01837, 1990.
- 1445  
1446 Slater, E. J., Whalley, L. K., Woodward-Massey, R., Ye, C., Lee, J. D., Squires, F., Hopkins, J. R., Dunmore,  
1447 R. E., Shaw, M., Hamilton, J. F., Lewis, A. C., Crilley, L. R., Kramer, L., Bloss, W., Vu, T., Sun, Y., Xu, W.,  
1448 Yue, S., Ren, L., Acton, W. J. F., Hewitt, C. N., Wang, X., Fu, P., and Heard, D. E.: Elevated levels of OH  
1449 observed in haze events during wintertime in central Beijing, *Atmos. Chem. Phys.*, 20, 14847-14871,  
1450 doi:10.5194/acp-20-14847-2020, 2020.
- 1451  
1452 Sommariva, R., Bloss, W. J., Brough, N., Carslaw, N., Flynn, M., Haggerstone, A. L., Heard, D. E., Hopkins,  
1453 J. R., Lee, J. D., Lewis, A. C., McFiggans, G., Monks, P. S., Penkett, S. A., Pilling, M. J., Plane, J. M. C., Read,  
1454 K. A., Saiz-Lopez, A., Rickard, A. R., and Williams, P. I.: OH and HO<sub>2</sub> chemistry during NAMBLEX: roles of  
1455 oxygenates, halogen oxides and heterogeneous uptake, *Atmos. Chem. Phys.*, 6, 1135-1153,  
1456 doi:10.5194/acp-6-1135-2006, 2006.
- 1457  
1458 Sommariva, R., Hollis, L. D. J., Sherwen, T., Baker, A. R., Ball, S. M., Bandy, B. J., Bell, T. G., Chowdhury,  
1459 M. N., Cordell, R. L., Evans, M. J., Lee, J. D., Reed, C., Reeves, C. E., Roberts, J. M., Yang, M., and Monks,  
1460 P. S.: Seasonal and geographical variability of nitryl chloride and its precursors in Northern Europe,  
1461 *Atmos. Sci. Lett.*, 19, e844, doi:10.1002/asl.844, 2018.
- 1462  
1463 Song, H., Chen, X., Lu, K., Zou, Q., Tan, Z., Fuchs, H., Wiedensohler, A., Moon, D. R., Heard, D. E., Baeza-  
1464 Romero, M. T., Zheng, M., Wahner, A., Kiendler-Scharr, A., and Zhang, Y.: Influence of aerosol copper on  
1465 HO<sub>2</sub> uptake: a novel parameterized equation, *Atmos. Chem. Phys.*, 20, 15835-15850, doi:10.5194/acp-  
1466 20-15835-2020, 2020.





- 1467  
1468 Spirig, C., Neftel, A., Ammann, C., Dommen, J., Grabmer, W., Thielmann, A., Schaub, A., Beauchamp, J.,  
1469 Wisthaler, A., and Hansel, A.: Eddy covariance flux measurements of biogenic VOCs during ECHO 2003  
1470 using proton transfer reaction mass spectrometry, *Atmos. Chem. Phys.*, 5, 465-481, doi:10.5194/acp-5-  
1471 465-2005, 2005.
- 1472  
1473 Stone, D., Whalley, L. K., and Heard, D. E.: Tropospheric OH and HO<sub>2</sub> radicals: field measurements and  
1474 model comparisons, *Chem. Soc. Rev.*, 41, 6348-6404, doi:10.1039/C2CS35140D, 2012.
- 1475  
1476 Stone, D., Sherwen, T., Evans, M. J., Vaughan, S., Ingham, T., Whalley, L. K., Edwards, P. M., Read, K. A.,  
1477 Lee, J. D., Moller, S. J., Carpenter, L. J., Lewis, A. C., and Heard, D. E.: Impacts of bromine and iodine  
1478 chemistry on tropospheric OH and HO<sub>2</sub>: comparing observations with box and global model  
1479 perspectives, *Atmos. Chem. Phys.*, 18, 3541-3561, doi:10.5194/acp-18-3541-2018, 2018.
- 1480  
1481 Taketani, F., Kanaya, Y., and Akimoto, H.: Kinetics of Heterogeneous Reactions of HO<sub>2</sub> Radical at Ambient  
1482 Concentration Levels with (NH<sub>4</sub>)<sub>2</sub>SO<sub>4</sub> and NaCl Aerosol Particles, *J. Phys. Chem. A*, 112, 2370-2377,  
1483 doi:10.1021/jp0769936, 2008.
- 1484  
1485 Taketani, F., Kanaya, Y., and Akimoto, H.: Heterogeneous loss of HO<sub>2</sub> by KCl, synthetic sea salt, and  
1486 natural seawater aerosol particles, *Atmos. Environ.*, 43, 1660-1665,  
1487 doi:10.1016/j.atmosenv.2008.12.010, 2009.
- 1488  
1489 Tan, D., Faloon, I., Simpas, J. B., Brune, W., Shepson, P. B., Couch, T. L., Sumner, A. L., Carroll, M. A.,  
1490 Thornberry, T., Apel, E., Riemer, D., and Stockwell, W.: HOx budgets in a deciduous forest: Results from  
1491 the PROPHET summer 1998 campaign, *J. Geophys. Res.: Atmos.*, 106, 24407-24427,  
1492 doi:10.1029/2001jd900016, 2001.
- 1493  
1494 Tan, Z., Fuchs, H., Lu, K., Hofzumahaus, A., Bohn, B., Broch, S., Dong, H., Gomm, S., Häsel, R., He, L.,  
1495 Holland, F., Li, X., Liu, Y., Lu, S., Rohrer, F., Shao, M., Wang, B., Wang, M., Wu, Y., Zeng, L., Zhang, Y.,  
1496 Wahner, A., and Zhang, Y.: Radical chemistry at a rural site (Wangdu) in the North China Plain:  
1497 observation and model calculations of OH, HO<sub>2</sub> and RO<sub>2</sub> radicals, *Atmos. Chem. Phys.*, 17, 663-690,  
1498 doi:10.5194/acp-17-663-2017, 2017.
- 1499  
1500 Tan, Z., Rohrer, F., Lu, K., Ma, X., Bohn, B., Broch, S., Dong, H., Fuchs, H., Gkatzelis, G. I., Hofzumahaus,  
1501 A., Holland, F., Li, X., Liu, Y., Liu, Y., Novelli, A., Shao, M., Wang, H., Wu, Y., Zeng, L., Hu, M., Kiendler-  
1502 Scharr, A., Wahner, A., and Zhang, Y.: Wintertime photochemistry in Beijing: observations of ROx radical  
1503 concentrations in the North China Plain during the BEST-ONE campaign, *Atmos. Chem. Phys.*, 18, 12391-  
1504 12411, doi:10.5194/acp-18-12391-2018, 2018.
- 1505  
1506 Tan, Z., Lu, K., Hofzumahaus, A., Fuchs, H., Bohn, B., Holland, F., Liu, Y., Rohrer, F., Shao, M., Sun, K., Wu,  
1507 Y., Zeng, L., Zhang, Y., Zou, Q., Kiendler-Scharr, A., Wahner, A., and Zhang, Y.: Experimental budgets of



- 15108 OH, HO<sub>2</sub>, and RO<sub>2</sub> radicals and implications for ozone formation in the Pearl River Delta in China 2014,  
15109 Atmos. Chem. Phys., 19, 7129-7150, doi:10.5194/acp-19-7129-2019, 2019.
- 15110  
15111 Tan, Z., Hofzumahaus, A., Lu, K., Brown, S. S., Holland, F., Huey, L. G., Kiendler-Scharr, A., Li, X., Liu, X.,  
15112 Ma, N., Min, K.-E., Rohrer, F., Shao, M., Wahner, A., Wang, Y., Wiedensohler, A., Wu, Y., Wu, Z., Zeng, L.,  
15113 Zhang, Y., and Fuchs, H.: No Evidence for a Significant Impact of Heterogeneous Chemistry on Radical  
15114 Concentrations in the North China Plain in Summer 2014, Environ. Sci. Technol., 54, 5973-5979,  
15115 doi:10.1021/acs.est.0c00525, 2020.
- 15116  
15117 Tan, Z., Fuchs, H., Hofzumahaus, A., Bloss, W. J., Bohn, B., Cho, C., Hohaus, T., Holland, F., Lakshmisha,  
15118 C., Liu, L., Monks, P. S., Novelli, A., Niether, D., Rohrer, F., Tillmann, R., Valkenburg, T., Vardhan, V.,  
15119 Kiendler-Scharr, A., Wahner, A., and Sommariva, R.: Seasonal variation of nitryl chloride and its relation  
15120 to gas-phase precursors during the JULIAC campaign in Germany, Atmos. Chem. Phys. Discuss., 2022, 1-  
15121 30, doi:10.5194/acp-2022-386, 2022.
- 15122  
15123 Tanaka, P. L., Riemer, D. D., Chang, S., Yarwood, G., McDonald-Buller, E. C., Apel, E. C., Orlando, J. J.,  
15124 Silva, P. J., Jimenez, J. L., Canagaratna, M. R., Neece, J. D., Mullins, C. B., and Allen, D. T.: Direct evidence  
15125 for chlorine-enhanced urban ozone formation in Houston, Texas, Atmos. Environ., 37, 1393-1400,  
15126 doi:10.1016/S1352-2310(02)01007-5, 2003.
- 15127  
15128 Teng, A. P., Crouse, J. D., and Wennberg, P. O.: Isoprene peroxy radical dynamics, J. Am. Chem. Soc.,  
15129 139, 5367-5377, doi:10.1021/jacs.6b12838, 2017.
- 15130  
15131 Thornton, J. A., Kercher, J. P., Riedel, T. P., Wagner, N. L., Cozic, J., Holloway, J. S., Dubé, W. P., Wolfe, G.  
15132 M., Quinn, P. K., Middlebrook, A. M., Alexander, B., and Brown, S. S.: A large atomic chlorine source  
15133 inferred from mid-continental reactive nitrogen chemistry, Nature, 464, 271-274,  
15134 doi:10.1038/nature08905, 2010.
- 15135  
15136 Vaughan, S., Ingham, T., Whalley, L. K., Stone, D., Evans, M. J., Read, K. A., Lee, J. D., Moller, S. J.,  
15137 Carpenter, L. J., Lewis, A. C., Fleming, Z. L., and Heard, D. E.: Seasonal observations of OH and HO<sub>2</sub> in the  
15138 remote tropical marine boundary layer, Atmos. Chem. Phys., 12, 2149-2172, doi:10.5194/acp-12-2149-  
15139 2012, 2012.
- 15140  
15141 Vilà-Guerau de Arellano, J., van den Dries, K., and Pino, D.: On inferring isoprene emission surface flux  
15142 from atmospheric boundary layer concentration measurements, Atmos. Chem. Phys., 9, 3629-3640,  
15143 doi:10.5194/acp-9-3629-2009, 2009.
- 15144  
15145 Wang, F., Hu, R., Chen, H., Xie, P., Wang, Y., Li, Z., Jin, H., Liu, J., and Liu, W.: Development of a field  
15146 system for measurement of tropospheric OH radical using laser-induced fluorescence technique, Optics  
15147 Express, 27, A419-A435, doi:10.1364/OE.27.00A419, 2019.
- 15148



- 1549 Whalley, L. K., Edwards, P. M., Furneaux, K. L., Goddard, A., Ingham, T., Evans, M. J., Stone, D., Hopkins,  
1550 J. R., Jones, C. E., Karunaharan, A., Lee, J. D., Lewis, A. C., Monks, P. S., Moller, S. J., and Heard, D. E.:  
1551 Quantifying the magnitude of a missing hydroxyl radical source in a tropical rainforest, *Atmos. Chem.*  
1552 *Phys.*, 11, 7223-7233, doi:10.5194/acp-11-7223-2011, 2011.
- 1553  
1554 Whalley, L. K., Stone, D., Dunmore, R., Hamilton, J., Hopkins, J. R., Lee, J. D., Lewis, A. C., Williams, P.,  
1555 Kleffmann, J., Laufs, S., Woodward-Massey, R., and Heard, D. E.: Understanding in situ ozone production  
1556 in the summertime through radical observations and modelling studies during the Clean air for London  
1557 project (ClearLo), *Atmos. Chem. Phys.*, 18, 2547-2571, doi:10.5194/acp-18-2547-2018, 2018.
- 1558  
1559 Whalley, L. K., Slater, E. J., Woodward-Massey, R., Ye, C., Lee, J. D., Squires, F., Hopkins, J. R., Dunmore,  
1560 R. E., Shaw, M., Hamilton, J. F., Lewis, A. C., Mehra, A., Worrall, S. D., Bacak, A., Bannan, T. J., Coe, H.,  
1561 Percival, C. J., Ouyang, B., Jones, R. L., Crilley, L. R., Kramer, L. J., Bloss, W. J., Vu, T., Kotthaus, S.,  
1562 Grimmond, S., Sun, Y., Xu, W., Yue, S., Ren, L., Acton, W. J. F., Hewitt, C. N., Wang, X., Fu, P., and Heard,  
1563 D. E.: Evaluating the sensitivity of radical chemistry and ozone formation to ambient VOCs and NO<sub>x</sub> in  
1564 Beijing, *Atmos. Chem. Phys.*, 21, 2125-2147, doi:10.5194/acp-21-2125-2021, 2021.
- 1565  
1566 Winiberg, F. A. F., Dillon, T. J., Orr, S. C., Groß, C. B. M., Bejan, I., Brumby, C. A., Evans, M. J., Smith, S. C.,  
1567 Heard, D. E., and Seakins, P. W.: Direct measurements of OH and other product yields from the HO<sub>2</sub>  
1568 + CH<sub>3</sub>C(O)O<sub>2</sub> reaction, *Atmos. Chem. Phys.*, 16, 4023-4042, doi:10.5194/acp-16-4023-2016, 2016.
- 1569  
1570 Wolfe, G. M., Thornton, J. A., Bouvier-Brown, N. C., Goldstein, A. H., Park, J. H., McKay, M., Matross, D.  
1571 M., Mao, J., Brune, W. H., LaFranchi, B. W., Browne, E. C., Min, K. E., Wooldridge, P. J., Cohen, R. C.,  
1572 Crouse, J. D., Faloona, I. C., Gilman, J. B., Kuster, W. C., de Gouw, J. A., Huisman, A., and Keutsch, F. N.:  
1573 The Chemistry of Atmosphere-Forest Exchange (CAFE) Model – Part 2: Application to BEARPEX-2007  
1574 observations, *Atmos. Chem. Phys.*, 11, 1269-1294, doi:10.5194/acp-11-1269-2011, 2011.
- 1575  
1576 Wolfe, G. M., Cantrell, C., Kim, S., Mauldin Iii, R. L., Karl, T., Harley, P., Turnipseed, A., Zheng, W., Flocke,  
1577 F., Apel, E. C., Hornbrook, R. S., Hall, S. R., Ullmann, K., Henry, S. B., DiGangi, J. P., Boyle, E. S., Kaser, L.,  
1578 Schnitzhofer, R., Hansel, A., Graus, M., Nakashima, Y., Kajii, Y., Guenther, A., and Keutsch, F. N.: Missing  
1579 peroxy radical sources within a summertime ponderosa pine forest, *Atmos. Chem. Phys.*, 14, 4715-4732,  
1580 doi:10.5194/acp-14-4715-2014, 2014.
- 1581  
1582